Robust Operation and Control Synthesis of Autonomous Mobile Rack Vehicle in the Smart Warehouse

Boc Minh Hung

A Dissertation Submitted in Partial Fulfillment of Requirements
For the Degree of Doctor of Philosophy

February 2018

Korea Maritime and Ocean University
Department of Refrigeration and Air-Conditioning Engineering

Supervisor Sam Sang You

본 논문을 BOC MINH HUNG 의 공학박사

학위논문으로 인준함

위 원장 김환성 (인)

위 원 유삼상 (인)

위 원 최형식 (인)

위 원 정석권 (인)

위 원 정태영 (인)

2018 년 1 월

한국해양대학교 대학원

Acknowledgement

I would like to thank Professor Sam-Sang You for his encouraging my research and for allowing me to grow as a research scientist. Thank to his guidance from beginner to now, so I can develop my best talent and improve quickly in my research. Your advice on both research and my future career have been priceless. I also would like to thank the committee members, professor Hwan-Seong Kim, professor Hyeung-Sik Choi, professor Seok-Kwon Jeong and professor Tae-Yeong Jeong for serving as my committee members even at hardship.

I would like to thank professor Hwan-Seong Kim who created the condition for me to join and finish this project. I would also like to thank all of my friends who supported me in writing and contribute ideas to complete my dissertation.

Korea Maritime and Ocean University, Busan, Korea

November 27th 2017

Boc Minh Hung

Robust Operation and Control Synthesis of Autonomous Mobile Rack Vehicle in the Smart Warehouse

Boc Minh Hung

Korea Maritime and Ocean University
Department of Refrigeration and Air – Conditioning Engineering

Abstract

Nowadays, with the development of science and technology, to manage the inventory in the warehouse more efficiency, so the warehouse must have the stability and good operation chain such as receive and transfer the product to customer, storage the inventory, manage the location, making the barcode...in that operation chain, storage the inventory in the warehouse is most important thing that we must consider. In addition, to reduce costs for larger warehouse or expand the floor space of the small warehouse, it is impossible to implement this with a traditional warehouse. The warehouse is called the traditional warehouse when it uses the fixed rack. To build this type of warehouse, the space for storage must be very large. However, the cost for renting or buying the large warehouse is too expensive, so to reduce cost and build the flexible warehouse which can store the huge quantity of product within limited area, then the smart warehouse is necessary to consider. The smart warehouse system with autonomous mobile rack vehicles (MRV) increases the space utilization by providing only a few open aisles at a time for accessing the racks with minimal intervention. It is always necessary to take into account the mobile-rack vehicles (or autonomous logistics vehicles).

This thesis deals with designing the robust controller for maintaining safe spacing with collision avoidance and lateral movement synchronization in the fully automated warehouse. The compact MRV dynamics are presented for the interconnected string of MRV with communication delay. Next, the string stability with safe working space of the MRV has been described for guaranteeing complete autonomous logistics in the extremely cold environment without rail rack. In addition, the controller order has been significantly reduced to the low-order system without serious performance degradation. Finally, this control method addresses the control robustness as well as the performances of MRV against unavoidable uncertainties, disturbances, and noises for warehouse automation.

Keywords: Logistics vehicle, H_∞ robust control, Uncertainty modeling, mobile rack vehicle, longitudinal control, nonlinear analysis, string stability, autonomous vehicle.

Contents

List of Tables

List of Figures

Chapter 1. Introduction

The intelligent warehouse is an essential part of the material-handling industry and has gained popularity in recent years. Efficient and sensitive warehousing with intelligent mobile rack vehicle and mobile robots is critical improve the overall productivity and simultaneously achieve high efficiency. The operation stability and synchronization movement problem of group mobile rack vehicle or mobile robot are a hot topic for warehouses. Several research efforts have been directed toward the control of a group of autonomous vehicle or robots. The reasons for multi-mobile rack vehicle system employing are widely different; however, one of the main motivations is that multi MRV can be used to increase the system effectiveness. A platoon of MRV can better perform a mission in terms of time and quality, can keep the safety distance between of each mobile racks to avoid the collision.

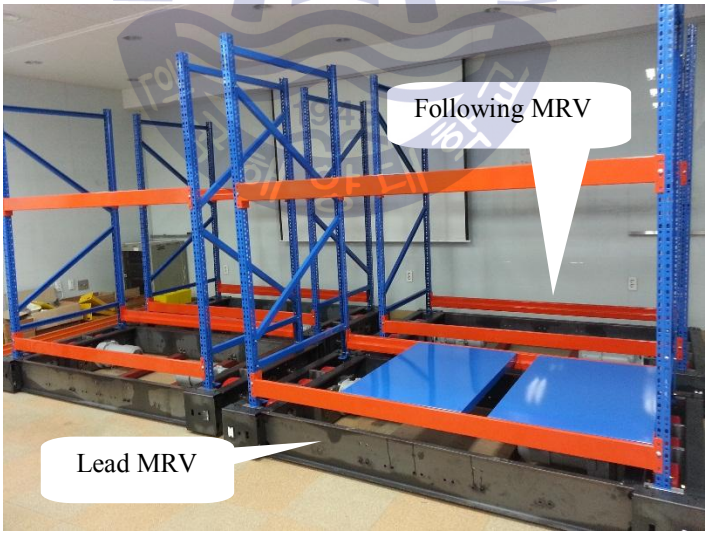

Fig. 1 The real model of MRV platoon in the warehouse

The word platoon MRV is a series of MRV following each other in the same lane. In a platoon, the forward most MRV also refers to as the leading MRV

independently, running at a constant speed whereas the following MRV try to follow the speed of the MRV while maintaining a short but safe distance to the preceding MRV, a real model of MRV in a platoon is described in Fig. 1. This formation will allow more vehicle to drive in the same lane which will increase the capacity of the road. A properly designed control system for a platoon will be attenuated the noise and resilient to different means of disturbances. The main objective of that competition was to drive several mobile rack vehicle developed by different participants in a platoon in the warehouse equipped with wireless communication to support the exchange of information between vehicles. The research addressed different problems in a mobile rack vehicle platoon and tried to minimize the effect by applying the ACC, a control strategy for connected vehicles driving in a platoon.

1.1 Mobile rack vehicle

In a mobile-rack warehouse, the neighboring racks need to be moved aside to access a specific aisle. Traditionally, a warehouse has aisles for storage and retrieval operations between racks, causing a dead space when there are no such operations. By moving racks and setting up space for materials handling only when such operations are in progress, the dead space can be effectively utilized for storage and this system is called the warehouse with a mobile-rack vehicle. A human picker or some storage and retrieval vehicle can access an open aisle in order to pick the stock keeping units defined by a pick list. The automated mobile-rack vehicle can be particularly used in cold storage warehouse for perishable items or frozen foods such as fish or meat. In this case, the floor surface is covered by ice, so the movement of the mobile-rack vehicle is a critical problem that the collision between mobile-racks occurs easily. The type of warehouse is depicted in Fig. 2. Fully loaded racks may become very heavy so that moving racks and opening another aisle needs considerable safe spacing and speed. The longitudinal motions have been controlled on the idea of adaptive cruise control (ACC) system

so far. In the fully automated process of a mobile-rack vehicle system, the user sets the desired position and velocity of the lead vehicle. Respectively, a distance sensor and the encoder attached to the front of the rack and the axle of the wheel are used to measure the preceding mobile-rack distance and velocity. The processing units receive the input signals from those sensors and send the output signals to the servomotor. Then the servomotor adjusts the position of the wheel or the safety distance in line with the command of the controller. Finally, the change in position or safety distance leads to the change in the speed of mobile-rack to obtain an optimal speed with an operation time. If a shorter or longer distance of mobile-rack is detected, the MRV collision could occur. Then the control units should slow down or speed up the mobile-rack to maintain the safety distance while avoiding those collisions.

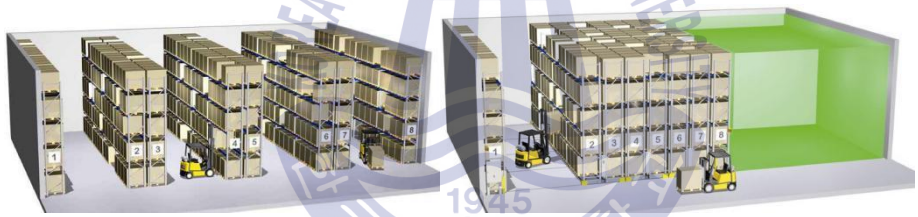

(a) Traditional ware house (b) Smart warehouse

Fig. 2 The type of the warehouse

A great *number of* research reports deal with the longitudinal control or ACC for the vehicles, concerned with the safe distance and velocity, for example, the pole placement control scheme (Godbole and Lygeros, 1994) The paper presents the longitudinal control law for the lead vehicle of a platoon in an automated highway, and the control laws successfully passed the simulation test. However, those results did not guarantee the performance under the noises and exogenous disturbances,

which affects the motion stability of the cruise control. In (Sivaji and Sailaja, 2013) the stability of inter-vehicle gap is based on the speed of host vehicle and headway. There are three major inputs to the ACC system, which are the speed of host vehicle read from memory unit, headway time set by the driver, and actual gap measured by the radar scanner. The PID control algorithm is applied to this research and the simulation results depict the response of the trial ACC model that the system stabilizes at a range of 20ms. The robust longitudinal velocity tracking of the vehicle has been presented using traction control and brake control based on a backstepping algorithm (Tai and Tomizuka, 2000). At each step of constructing a candidate Lyapunov function, a scaling parameter is introduced for each added term to take into account badly scaled system states. The simulation results are described in two cases, where all the parameters of the model are known, and the model with actual slip coefficient has a good velocity response. However, the system would be unstable under disturbances and noises. (Hsu *et al.*, 2005) proposed a collision prevention control using a wavelet neural network (WNN). The intelligent wavelet neural network (IWNN) scheme is comprised of a WNN controller and a robust controller. The simulation results demonstrate that the proposed control system can achieve favorable tracking performance while the leading vehicle velocity and the following safe spacing are changing. Some advanced control schemes have been presented using robust control synthesis (Gao *et al.*, 2016; Gao *et al.*, 2017). A control approach with linear matrix inequality (LMI) is presented for a heterogeneous platoon with uncertain vehicle dynamics and uniform communication delays. Other papers provided a decoupled control strategy for vehicular platoons with a rigid communication topology which applying eigenvalue decomposition on communication matrix to solve the limitation of the norm. (Guo *et al.*, 2012) designed a controller considering parametric uncertainties, communication delays, and disturbance attenuation. However, this study only works for a vehicular platoon with a specific length. To overcome these issues, (Stankovic *et al.*, 2000) designed a state feedback sub-optimal controller based on a three-order vehicle model. (Herman *et al.*, 2015)

proposed an asymmetric bidirectional controller to ensure string stability without the lead vehicle information. (Rajamani *et al.*, 2001) employed a hierarchical structure, whose upper–level controller is to maintain safe and stable operation, and the lower-level controller determines throttle/ brake commands.

1.2 Leader and following vehicle

1.2.1 Cruise control

Cruise control system is one of the advanced systems and has become a common feature in automobiles nowadays. Instead of driver frequently checking out the speedometer and adjusting the pressure on the throttle pedal or the brake.

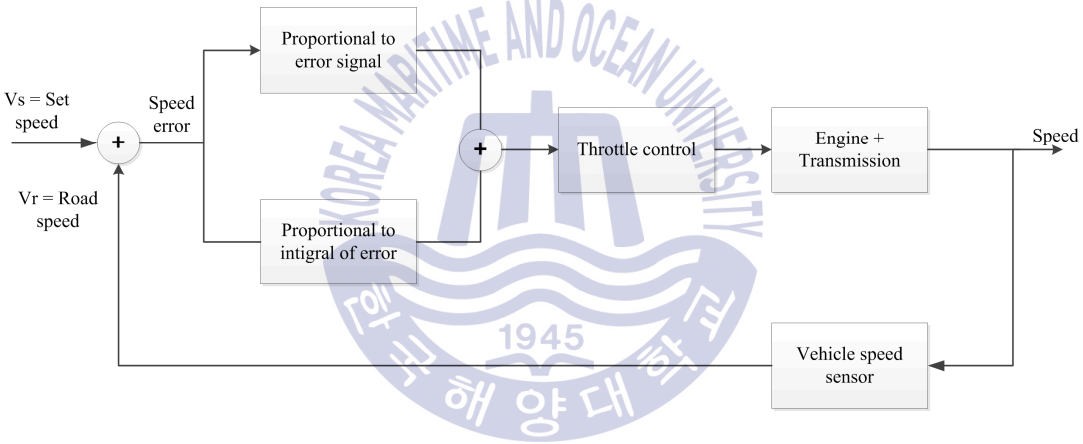

Fig. 3 The block diagram of cruise control model

Cruise control system takes over the control the speed of the car by maintaining the constant speed set by the driver. Therefore, this system can help in reducing driver's fatigue in driving a long road trip. In the process of the cruise control system. Firstly, the driver sets the desired speed of the car by turning on the cruise control mode at the desired speed, such that the car is traveling at the set speed and hits the button. An alternate way to set the desired speed of the car is by tapping the set/acceleration button to increase the speed of the car or by tapping the coast button to decrease the speed of the car. Secondly, the processing unit in the system receives the input signal, and progress the output signal to the actuator. Thirdly, the

actuator adjusts the throttle position according to the command of the controller. Finally, the changes in the throttle position lead to the change in the speed of the car traveling and obtain the desired speed. The actual speed of the car is continuously monitored by a sensor and fed to the processor. The process of transmitting the current speed of the car continues to the processor to maintain the desired speed, as long as the cruise control is engaged.

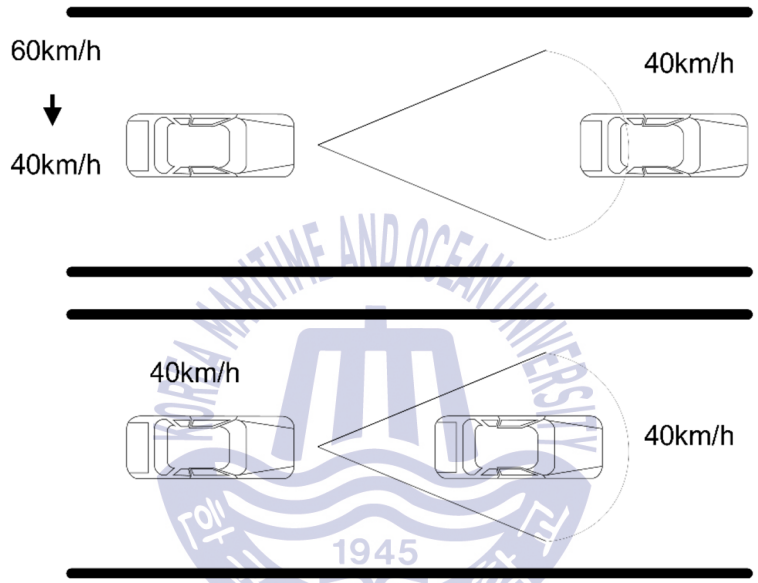

Fig. 4 The cruise control system description

The basic operation of a cruise controller is to sense the speed of the vehicle, compare this speed to the desired reference, and then accelerate or decelerate the car as required. A simple control algorithm for controlling the speed is to use a proportional plus integral feedback.

1.2.2 Adaptive cruise control

The history of research in a vehicle following strategies goes back until 1960's. However, the commercial deployment started in late 2000's when industry grade

Electronic Control Unit and sophisticated electronic sensors came to market. Intelligent cruise control (ACC) is a modern which assists the driver to maintain primarily longitudinal control of the vehicle. During a motorway driving, an ACC performs longitudinal control of the vehicle while the lateral maneuver remains the drivers' responsibility. While driving in ACC mode, it is mandatory for the driver to monitor the situation at all times and prepare to take over control at any unanticipated event. ACC is an extension of the CC system. In an ACC system, the driver specifies the desired distance from the vehicle in front and a maximum speed which the system should not exceed. The control algorithm of the ACC maintains the distance to the preceding vehicle measured typically by a RADAR and sends acceleration or deceleration signals to the engine system.

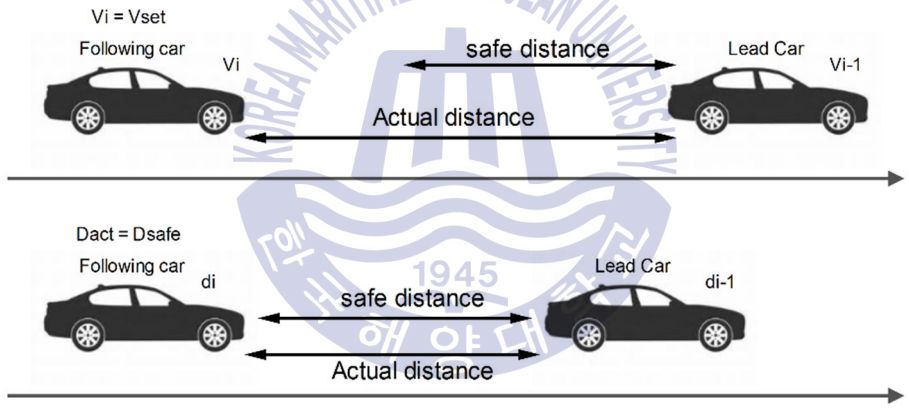

Fig. 5 Structure of Intelligent cruise control

The core of an ACC system relies on the selection of an inter-vehicle spacing policy. Among different vehicle following speed control methods proposed over the years (Steven. E. S, 1995) only a handful of them have been proven for real-world application. The most popular gap regulation strategies are (Steven. E. S et al., 2015)

- Constant Clearance or Constant Distance Gap:

In this strategy, the distance between vehicles (measured in meters) remains constant regardless of the change in speed. Achieving constant clearance requires an ideal platoon formation and noise free sensor measurements. According to studies, it is very likely that a CDG platoon will be prone to string instability (Chi. Y. L and Huei. P, 2000). The constant clear policy is not favorable for non-interconnected platoons in general (Jing. Z and Huei. P, 2005).

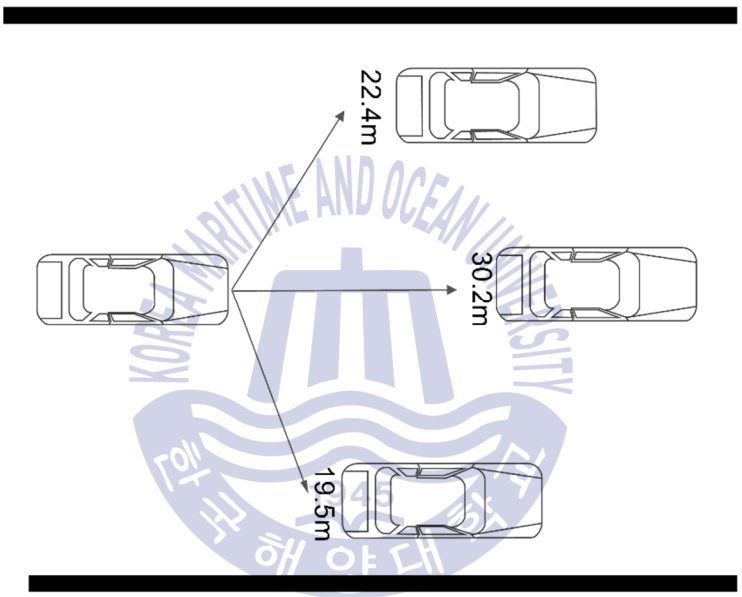

Fig. 6 ACC system monitors the distance from preceding vehicle

- Constant Time Gap (CTG) or Constant Time Headway (CTH):

The CTG policy proposed a linear relation between inter-vehicle space and vehicle speed (Jing. Z and Huei. P, 2005). This resembles to how human drivers behave on a motorway. In CTH, inter-vehicle distance increase when the speed of the ego vehicle is increasing and vice versa, which appears to be very convenient and safe to the driver. The space between two vehicles is expressed in terms of time

which is also known as time headway. The formal definition of time headway is the time between, when the front bumper of the leading vehicle and the front bumper of the following vehicle, pass a fixed point on the road (measured in seconds). CTH is the most common strategy in the research of ACC. Mathematically desired distance in CTH for the i^{th} vehicle is calculated by

$$D_{i,des}(t) = D_{\min} + h_i v_i(t) \tag{1}$$

where:

$D_{i,des}(t)$ desired distance (m)

$D_{\min}$ desired standstill distance (m)

h_i time headway (s)

$v_i(t)$ vehicle speed (m/s^2)

In (Joseph. T and Zoltan A. N, 1970) researcher have monitored real-world traffic and found that about 50% of the drivers maintained a time headway between 1s and 2s. There were less than 20% which was driving with a headway time below 1s.

- Constant Safety –factor Criterion (CSFC):

This policy defined a concept which is different from CTH. In this strategy inter-vehicle, spacing has a nonlinear relation to the vehicle speed (Ioannis. A. N et al., 2015). The CSFC calculates inter-vehicle space which is proportional to the square of the cruising speed (Steven. E. S et al., 2015). However, this method is still under development. Generally, the structure of an ACC system is consists of a two-layer control system namely high-level or supervisory level and low-level control or servo level. The supervisory level controller measures the range to the preceding vehicle, if it is out of range or not present at all, the CC controller is activated to drive at the desired speed. In the scenario where the preceding vehicle is in range, the supervisory level controller switches to ACC mode measures range

and range rate and calculates all the kinematics required to maintain the inter-vehicle gap set by the driver. The low level or servo level control is identical for an ACC and a CC system. It translates the speed or acceleration input from the supervisory level into an engine signal for acceleration or deceleration. An ACC system should ensure road safety and driver comfort, any change in the environment should be dealt with in a rational way so that it does not amplify any disturbances.

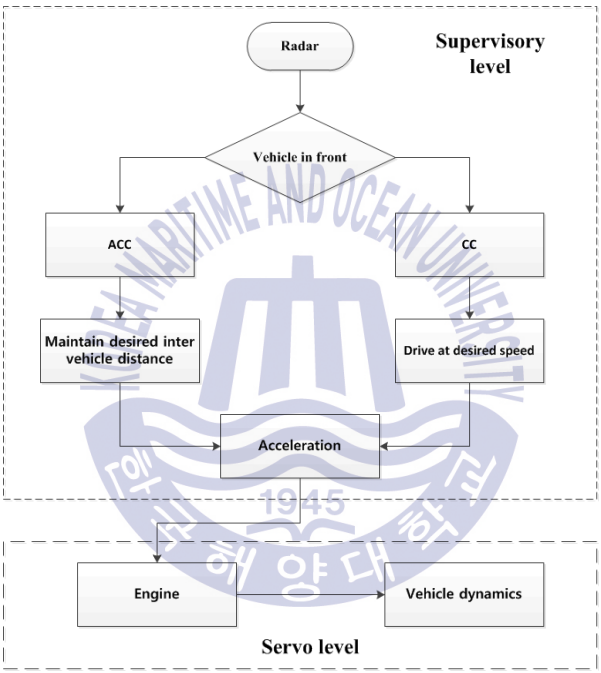

Fig. 7 Controller structure of ACC and selection between ACC and CC

1.2.3 String stability of longitudinal vehicle platoon

In this thesis, the controller is built which based on the adaptive cruise control theorem. So the string stability of mobile rack platoon is established that satisfied the condition of ACC system. The notion of string stability in automated vehicular platoon has been introduced in (Caudill et al., 1977). A platoon of vehicles on the

road is referred to as a vehicle string. A string of vehicles is said to be “string stable” if the range error does not amplify as it propagates along the string but rather decrease towards zero. In general, a platoon is string stable if any change in the speed of a lead vehicle will not result in a fluctuation in the space error for the following vehicles. Mathematically string stability is defined as, if the transfer function from the range error of a vehicle to that of its following vehicle has a magnitude less than or equal to 1 (Swaroop. D et al., 1996). The motion of the leading vehicle is measured by several sensors. The delays in sensor data acquisition are incorporated with the control system response time.

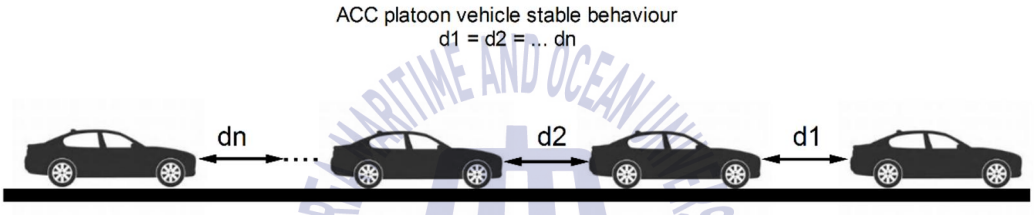

Fig. 8 The string stable platoon behavior

For an ACC equipped vehicle, if the accumulated time delay from sensor data acquisition, processioning, controller, and dynamics is 1.5s, it will take 4.5s for the 4th vehicle in the platoon to sense the change in motion of the lead vehicle (Steven. E. S et al., 2015).

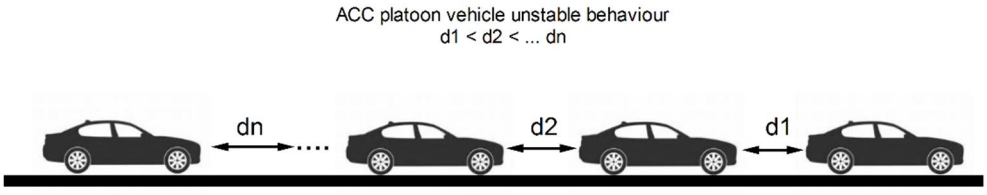

Fig. 9 The string unstable platoon behavior

California PATH project demonstrated that in a platoon, if the leading vehicle decelerates at $0.1 m/s^2$, the declaration will amplify and when it 4th reacts the deceleration will peak to $0.3 m/s^2$ (Vicente. M et al., 2014).

1.2.3.1 Longitudinal vehicle string stability definition

a) Uniform vehicle strings

Consider a uniform vehicle string, that is, all vehicles in the string are identical, i.e. $G_i = G$ and $h_i = h \forall_i$. It is clear that the range error output must be smaller than or equal to the range error input to avoid range errors propagate indefinitely along the string. For this uniform vehicle string, a string-stability definition is widely used and is described as following:

❖ **Definition:**

A uniform vehicle string is string stable if:

$$\left\| \varepsilon_{i+1} \right\|_2 \leq \left\| \varepsilon_i \right\|_2 \tag{2}$$

In a uniform vehicle string, the propagation transfer function $\bar{G}_{i,1}$ from the range error (ε_i) of one vehicle to the range error (ε_{i+1}) of its followers can be written as:

$$\frac{\varepsilon_{i+1}}{\varepsilon_i} = \bar{G}_{i,1} = G_i . \frac{(1 - G_{i+1} - s.h_{i+1}.G_{i+1})}{(1 - G_i - s.h_i.G_i)} = G_i = G \tag{3}$$

To achieve string stability, the inequality $\|G\|_\infty \le 1$ needs to be satisfied. Therefore, the string stability of an uninformed vehicle string can be determined by the car following algorithm G .

b) Mixed vehicle string

In the previous section, string stability is defined under the assumption of uniform vehicle strings. On the real highway, however, a vehicle strings consist of different types of vehicles, including manual and automated, string stable and string unstable vehicles. What is the string-stability property of such a mixed vehicle string? More specifically, if we consider a mixed vehicle string consisted of string-unstable manual vehicles and string-stable semi-automated vehicles, the string-stability definition in:

❖ **Definition:**

For a mixed vehicle string, the string stability from vehicle to the vehicle has become meaningless because no simple expression can represent all vehicles in this mixed vehicle string. The assumption, the string vehicle with a constant time headway $h = 1$ s.

$$\|G_1\|_\infty \le 1, \|G_2\|_\infty \le 1, \|G_3\|_\infty \le 1 \qquad (4)$$

The two propagation transfer functions are as follows

$$\bar{G}_{1,1} = \frac{\varepsilon_2}{\varepsilon_1} = G_1 . \frac{1 - G_2 - s.h.G_2}{1 - G_1 - s.h.G_1}$$
$$\bar{G}_{2,1} = \frac{\varepsilon_3}{\varepsilon_2} = G_2 . \frac{1 - G_3 - s.h.G_3}{1 - G_2 - s.h.G_2} \quad (5)$$

and we found that

$$\left\| \bar{G}_{1,1} \right\|_\infty > 1, \left\| \bar{G}_{2,1} \right\|_\infty < 1 \quad (6)$$

It is obviously that no conclusion about the string stability of this mixed string can be drawn in this numerical example. In the following, we will propose a string stability definition for mixed vehicle strings. Consider a mixed vehicle string (S_1) of k vehicles. If this string is repeated to form an infinitive string, then the propagation transfer function from the first vehicles rang error (ε_{nk+1}) of on sub-string (S_n) to that $(\varepsilon_{(n+1)k+1})$ of the following sub-string (ε_{n+1}) is as follows:

$$\bar{G}_{nk+1,k} = \frac{\varepsilon_{(n+1)k+1}}{\varepsilon_{nk+1}} = G_{nk+1} . G_{nk+2} ... G_{nk+k} . \frac{(1 - G_{(n+1)k+1} - s.h_{(n+1)k+1} . G_{(n+1)k}}{(1 - G_{nk+1} - s.h_{nk+1} . G_{nk+1})}$$
$$n = 0..\infty \quad (7)$$

Because $G_{nk+1} = G_1, G_{nk+2} = G_2, ..., G_{nk+k} = G_k$ and $h_{nk+1} = h_1$ becomes
$\bar{G}_{nk+1,k} = G_1 . G_2 ... G_k \quad n = 0..\infty$

It is clear that to avoid any range error being amplified unboundedly along this imaginary infinite vehicle string, the magnitude of $\bar{G}_{nk+1,k}$ must be less than or equal to 1.

1.2.3.2 String stability margin

String stability has become an important design issue in the vehicle longitudinal control. Researchers have been done on the proof and analysis of string stability. However, no quantitative measurement of string stability has been provided. As a result, there is no way we can determine if one ACC design is "marginally" string stable? Or if one ACC design is more string stable than the other? In this section, we will define a string-stability margin (SSM) and determine the string stability of ACC designs in the context of SSM. The margin is basically measured of how close an ACC design comes to the marginal string stability, i.e. $\|G\|_\infty = 1$. The operational definition of SSM is stated below.

❖ **Definition:**

Consider a mixed vehicle string condition of n standard manual vehicles with their car following algorithm represented by G_{MV} and ACC controlled vehicle with its car-following algorithm represented by G_{ACC}. Increase n from zero until $n_{\max}$ so that the following inequality is not satisfied.

$$\left\| \underbrace{G_{MV}.G_{MV}...G_{MV}}_{n}.G_{ACC} \right\|_\infty \le 1 \qquad (8)$$

The $n_{\max}$ is the SSM for this ACC controlled vehicle.

1.2.4 String stability of lateral vehicle platoon

In this case, the lateral error from the first follower propagates back and is amplified, it can lead to vehicles further down the platoon cutting corners or

leaving the lane due to too large errors. Therefore, the stability of lateral control must be considered to keep the stability of the mobile rack vehicle platoon.

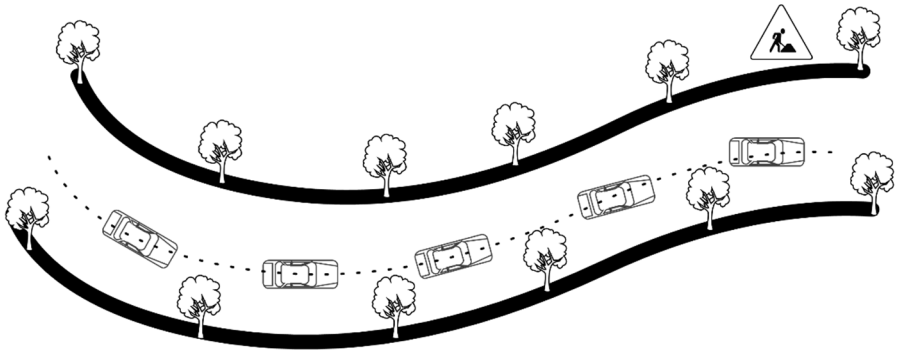

Fig. 10 The lateral string stability of vehicle

1.2.4.1 Lateral vehicle string stability definition

Let $\xi_e^i(t)$ denote the measure lateral error from vehicle i to vehicle $i-1$. A platoon of n vehicles is said to be string stable in the L_2 norm sense if for every $i \in [2, n]$, the relation $\left\|\xi_e^{(i)}(t)\right\|_2 < \left\|\xi_e^{(i-1)}(t)\right\|_2$. If string-stability holds, a disturbance in the system will always attenuate as it propagates throughout the platoon. This approach is different from the one discussed in (Papadimitriou. I et al., 2004), where the L_∞ norm is considered instead of the L_2 norm. That former approach imposes a condition on the infinity norm $\left\|H(j\omega)\right\|_\infty$ as well as having the sign of the impulse response of $\left\|H(j\omega)\right\|$ be non-changing which proved to be difficult to analyze. A translation of the definition above to the frequency domain would mean that if the transfer function from the error of a vehicle to that of its following vehicle has a magnitude less than 1, string stability is ensured. Thus, the condition is

$$\left\|H(j\omega)\right\|_{\infty} = \left\|\frac{\varepsilon_i(j\omega)}{\varepsilon_{i-1}(j\omega)}\right\| < 1 \rightarrow \left|\frac{\varepsilon_i(j\omega)}{\varepsilon_{i-1}(j\omega)}\right| < 1 \forall \omega \tag{9}$$

where $\varepsilon_i(j\omega)$ denotes the Laplace transform of the lateral error $\xi_e^i(t)$ from vehicle i to the preceding vehicle, and $\varepsilon_{i-1}(j\omega)$ similarly from vehicle $i-1$ to its preceding vehicle. The requirement is therefore that the infinity norm $\left\|H(j\omega)\right\|_{\infty}$ is strictly less than one. In order to investigate whether the system is string stable or not, proper error functions must be determined. Hence, since the error would in this case be the lateral deviation, the following relations are set up. Let the error from vehicle i to vehicle $i-1$ be defined as the projected lateral offset from the center of gravity of the following vehicle to the rear bumper of the leader.

$$\dot{\xi}_e^{(i)} = \Delta\dot{\xi}_i = L\dot{\psi}_i + V_x\psi_i + V_x\beta_i - V_x\psi_{i-1} - V_x\beta_{i-1} + l_{rb}\dot{\psi}_{i-1} \tag{10}$$

where the term $l_{rb}\dot{\psi}_{i-1}$ is introduced from following the rear bumper. Since every MRV in the platoon is assumed to be identical and thus having the same controller acting on the lateral error, the control signal for vehicle i can be written as $u_i = -C\varepsilon_i$ where C is the controller used by the vehicle. It is assumed at this point that there is no communication between the vehicles in the platoon. Thus, by performing a Laplace transform, the previous relation can be rewritten as

$$s * \varepsilon_i = (LG_{\dot{\psi}_i} + V_x G_{\psi_i} + V_x G_{\beta i})u_i - (-l_{rb}G_{\dot{\psi}_{i-1}} + V_x G_{\psi_{i-1}} + V_x G_{B_{i-1}})u_{i-1} \tag{11}$$

Since it has been assumed that all the vehicles are identical, $G_{\dot{\psi}_i} = G_{\dot{\psi}_{i-1}}$ must hold and similarly for the rest of the expressions. Hence, the indices can be omitted and the relation can be written as

$$\varepsilon_i = \frac{(LG_{\dot{\psi}} + V_x G_{\psi} + V_x G_{\beta})}{s} u_i - \frac{(-l_{rb} G_{\dot{\psi}} + V_x G_{\psi} + V_x G_B)}{s} u_{i-1} \tag{12}$$

The expression $\frac{(LG_{\dot{\psi}} + V_x G_{\psi} + V_x G_{\beta})}{s}$ can be written as $G_{\Delta y}$, whereas the other expression $\frac{(-l_{rb} G_{\dot{\psi}} + V_x G_{\psi} + V_x G_B)}{s}$ represents the dynamic of the movement of the point on the rear bumper that is to be tracked by the sensor. It is similar to that of $G_{\Delta y}$ but with L replaced by $-l_{rb}$ and will for distinction be denoted G_{rb}.

$$G_{\Delta y}(s) = \frac{(e_0 + f_0 L)s^2 + \left(\frac{(c_0 e_0 - a_0 f_0)(L + l_r)}{v_x}\right)s + (c_0 e_0 - a_0 f_0)}{s^4 - \left(\frac{a_0 + d_0}{v_x}\right)s^3 + \left(\frac{a_0 d_0 - b_0 c_0}{v_x^2} + c_0\right)s^2} \tag{13}$$

$$G_{rb}(s) = \frac{(e_0 + f_0 l_{rb})s^2 + \left(\frac{(c_0 e_0 - a_0 f_0)(-l_{rb} + l_r)}{v_x}\right)s + (c_0 e_0 - a_0 f_0)}{s^4 - \left(\frac{a_0 + d_0}{v_x}\right)s^3 + \left(\frac{a_0 d_0 - b_0 c_0}{v_x^2} + c_0\right)s^2} \tag{14}$$

In addition

$$\varepsilon_i = G_{\Delta y} u_i - G_{rb} u_{i-1} \tag{15}$$

By substituting for the control signals the relation can be written as

$$\varepsilon_i = G_{\Delta y} u_i - G_{rb} u_{i-1} = G_{\Delta y}(-C\varepsilon_i) - G_{rb}(-C\varepsilon_{i-1}) \tag{16}$$

Thus the ratio of the errors can finally b written as follows:

$$\frac{\varepsilon_i}{\varepsilon_{i-1}} = \frac{G_{rb}C}{1+G_{\Delta y}C} \tag{17}$$

From the remarks above, it is clear that at best when the system is controlled to achieve an over-damped response, the ratio will be $\left\| \frac{\varepsilon_i(j\omega)}{\varepsilon_{i-1}(j\omega)} \right\|_\infty \leq 1$ with equality. It means that for low frequencies, the error will propagate equally along the platoon. In the case where the controlled system experiences overshoot, that overshoot will propagate down the platoon causing the error to grow with respect to the leader. Although all vehicles will converge to the path of the leader eventually, the system is bound by the lane it is moving within and should not move unnecessarily in the lateral direction since it might cause the cars to cross into the other lanes. Thus, for the decentralized platoon, it should hold that the controlled system should not have any overshoot at all. Next, inter-vehicle communication is considered where feed-forward from previous vehicles in the platoon is conveyed down the platoon.

1.2.4.2 Communication from preceding vehicle

The lateral deviation of the preceding vehicle is transmitted to the vehicle immediately following it, as illustrated in the Fig. 26. The control signals for vehicles i and $i-1$ are defined as:

$$\begin{aligned} u_i &= -C\varepsilon_i + F\varepsilon_{i-1} \\ u_{i-1} &= -C\varepsilon_{i-1} + F\varepsilon_{i-2} \end{aligned} \tag{18}$$

where F is the feed-forward filter and is assumed to be the same for all followers. Substituting the signal in (61) the relation between the errors can be written as

$$\varepsilon_i = -G_{\Delta y}C\varepsilon_i + G_{\Delta y}F\varepsilon_{i-1} + G_{rb}C\varepsilon_{i-2} \tag{19}$$

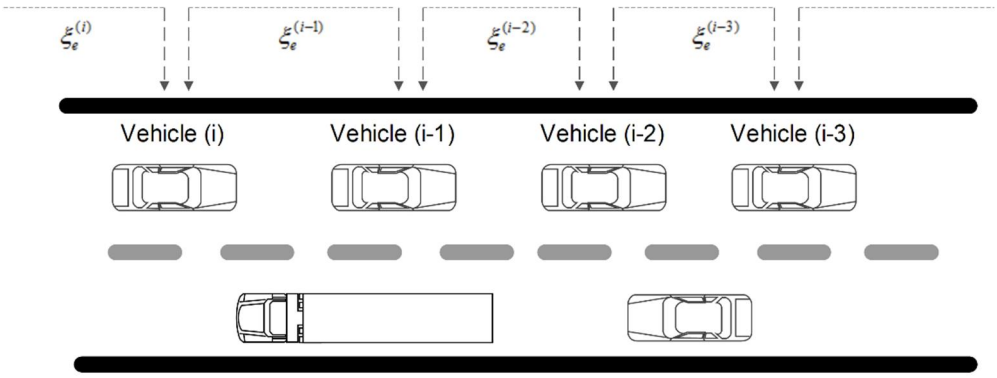

Fig. 11 Communication from preceding vehicle only

Grouping the similar error terms yields

$$(1+G_{\Delta y}C)\varepsilon_i = \left(G_{\Delta y}F + G_{rb}C\right)\varepsilon_{i-1} - G_{rb}F\varepsilon_{i-2} \tag{20}$$

1.3 Problem definition

In the operation of mobile rack vehicle, one of the major challenges is string stability, or rather string stability. In a platoon, the ego MRV aim is to maintain a constant inter-vehicular distance to the preceding MRV by using distance measurement sensor such as radar sensor. These sensors are used by adaptive cruise control and/or collision avoidance systems. Most existing headway sensors use 76.5 GHz radar, but other frequencies (e.g 24Ghz, 35Ghz and 79 GHz) are also in use. Some systems use infrared sensors instead of the radar sensor. There are two primary methods of measuring distance using radar. The first is known as the direct propagation method and measures the delay associated with reception of the reflected signal which can be correlated to the distance of the reflecting object as a function of the speed of light and the period or rather, the time delay in the transmission and receiving of the waves. The second method is known as the

indirect propagation method or the Frequency Modulated Wave (FMCW) method. For indirect propagation, a modulated frequency is sent and received, the difference in the frequency can be used to directly determine the distance as well as the relative speed of the object. Radar signals are very good at detecting objects that strongly reflect electromagnetic radiation (e.g metal objects). Because of the operation at wavelengths on the order of a few millimeters, automotive radar systems are pretty good at detecting objects that are several centimeters or larger. They are also good at looking through (i.e ignoring objects that are small relative to a wavelength). Therefore, any sudden changes in acceleration or deceleration of the leading or preceding MRV will generate a transient resulting in an inter-vehicular spacing error which will increase along the string. This behavior is known as string instability. One example of string instability is when the preceding MRV acceleration or deceleration, then the following MRVs have to speed up or slow down. In addition, the mass of each MRV is very heavy, so the inertia of movement is very high. Then the spacing errors between each MRV is increased and the collision of each other in the platoon is easily occurred, this is very undesirable.

1.4 Purpose and aim

This dissertation aims to develop the mobile-rack system operated in refrigerated logistical areas without rail rack. Therefore, the road condition is a critical issue for maintaining the safe motions. Due to the dense fog under adverse weather conditions, the measurement sensors used for detecting, locating, and tracking are affected by unavoidable noises. In addition, the cargo in the warehouse are varied, so the MRV mass shall be changed frequently depending on loading conditions. In turn, many system variables will also be changed. The robust controller can eliminate the measurement noises from sensors and the exogenous disturbances from the road or acceleration. Moreover, the complete control system is also stable under the parameter variations as well as model uncertainties of the mob. Assume that the lead mobile-rack is equipped with sensors, which can

provide the relative distance and speed of the mobile-rack in front. In addition, the delay time is very small and this is an autonomous system without communication between each mobile-rack. With these assumptions, the longitudinal control synthesis for the mobile-rack system is presented in this research.

The sequel of this dissertation is organized as follows:

Chapter 2: Robust control synthesis.

Chapter 3: Dynamical model of mobile rack vehicle.

Chapter 4: Mobile rack vehicle controller design.

Chapter 5: Numerical simulation results and discussion.

Chapter 6: Conclusion

1.5 Contribution

Based on the problem definition in section 1.3, the main problem of MRV platoon is to control the longitudinal and lateral movement that it has to satisfy the condition of vehicle platoon. Therefore, this paper aim to make the evaluation of the proposed controller which based on robust control synthesis to solve the string stability problem and the lateral position of mobile rack vehicles in a platoon. Demonstrated the ability of the mobile rack vehicles controller can cope with the system uncertainty and can attenuate the noise, disturbance from sensors and the road or harsh environment…

Chapter 2. Robust control synthesis

2.1 Introduction

Throughout the 1960s and 1970s, the optimal linear quadratic (LQ) control was popular, largely applied in controlling with the work of Kalman. In the late 1970s, the control practice showed some limitations of LQ control. Doyle (1978) showed that there is no assurance for the stability of LQG, which is an LQR control combined with a Kalman filter.

The control theory literature started to look for a more robust approach. Zames (1981) developed H_∞ control which is more robust than LQ control. Since in LQ control, the performance is measured with a 2-norm across frequencies, while H_∞ control uses a ∞-norm that cares the peak of the losses across frequencies. It can be interpreted as the maximum magnitude of the disturbances affects the outputs.

The uncertainty sets in the H_∞ approach are unstructured. They illustrate perturbations of the model. This perturbation is bounded but has no particular form. Recently, the structured perturbations have been studied such as parametric uncertainty, diagonal uncertainty or uncertainty in some particular channel. The robust control theory with structured uncertainty uses the structured singular value (μ-synthesis) rather than the ∞-norm as a measure of performance. μ-synthesis has been getting some important stability and performance achievements. However, the design procedure is a more daunting task and the theory is not as fully developed as the unstructured case.

2.2 Uncertainty modeling

Uncertainties are unavoidable in every real system. Uncertainties can be classified into two types: disturbance and dynamics perturbations. The former includes exogenous disturbance and sensor noises. The latter comes from the gap

between mathematical model and the actual dynamics of the system. It is known that mathematical model is just an approximation with some assumptions to simplify the real system. Furthermore, in the modeling, some nonlinearities is ignored and there are no varying parameters as in real systems. The dynamics perturbations may adversely affect the stability and performance of a control system. Therefore, this kind of uncertainty is described in this section so that they are well considered under robust control analysis.

2.2.1 Unstructured uncertainties

Dynamics perturbations such as unmodelled dynamics can occur at different parts in a system. However, they can be lumped into a single uncertainty block Δ. Since there is no information about the uncertainty except it bound, it is also referred as unstructured uncertainty.

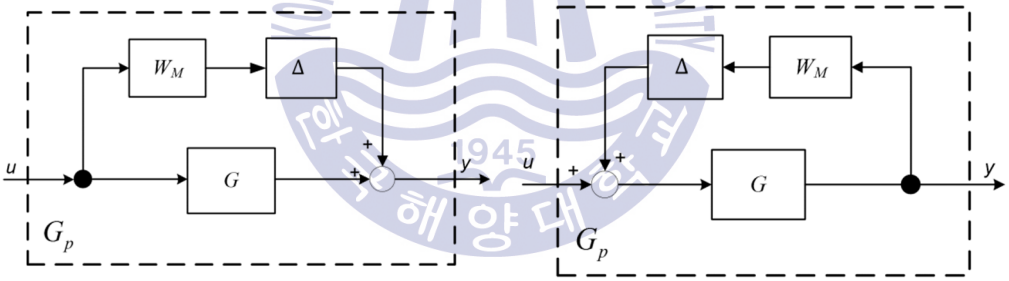

a) *Additive uncertainty*

$$G_p(s) = G(s) + \Delta(s)W_M(s)$$

b) *Inverse additive uncertainty*

$$G_p(s) = G(s)(I - \Delta(s)W_M(s)G(s))^{-1}$$

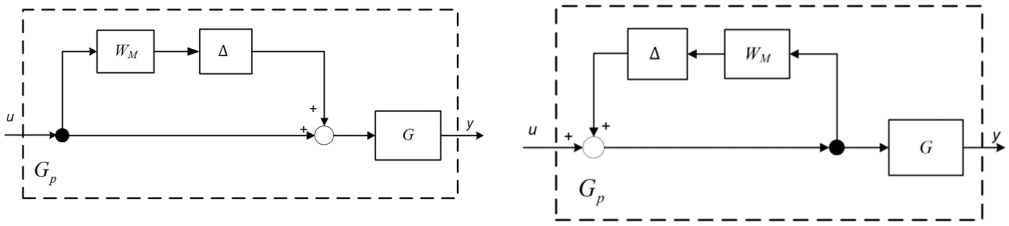

c) *Input multiplicative uncertainty*

$$G_p(s) = G(s)(I + \Delta(s)W_M(s))$$

d) *Inverse input multiplicative unc.*

$$G_p(s) = G(s)(I - \Delta(s)W_M(s))^{-1}$$

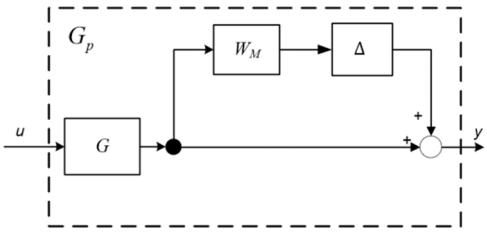

e) *Output multiplicative uncertainty*

$$G_p(s) = (I + \Delta(s)W_M(s))G(s)$$

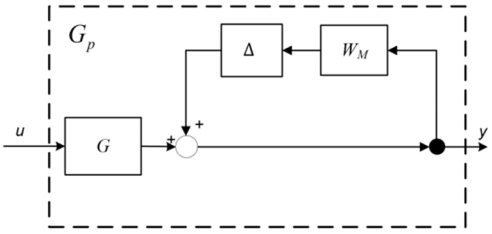

f) *Inverse output multiplicative unc.*

$$G_p(s) = (I - \Delta(s)W_M(s))^{-1}G(s)$$

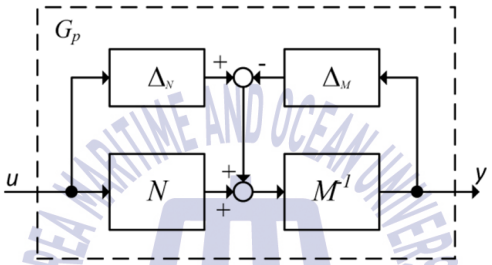

g) *Left coprime factor uncertainty*

$$G_p(s) = (M(s) + \Delta_M(s))^{-1}(N(s) + \Delta_N(s))$$

Fig. 12 Some common kinds of unstructured uncertainty

This uncertainty can be described by different frameworks, as following, where $G_p(s)$ denotes perturbed uncertain system and $G_o(s)$ refers to the nominal system.

2.2.2 Parametric uncertainties

The unstructured uncertainty describes unmodelled dynamics and neglected nonlinearities occurring mostly in high-frequency ranges. However, in a real system, the dynamics perturbations also come from variations of certain parameters. They occur in low-frequency ranges and is called “parametric uncertainties”. Parametric uncertainty is sometimes called “structured uncertainty” since it models

the uncertainty is a structured manner. It is often expressed along with transfer function or state-space representation. For example, the parametric uncertainties of three components in a mass-spring-damper system can be represented in the following structure, using state-space representation:

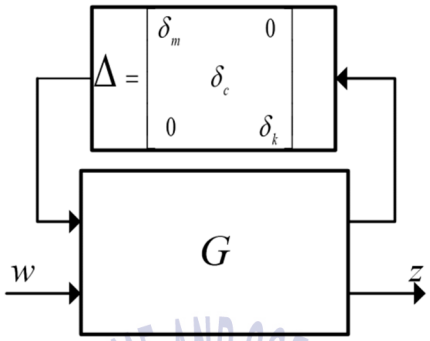

Fig. 13 Parametric uncertainty

2.2.3 Structured uncertainties

In some robust design problem, the uncertainties would include structured uncertainties, such as unmodeled dynamics as well as parametric uncertainty. The whole system then can be rearranged in a standard configuration of linear fractional transformation $F(M, \Delta)$. The uncertainty block now has the structure:

$$\Delta = diag[\delta_1 I_{r_1}, ..., \delta_s I_{r_s}, \Delta_1, ..., \Delta_f], \quad \delta_i \in C, \Delta_j \in C^{m_j x m_j} \tag{21}$$

where $\sum_{i=1}^{s} r_i + \sum_{f=1}^{f} m_j = n$, and n is the dimension of the uncertainty block Δ.

The total uncertainty block Δ now has two kinds of uncertainty: s is the repeated scalar blocks and f full blocks.

2.2.4 Linear fractional transformation

Linear fractional transformation (LFT) is a standard configuration to account the uncertainties into a system. There are two categories, say upper and lower LFT.

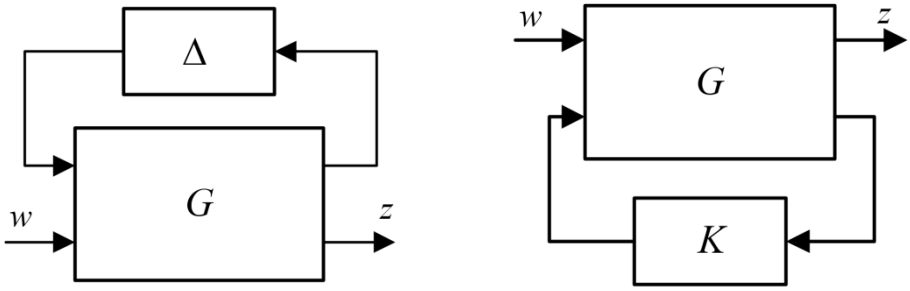

Fig. 14 Upper linear fractional transformation (left) and lower LFT (right)

Providing that the system G is partitioned as $G = \begin{bmatrix} G_{11} & G_{12} \\ G_{21} & G_{22} \end{bmatrix}$ the input and output relation in upper LFT is derived as:

$$z = \left[G_{22} + G_{21}\Delta(I - G_{11}\Delta)^{-1} G_{12} \right] w = F_u(G, \Delta) w \tag{22}$$

The lower LFT is calculated using:

$$F_l(G, K) = \left[G_{11} + G_{12} K (I - G_{22} K)^{-1} G_{21} \right] \tag{23}$$

2.2.5 Coprime factor uncertainty

2.2.5.1 Coprime factor uncertainty and robust stability

The robust stabilization problem for linear plants with a normalized left coprime factor uncertainty characterization was solved in (Glover and McFarlane, 1992), based on a solution to the H_∞ control problem for generalized plants.

Coprime factors are a powerful tool for characterizing plant uncertainty since they capture both stable and unstable pole and zero uncertainty. It forms the basis for the H_∞ loop shaping controller design method, in which a stabilizing controller is synthesized for a plant shaped using input/output weights chosen to achieve performance objectives.

Let a left Coprime factorization of P be given by $\{\tilde{M}_0 = R\tilde{M}, \tilde{N}_0 = R\tilde{N}\}$, where $\{\tilde{M}, \tilde{N}\}$ is normalized and $R \in \wp H_\infty$ is denormalization factor. The perturbed plant is given by

$$P_\Delta = \tilde{M}_{\Delta,0}^{-1}\tilde{N}_{\Delta,0} = (\tilde{M}_0 - \Delta_{\tilde{M}})^{-1}(\tilde{N}_0 + \Delta_{\tilde{N}}) \tag{24}$$

For the purpose of starting robust stability and robust performance theorems for left Coprime factor uncertainty, recall the following definitions from (Lanzon and Papageorgiou, 2009)

- Definition 1: (Lanzon and Papageorgiou, 2009) Given two plants $P, P_\Delta \in R^{p\times q}$ with normalized graph symbols $\tilde{G}$ and G_Δ and a denormalization factor $R \in \wp H_\infty$ define the distance measure for left Coprime factor uncertainty structure as implied by R as

$$d_{lcf}^R(P, P_\Delta) = \left\| R\tilde{G}G_\Delta \right\|_\infty \tag{25}$$

- Definition 2: (Lanzon and Papageorgiou, 2009) Given a positive feedback interconnection [P,C] of a plant $P \in R^{p\times q}$ with left Coprime factorization $\{\tilde{M}_0, \tilde{N}_0\} = \{R\tilde{M}, R\tilde{N}\}$, where $R \in \wp H_\infty$ is a denormalization factor, and a controller $C \in R^{q\times p}$, define the robust stability margin in the left Coprime factor uncertainty structure as:

$$b_{lcf}^{R}(P,\mathrm{C}) := \begin{cases} \left\| \begin{bmatrix} I \\ C \end{bmatrix} (I - PC)^{-1} \tilde{M}_0^{-1} \right\|_{\infty}^{-1} & if\,[P,C]\,\text{is internally stable;} \\ 0 & otherwise \end{cases} \tag{26}$$

It is easy to show that when [P,C] is internally stable, $b_{lcf}^{R}(P,C) = \left\| (R\tilde{G}K)^{-1} \right\|_{\infty}^{-1}$, where $\tilde{G}$ is a normalized left graph symbol of P and K is a normalized inverse right graph symbol of C. The superscript R denotes the dependence on the denormalization factor R of the coprime factorization $\left\{ \tilde{N}_0 = R\tilde{N}, \tilde{M}_0 = R\tilde{M} \right\}$. The significant difference between Coprime factor uncertainty and four –block uncertainty lies in the additional degree of freedom offered by the denormalization factor R. note that when R is unitary, the two uncertainty structures are identical. In that case, $b_{lcf}^{R}(P,C) = b(P,C)$ as defined in (McFarlane and Glover) and $d_{lcf}^{R}(P,P_{\Delta}) = b(P,C)$ as defined in (Vinnicombe, 1993).

The ratio $\dfrac{d_{lcf}^{R}(P,P_{\Delta})}{b_{lcf}^{R}(P,C)}$ is crucial for quantifying robust stability and robust performance, as will be shown in the following. Its infimum over $R \in \wp H_{\infty}$ is given by $\left\| (\tilde{G}K)^{-1} \tilde{G} G_{\Delta} \right\|_{\infty}$ when $[P,C]$ is internally stable. The robustness ratio is precisely this infimum and is given below.

- Definition 3: Given plants $P, P_{\Delta} \in R^{p \times q}$ and a controller $C \in R^{q \times p}$, define the robustness ratio:

$$r(P,P_{\Delta},\mathrm{C}) := \begin{cases} \left\| (\tilde{G}K)^{-1} \tilde{G} G_{\Delta} \right\|_{\infty} & if\,[P,C]\,\text{is internally stable;} \\ \infty & otherwise \end{cases} \tag{27}$$

Using the definition of the robustness ratio $r(P,P_\Delta,\mathrm{C})$, the following corollary to describes the set of plants guaranteed to be robustly stable given a nominal closed-loop system.

- Corollary 1: Given a plant $P \in R^{p\times q}$, a controller $C \in R^{q\times p}$, the following set of feedback systems is internally stable, where $P_\Delta \in R^{p\times q}$:

$$P_{cf} := \left\{ \begin{matrix} P_\Delta \in R^{p\times q} : r\left(P,P_\Delta,C\right) < 1, \bar{\sigma}\left(\tilde{G}G_\Delta\right)(\infty) < 1 \\ wno\det\left(G_\Delta^* G\right) = 0 \end{matrix} \right\} \tag{28}$$

Furthermore, where

$$P_v := \left\{ \begin{matrix} P_\Delta \in R^{p\times q} : b\left(P,C\right) < \delta_v(P,P_\Delta), \bar{\sigma}(\tilde{G}G_\Delta)(\infty) < 1 \\ wno\det\left(G_\Delta^* G\right) = 0 \end{matrix} \right\} \tag{29}$$

2.2.5.2 Coprime factor uncertainty and Coprime factor performance

In typical control problems, robust performance is at least as important as robust stability. This section describes bounds on the robust performance degradation under perturbation (in a fractional form). A corollary to (Lanzon and Papageorgiou, 2009) shows that the performance of the perturbed system is bounded by the robustness ratio $r\left(P,P_\Delta,C\right)$. The generalized plant H for a fractional interconnection with left Coprime factor uncertainty is given by

$$H := \left[\begin{array}{c|c} \tilde{M}_0^{-1} & P \\ 0 & I \\ \hline \tilde{M}_0^{-1} & P \end{array} \right] \tag{30}$$

and H_Δ is obtained by replacing $\tilde{M}_0$ by $\tilde{M}_{\Delta,0}$ and P by P_Δ .

- Corollary 2: Given the suppositions of corollary 1 and give $P_\Delta \in P_{cf}$ as defined in (2.2.5.2), then

$$1 - r(P, P_\Delta, C) \le b_{lcf}^{R}(P_\Delta, C)\Big|_{R=(\tilde{G}K)^{-1}} \le 1 + r(P, P_\Delta, C) \tag{31}$$

$$\left.\frac{\left\|\rho_l(H_\Delta, C) - \rho_l(H, C)\right\|_\infty}{\left\|\rho_l(H, C)\right\|_\infty}\right|_{R=(\tilde{G}K)^{-1}} = \left\|\left(\tilde{G}_\Delta K\right)^{-1}\tilde{G}K - I\right\|_\infty \le \frac{r\left(P, P_\Delta, C\right)}{1 - r\left(P, P_\Delta, C\right)} \tag{32}$$

2.3 Stability criterion

2.3.1 Small gain theorem

Consider a feedback configuration as in Fig. 15. Providing that G_1 and G_2 are the transfer function of LTI system.

Theorem 2.3.1: If G_1 and G_2 are stable, i.e $G_1, G_2 \in H_\infty$, then the closed-loop system is internally stable if and only if $\left\|G_1 G_2\right\|_\infty < 1$ and $\left\|G_2 G_1\right\|_\infty < 1$.

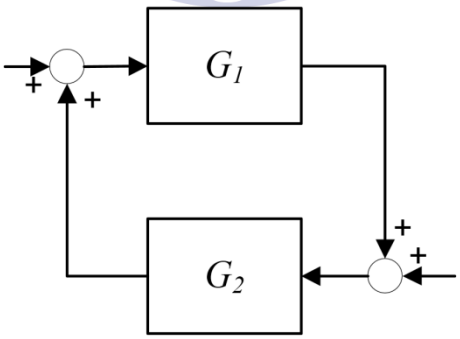

Fig. 15 A feedback configuration

Note that the small theorem consider the norm of the closed-loop system, therefore it is independent on the sign of feedback.

The theorem actually came from Nyquist stability condition as stated in the following. Consider an uncertain feedback system as in Fig. 16 where there is input multiplicative uncertainty magnitude of $\|W_M(j\omega)\|_\infty$.

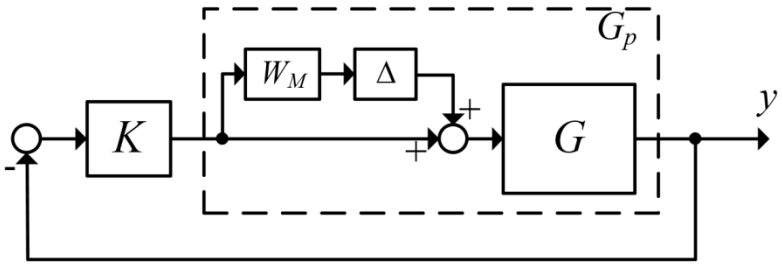

Fig. 16 Uncertain feedback system

The uncertainty loop transfer function becomes:

$$L_p = G_p K = GK(1+W_M\Delta) = L + W_M L\Delta, |\Delta(j\omega)| \le 1, \forall\omega \tag{33}$$

According to Nyquist stability condition, the closed-system is robust stable if L_p does not encircle the point -1 in the Nyquist diagram,

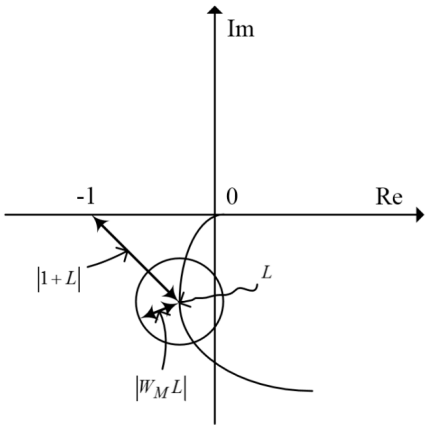

Fig. 17 Nyquist plot of closed-loop system for robust stability

From the Fig. 17, one can see that $|1+L|$ is the distance from the point -1 to the center of the disc representing L_p, and that $|W_M L|$ is the radius of the disc. Encirclements are avoided if none of the discs cover -1, it is also expressed as:

$$\begin{aligned} &\text{RS} <=> |W_M L| < |1+L|, \forall \omega \\ &<=> \left|\frac{W_M L}{1+L}\right| < 1, \forall \omega <=> |W_M T| < 1, \forall \omega \\ &<=> \|W_M T\|_\infty < 1 \end{aligned} \tag{34}$$

2.3.2 Structured singular value (μ) synthesis brief definition

If there exists a M - Δ structure as in Fig. 18

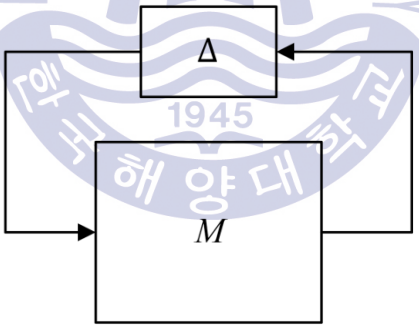

Fig. 18 M - Δ structure

For $M \in C^{n_x n}$, the structured singular value w.r.t M, μ_Δ is defined as in (Doyle, 1982):

$$\mu_{\Delta}(M)=\frac{1}{\min\{\bar{\sigma}(\Delta)\,|\,\Delta\in\Delta,\det(I-M\Delta)=0\}}$$
$$\Rightarrow \min\{\bar{\sigma}(\Delta)\,|\,\Delta\in\Delta,\det(I-M\Delta)=0\}=\frac{1}{\mu_{\Delta}(M)} \tag{35}$$

where $\bar{\sigma}(\Delta)$ is the maximum value of the uncertainty matrix Δ.

Suppose the peak (across frequency ω) of the $\mu_{\Delta}(M)$ is β. This means that for all perturbation matrices Δ with the appropriate structure, and satisfy $\max_{\omega}\bar{\sigma}[\Delta(j\omega)]<1/\beta$, the perturbed system is stable. Normally, $\beta<1$ is the requirement for a maximum perturbation size 1.

2.4 Robustness analysis and controller design

2.4.1 Forming generalized plant and N-$\hat{\Delta}$ structure

Consider a typical control system as in Fig. 19 with the nominal system *G*, the multiplicative input uncertainty expressed by W_M and Δ, the controller *K*. Inputs to the system include *r*, *d*, *n*, which are reference, disturbance at system output, and noise, respectively. These three inputs are weighted by their respective weighting function, W_r, W_d, W_n.

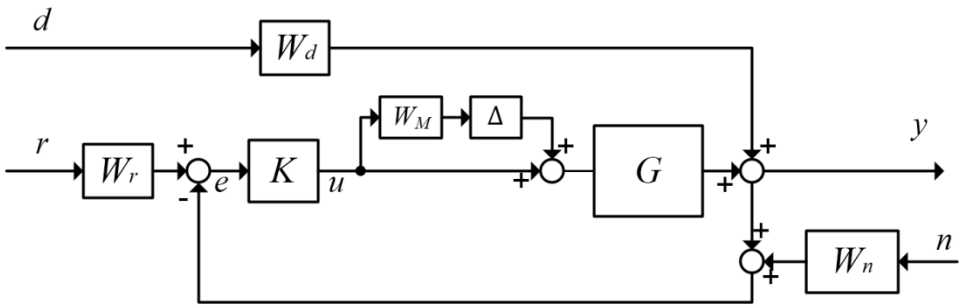

Fig. 19 A typical control system

They may be constant or dynamic which respectively describe the frequency content of the set points, disturbances, and noise signals. u is the control signal, e is the error and y is the measured output. In the procedure to create the M-Δ-like structure as in Fig. 18, the block diagram in Fig. 19 is reconstructed as in Fig. 20. In this new formulation, a weighting function W_P is added at the output to represent the performance requirement level. Δ_P is the fictitious perturbation used in case of robust performance analysis. The uncertainty block Δ is isolated and forms generalized plant P blocked in the dashed rectangular. Z is the regulated output.

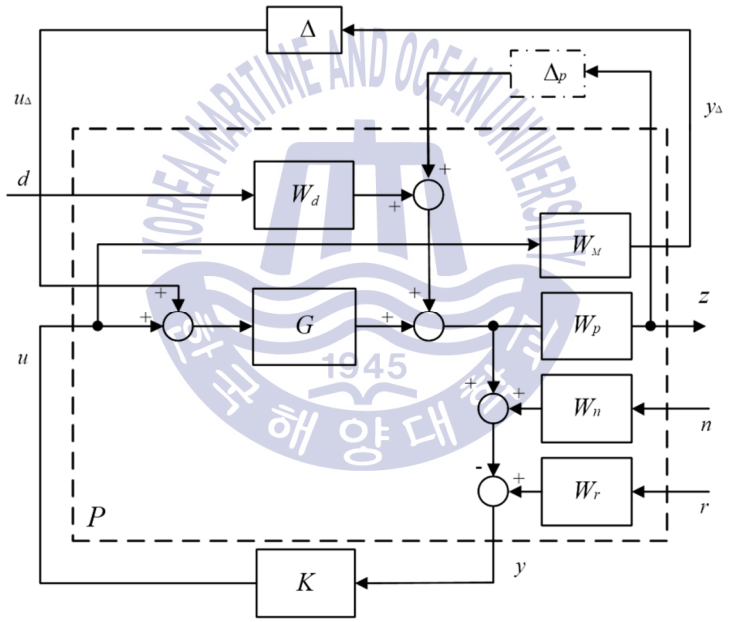

Fig. 20 Block diagram of generalized plant P

From the block diagram in Fig. 20, a generalized P block can be formed by grouping the blocks in the dashed rectangular. It shows that the generalized plant P is further written as

$$\begin{bmatrix} y_\Delta \\ z \\ \hline y \end{bmatrix} = \underbrace{\left[\begin{array}{cccc|c} 0 & 0 & 0 & 0 & W_M \\ W_p G_{de} & W_p W_d & 0 & 0 & W_p G_{de} \\ \hline -G_{de} & -W_d & -W_n & W_r & -G_{de} \end{array}\right]}_{P} \begin{bmatrix} u_\Delta \\ d \\ n \\ r \\ \hline u \end{bmatrix} \tag{36}$$

with $u_\Delta = \Delta y_\Delta$ and $u = Ky$

The current block diagram is then redrawn in a compact form as in Fig. 21

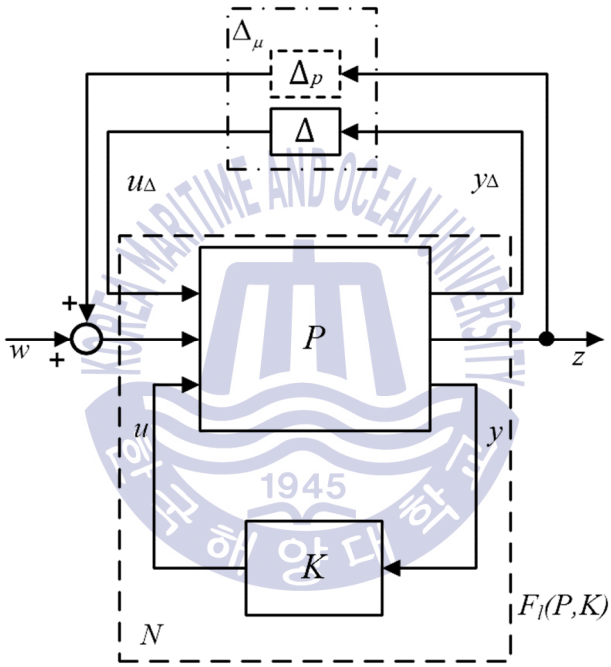

Fig. 21 *P-K* grouping and N - $\hat{\Delta}$ structure

In Fig. 21, the closed-loop transfer matrix N that connects the generalized plant P with the controller K via a lower linear fractional transformation (LFT), is defined by

$$\begin{bmatrix} y_\Delta \\ z \end{bmatrix} = \underbrace{F_L(P,K)}_{N} \begin{bmatrix} u_\Delta \\ w \end{bmatrix} \tag{37}$$

where $w = \begin{bmatrix} d & n & r \end{bmatrix}^T$

$$
\begin{aligned}
N &= F_l(P,K) = P_{11} + P_{12}K(I - P_{22}K)^{-1}P_{21} \\
&= \left[\begin{array}{c|ccc} -W_M T_i & -W_M KS_o Wd & -W_M KS_o W_n & W_M KS_o W_r \\ \hline W_P S_o G_{de} & W_P S_o W_d & -W_P T_o W_n & W_P T_o W_r \end{array}\right] \\
&= \left[\begin{array}{c|ccc} N_{11} & N_{12} & N_{13} & N_{14} \\ \hline N_{21} & N_{22} & N_{23} & N_{24} \end{array}\right] = \left[\begin{array}{c|c} N_{y_\Delta u_\Delta} & N_{y_\Delta w} \\ \hline N_{zu_\Delta} & N_{zw} \end{array}\right]
\end{aligned}
\tag{38}
$$

with $T_i = KG_{de}(I + KG_{de})^{-1}$, $T_o = G_{de}K(I + G_{de}K)^{-1}$ and $S_o = (I + G_{de}K)^{-1}$. $N_{y_\Delta u_\Delta}$ is the transfer matrix from u_Δ to y_Δ, $N_{y_\Delta w}$ the transfer matrix from w to y_Δ, N_{zu_Δ} the transfer matrix from u_Δ to z and N_{zw} the transfer matrix from w to z.

In this final form, the N - $\hat{\Delta}$ structure is similar to M- Δ one, so that the robust control synthesis based on small gain theorem and structured singular value can be applied. Note that $\hat{\Delta}$ block includes the unmodelled block Δ and the fictitious block Δ_p.

2.4.2 Robustness analysis

The objectives of the H_∞ robust controller for any control system include:

- Nominal stability (NS): The system is internally stable with the nominal model (no model uncertainty). A system is internally stable if all the transfer functions of the closed-loop system are stable, i.e. there is no pole staying in the right half plane of the complex plane.
- Nominal Performance (NP): The system satisfies the performance specifications with the nominal model (no model uncertainty). The nominal system performance depends on the sensitivity (S_o), which is a very good indicator of the disturbance attenuation ability. To attenuate the disturbance effects, the

singular value of S_o in the element N_{22} in Eq. (18) must be small. Therefore, to limit the value of S_o, the performance weighting function W_P is selected and the controller is designed so that

$$\|W_P S_o W_d\|_\infty < 1 \Leftrightarrow \mu_\Delta(N_{22}(j\omega)) < 1, \ ^\forall\omega \tag{39}$$

where $\mu_\Delta(N_{22}(j\omega))$ is the structured singular value of the nominal system that respects to the uncertainty Δ.

Nominal performance includes disturbances and noise attenuation. To reduce noise, the singular value of complementary sensitivity (T_o) in the element N_{23} in Eq. (18) must be small. Note that $T_o+S_o=1$. This implies that the disturbances and noise reduction cannot be achieved in the same frequency range. Depending on the characteristics of disturbances and noises, disturbances attenuation should be achieved in low-frequency range and noise reduction should be achieved in the high-frequency range.

- Robust stability (RS): The system is stable for all perturbed plants about the nominal model, up to the worst-case model uncertainty (including the real plant). The robust stability criterion is written as

$$\|W_M T_i\|_\infty < 1 \ \Leftrightarrow \ \mu_\Delta(N_{11}(j\omega)) < 1, \ ^\forall\omega \tag{40}$$

where $\mu_\Delta(N_{11}(j\omega))$ is the structured singular value of the system that respects to parametric uncertainty Δ.

- Robust performance (RP): The system satisfies the performance specifications for all perturbed plants about the nominal model, up to the worst-case model uncertainty (including the real plant). The robust performance property is guaranteed if

$$\|F_u(N,\Delta)\|_\infty = \left\|N_{zw} + N_{zu_\Delta}\Delta(I - N_{y_\Delta u_\Delta}\Delta)^{-1}N_{y_\Delta w}\right\|_\infty < 1, \quad \forall\Delta, \|\Delta\|_\infty < 1,$$
and robust stability
$$\Leftrightarrow \mu_{\hat{\Delta}}(N) < 1, \ ^{\forall}\omega, \ \hat{\Delta} = \begin{bmatrix} \Delta & 0 \\ 0 & \Delta_P \end{bmatrix} \tag{41}$$

where uncertain perturbation $\hat{\Delta}$ includes Δ and fictitious perturbation Δ_P that represents the H_∞ performance specification in the framework of μ approach. $\mu_{\hat{\Delta}}(N)$ is the structured singular value of the system that respects to $\hat{\Delta}$.

After having all the initial weighting functions, the DK-iteration of μ-synthesis toolbox in Ma

The key design issue is to choose reasonable weighting functions W_M and W_P satisfying all the above requirements. The controller design procedure is a loop including tries and tuning. The steps to design the controller are summarized as follows:

Step 1. Model the uncertainty

Step 2. Weight the input signals by reasonable dynamics weighting functions or constants

Step 3. Choose the uncertainty weighting function W_M and performance weighting function W_P

Step 4. Create a generalized plant and forming M- Δ structure

Step 5. Design a robust controller using Matlab toolboxes, check the performance, if not satisfied, go back to step 3.

2.5 Robust controller using loop shaping design

This method, which is highly attractive because of its simplicity, consists of solving two LQG-type Riccati equations. In its 4-blocks equivalent representation, it is a particular case of the standard H_∞ approach to robust control. Noting that we can model the direct and complementary sensitivity functions by modeling the open loop response, and seeing that any loop transfer is proportional to those

sensitivity functions, therefore it is possible to model any loop transfer by working on a single transfer – the open-loop response. This is the principle upon which loop-shaping synthesis is founded. Drawing inspiration from frequency-shaped LQG synthesis, we shape the singular values of the open-loop response using weighting functions on the input and output of the system, thereby creating a loop-shape for which a stabilizing controller can be calculated. This is the definition of H_∞ loop-shaping synthesis.

Let us now consider a nominal transfer matrix system $H(s)$ with m inputs and p outputs, subject to modeling uncertainties which can transform that matrix into $\tilde{H}(s)$. If $H(s)$ is factorized in one of the above two forms, we can consider a family of plants by introducing a norm-bounded uncertainty on both of the factors: right factorization and left factorization.

- Right factorization

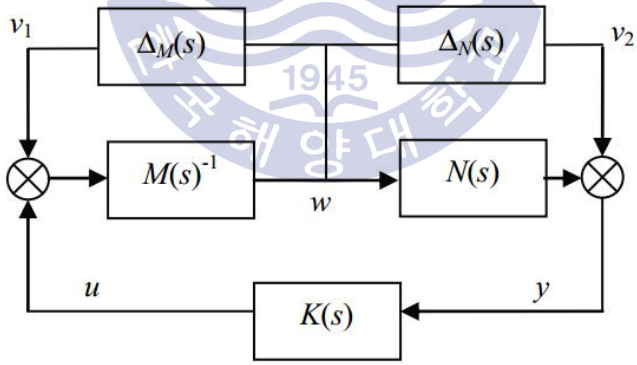

Fig. 22 Right factorization and uncertainties on the coprime factors

$$\psi = \left\{ \begin{array}{l} \tilde{H}(s) = \left(N(s) + \Delta_N(s)(M(s) + \Delta_M(s)\right)^{-1}; \\ \Delta_N, \Delta_M \in RH_\infty; \left\| \begin{bmatrix} \Delta_N \\ \Delta_M \end{bmatrix} \right\|_\infty \le \varepsilon \end{array} \right\} \tag{42}$$

The uncertainty on the transfer $M^{-1}(s)$ is represented in inverse additive form (which is equivalent to representing the uncertainty on the $M(s)$ in direct additive form). The uncertainty on the transfer $N(s)$ is represented in direct additive form.

- Left factorization

$$\bar{\psi} = \left\{ \begin{array}{l} \tilde{H}(s) = \left(\bar{M}(s) + \Delta_{\bar{M}}(s)\right)^{-1} \left(\bar{N}(s) + \Delta_{\bar{N}}(s)\right); \\ \Delta_{\bar{N}}, \Delta_{\bar{M}} \in RH_\infty; \left\| \left[\Delta_{\bar{M}} \quad \Delta_{\bar{N}} \right] \right\|_\infty \le \bar{\varepsilon} \end{array} \right\} \tag{43}$$

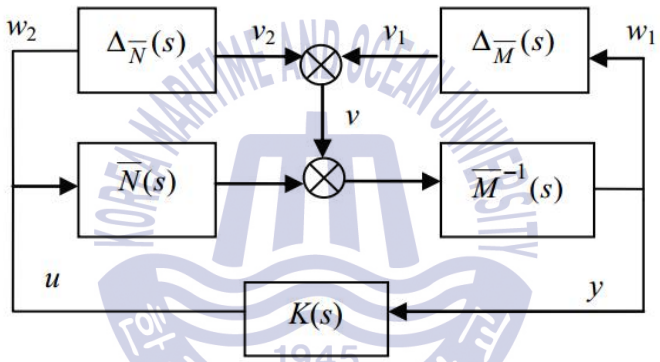

Fig. 23 Left factorization and uncertainties on the coprime factors

The uncertainty on the transfer $\bar{M}^{-1}(s)$ is represented in inverse additive form. The uncertainty on the transfer $\bar{N}(s)$ is represented in direct additive form.

2.5.1 Stability robustness for a coprime factor plant description

- Right coprime factorization

The application of the small gain theorem require us to put the loop in the standard form for robustness analysis with:

$$v = \begin{pmatrix} v_1 \\ v_2 \end{pmatrix} = \begin{pmatrix} \Delta_M \\ \Delta_N \end{pmatrix} w = \Delta(s) w \tag{44}$$

In that case:

$$v = \begin{pmatrix} v_1 \\ v_2 \end{pmatrix} = \begin{pmatrix} \Delta_M \\ \Delta_N \end{pmatrix} w = \Delta(s) w \tag{45}$$

That is:

$$M(s)w = v_1 + K(s)v_2 + K(s)N(s)w \tag{46}$$

This means that:

$$\left(I_m - K(s)H(s)\right) M(s)w = v_1 + K(s)v_2 \tag{47}$$

Finally, we can deduce that:

$$\begin{aligned} w &= M(s)^{-1}(I_m - K(s)H(s))^{-1}(v_1 + K(s)v_2) \\ &= M(s)^{-1}(I_m - K(s)H(\mathrm{s}))^{-1} \begin{pmatrix} I_m \\ K(s) \end{pmatrix} v \end{aligned} \tag{48}$$

According to the small gain theorem, the system is stable for all plant uncertainties $\Delta_M(s), \Delta_N(s) \in RH_\infty$, on the right normalized coprime factors such that $\left\| \begin{matrix} \Delta_N \\ \Delta_M \end{matrix} \right\| \le \varepsilon$, iff:

$$\begin{aligned} &\left\| M(s)^{-1}(I_m - K(s)H(s)^{-1} \begin{pmatrix} I_m \\ K(s) \end{pmatrix} \right\|_\infty \\ &= \left\| M(s)^{-1} \begin{pmatrix} S_u(s) & S_u(s)K(s) \end{pmatrix} \right\|_\infty < \varepsilon^{-1} \end{aligned} \tag{49}$$

where $S_u(s) = \left(I_m - K(s)H(s)\right)^{-1}$

- Left coprime factorization

Let apply a similar process of reasoning to the loop, we set:

$$v = v_1 + v_2 = \Delta_{\bar{M}}(s)w_1 + \Delta_{\bar{N}}(s)w_2 = \begin{pmatrix}\Delta_{\bar{M}}(s) & \Delta_{\bar{N}}(s)\end{pmatrix}\begin{pmatrix}w_1 \\ w_2\end{pmatrix} = \Delta(s)w \tag{50}$$

and: $w_1 = y$ and $w_2 = u$

In addition:

$$w_1 = y = \bar{M}^{-1}(s)\left(v_1 + v_2 + \bar{N}(s)K(s)y\right) = \bar{M}^{-1}(s)v + H(s)K(s)w_1 \tag{51}$$

Thus:

$$w_1 = \left(I_p - H(s)K(s)\right)^{-1}\bar{M}^{-1}(s)v \tag{52}$$

and:

$$w_2 = u = K(s)w_1 = K(s)\left(I_p - H(s)K(s)\right)^{-1}\bar{M}^{-1}(s)v \tag{53}$$

Finally:

$$\begin{pmatrix}w_1 \\ w_2\end{pmatrix} = \begin{pmatrix}\left(I_p - H(s)K(s)\right)^{-1}\bar{M}^{-1}(s) \\ K(s)\left(I_p - H(s)K(s)\right)^{-1}\bar{M}^{-1}(s)\end{pmatrix} \tag{54}$$

Or indeed:

$$w = \begin{pmatrix} I_p \\ K(s) \end{pmatrix} \left(I_p - H(s)K(s) \right)^{-1} \bar{M}^{-1}(s) v \tag{55}$$

According to the small- gain theorem, the system is stable for all plant uncertainties $\Delta_{\bar{M}}(s), \Delta_{\bar{N}}(s) \in RH_\infty$ on the left normalized coprime factors such that $\left\| \begin{pmatrix} \Delta_{\bar{M}} & \Delta_{\bar{N}} \end{pmatrix} \right\|_\infty \le \bar{\varepsilon}$, iff:

$$\left\| \begin{pmatrix} I_p \\ K(s) \end{pmatrix} \left(I_p - H(s)K(s) \right)^{-1} \bar{M}^{-1}(s) \right\|_\infty = \left\| \begin{pmatrix} S_y(s) \\ K(s)S_y(s) \end{pmatrix} \bar{M}^{-1}(s) \right\|_\infty \le \bar{\varepsilon}^{-1} \tag{56}$$

where $S_y(s) = \left(I_p - H(s)K(s) \right)^{-1}$

2.6 Reduced controller

The achieved controller is efficient, however, its order is very high. This high-order controller is very complex to be implemented practically. A high-order controller will lead to high cost, difficult commissioning, poor reliability and a potential problem in maintenance. Therefore, it's necessary to simplify the controller into a lower-order controller that achieves the same level of performance, so that it is easier to be applied in RO system.

The basis of model reduction is addressed as following. Given a stable model *G(s)* of order *n*, with state space form is given as:

$$\begin{aligned} \dot{x}(t) &= Ax(t) + Bu(t) \\ y(t) &= Cx(t) + Du(t) \end{aligned} \tag{57}$$

where $x(t) \in \Re^n, A \in \Re^{n \times n}, B \in \Re^{n \times m}, C \in \Re^{k \times n}, u(t) : \Re \to \Re^m, y(t) : \Re \to \Re^k$

Assuming the system is stable, i.e matrix A is Hurwitz. Find a reduced order model $G_r(s)$ of degree k (McMillan degree) such that the infinity norm of the error $\|G(s)-G_r(s)\|_\infty$ is minimized, w.r.t the same input $u(t)$.

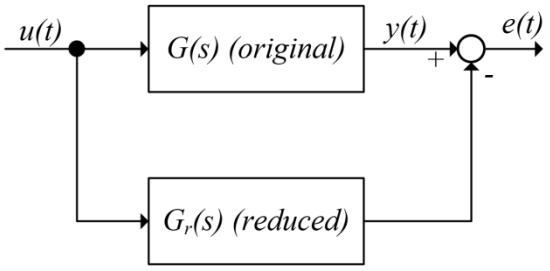

Fig. 24 The idea of order reduction

In general, there are three main methods to obtain a lower-order controller for a relatively high-order one: balanced truncation, balanced residualization, and optimal Hankel norm approximation. Each method gives a stable approximation and a guaranteed bound on the error in the approximation. In this dissertation, Hankel norm approximation is chosen to reduce controller's order. Therefore, the Hankel reduction algorithm will be stated carefully in this section.

2.6.1 Truncation

Let (A, B, C, D) be a minimal realization of a stable system $G(s)$, and partition the state vector x, of dimension n, into $\begin{bmatrix} x_1 \\ x_2 \end{bmatrix}$ where x_2 is the vector of n-k states that we want to remove. The state-space form becomes:

$$\begin{aligned} \dot{x}_1 &= A_{11}x_1 + A_{12}x_2 + B_1u \\ \dot{x}_2 &= A_{21}x_1 + A_{22}x_2 + B_2u \\ y &= C_1x_1 + C_2x_2 + Du \end{aligned} \tag{58}$$

A k^{th}-order truncation of the full system is given by $G_a = (A_{11}, B_1, C_1, D)$. The truncated model G_a is equal to G at infinite frequency. Matrix A is in Jordan form so it is easy to reorder the states so that x_2 corresponds to a high frequency or fast mode.

For simplicity, assume that A is diagonalized as:

$$A = \begin{bmatrix} \lambda_1 & 0 & \cdots & 0 \\ 0 & \lambda_2 & \cdots & 0 \\ \vdots & \vdots & \ddots & \vdots \\ 0 & 0 & \cdots & \lambda_n \end{bmatrix} \tag{59}$$

and

$$B = \begin{bmatrix} b_1^T \\ b_1^T \\ \vdots \\ b_n^T \end{bmatrix}, C = \begin{bmatrix} c_1 & c_2 & \cdots & c_n \end{bmatrix} \tag{60}$$

Then, if the eigenvalues are ordered so that $|\lambda_1|<|\lambda_2|...$, the fastest modes are removed from the model after truncation. The error between G and G_a is given as follow (Skogestad and Postlethwaite, 2005):

$$\left\| G - G_a \right\|_\infty \le \sum_{i=k+1}^{n} \frac{\bar{\sigma}(c_i b_i^T)}{\left| \mathrm{Re}(\lambda_i) \right|} \tag{61}$$

2.6.2 Residualization

In truncation as stated above, all states and dynamic associated with x_2 are removed. In residualization, $\dot{x}_2$ is set to zero in the state space. Then x_2 can be calculated based on x_1 and u, back substitution of x_2 gives:

$$\begin{aligned} \dot{x}_1 &= (A_{11} - A_{12}A_{22}^{-1}A_{21})x_1 + (B_1 - A_{12}A_{22}^{-1}B_2)u \\ y &= (C_1 - C_2A_{22}^{-1}A_{21})x_1 + (D - C_2A_{22}^{-1}B_2)u \end{aligned} \tag{62}$$

Providing that A_{22} is invertible and define

$$A_r \triangleq A_{11} - A_{12}A_{22}^{-1}A_{21} \tag{63}$$

$$B_r \triangleq B_1 - A_{12}A_{22}^{-1}B_2 \tag{64}$$

$$C_r \triangleq C_1 - C_2A_{22}^{-1}A_{21} \tag{65}$$

$$D_r \triangleq D - C_2A_{22}^{-1}B_2 \tag{66}$$

then the residualization of $G(s)$ is the reduced order model $G_a(s) = (A_r, B_r, C_r, D_r)$

It is noted that truncation is better for the systems that require accuracy at high frequency while residualization works well for the low-frequency system.

2.6.3 Balanced realization

Balanced realization is an asymptotically stable minimal realization where the controllability and observability Gramians are equal and diagonal.

Let (A, B, C, D) be a minimal realization of a stable, rational transfer function $G(s)$. Then, (A, B, C, D) is called balanced if the controllability and observability Gramian (P, Q) satisfy following Lyapunov equations:

$$A^TQ + QA = -C^TC \tag{67}$$

$$AP + PA^T = -BB^T \tag{68}$$

where

$$Q = \int_0^\infty e^{A^T t} C^T C e^{At} dt \tag{69}$$

$$P = \int_0^\infty e^{A^T t} B B^T e^{At} dt \tag{70}$$

Any minimal realization of a stable transfer function can be balanced by state similarity transformation, in other words, by changing of the basis of state and Gramians into quadratic forms:

$$x \to Tx, P \to TPT^T, Q \to (T^T)^{-1} Q T^{-1} \tag{71}$$

Then the balanced realization between controllability and observability Gramian can be achieved as:

$$P = Q = diag(\sigma_1, \sigma_2, ..., \sigma_n) = \Sigma = \begin{pmatrix} \Sigma_1 & 0 \\ 0 & \Sigma_2 \end{pmatrix}, \sigma_1 \geq \sigma_2 \geq ... \geq \sigma_n > 0 \tag{72}$$

The σ_i are the ordered Hankel singular value of $G(s)$, defined as:

$$\sigma_i = \sqrt{\lambda_i(PQ)} \tag{73}$$

A full model then can be reduced by using balanced truncation, balanced residualization or optimal Hankel norm approximation. The latest is the most popular so it will be well stated in the next section.

2.6.4 Optimal Hankel norm approximation

Given a stable model *G(s)* of order *n*, with state space form is given as:

$$\begin{aligned} \dot{x}(t) &= Ax(t) + Bu(t) \\ y(t) &= Cx(t) + Du(t) \end{aligned} \tag{74}$$

where

$$x(t) \in \Re^n, A \in \Re^{n\times n}, B \in \Re^{n\times m}, C \in \Re^{k\times n}, u(t) : \Re \to \Re^m \text{: inputs}, y(t) : \Re \to \Re^k \text{:outputs}$$

The Hankel norm of a system $G = (A, B, C, D)$ is defined by:

$$\|G\|_H^2 = \sup \frac{\int_0^\infty y(t)^2 dt}{\int_{-\infty}^0 u(t)^2 dt} \tag{75}$$

Note that for any *G* and G_r,

$$\|G - G_r\|_\infty \geq \left\|\Gamma_{G-G_r}\right\| = \left\|\Gamma_G - \Gamma_{G_r}\right\| = \|G(s) - G_r(s)\|_H \tag{76}$$

The problem equals to find a Hankel operator $\Gamma_G : L_2(-\infty, 0] \to L_2[0, \infty)$ which solves:

Minimize $\left\|\Gamma_G - \Gamma_{G_r}\right\|$ subject to Γ_{G_r} is the Hankel operator for some G_r that rank (Γ_{G_r}) = *r*, or it equals to find a reduced order model $G_r(s)$ of degree *k* (McMillan degree) such that the Hankel norm of the approximation error, $\|G(s) - G_r(s)\|_H$ is minimized, where the Hankel norm of a stable transfer function $E(s)$ is defined as:

$$\|E(s)\|_H = \sqrt{\rho(PQ)} = \sqrt{\lambda_{\max}(PQ)} \tag{77}$$

where P and Q are the controllability and observability Gramians of $E(s)$. ρ is the spectral radius (maximum eigenvalue) of PQ.

The Hankel operator maps past inputs to future system outputs. It ignores any system response before time 0. In Hankel operator, the interest is to know how energy is transferred between the input to state and to the output of the system. In other words, the problem is to observe how much energy is released from some state $x(0)$ to the output and what is the minimal energy of input signal needed to drive system to the state $x(0)$.

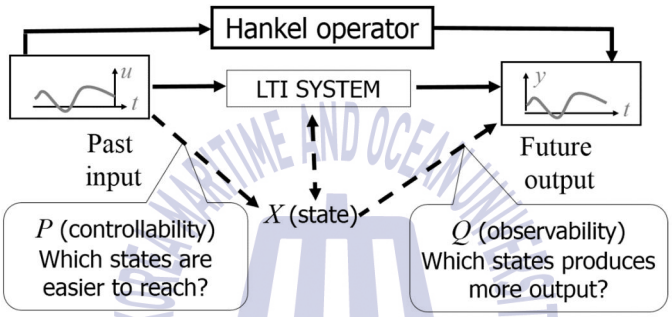

Fig. 25 Hankel operation

Let $G(s)$ be a stable, square, transfer function with Hankel singular values such as

$$\sigma_1 \geq \sigma_2 \geq \ldots \geq \sigma_k \geq \sigma_{k+1} = \sigma_{k+2} = \ldots = \sigma_{k+l} > \sigma_{k+l+1} \geq \ldots \geq \sigma_n > 0 \qquad (78)$$

then an optimal Hankel norm approximation of order $k, G_r(s),$ can be calculated as follows:

Let (A, B, C, D) be a balanced realization of $G(s)$ with the Hankel singular values reordered so that the Gramian matrix is

$$\Sigma = diag(\sigma_1, \sigma_2, ..., \sigma_k, \sigma_{k+l+1}, ..., \sigma_n, \sigma_{k+1}, ..., \sigma_{k+l}) \\ \equiv diag(\Sigma_1, \sigma_{k+1} I) \tag{79}$$

Partition matrices (A, B, C, D) to fit with Σ:

$$A = \begin{bmatrix} A_{11} & A_{12} \\ A_{21} & A_{22} \end{bmatrix}, B = \begin{bmatrix} B_1 \\ B_2 \end{bmatrix}, C = \begin{bmatrix} C_1 & C_2 \end{bmatrix} \tag{80}$$

Define $(\hat{A}, \hat{B}, \hat{C}, \hat{D})$ by:

$$\hat{A} \equiv \Gamma^{-1}(\sigma_{k+1}^2 A_{11}^T + \Sigma_1 A_{11} \Sigma_1 - \sigma_{k+1} C_1^T U B_1^T) \tag{81}$$

$$\hat{B} \equiv \Gamma^{-1}(\Sigma_1 B_1 - \sigma_{k+1} C_1^T U) \tag{82}$$

$$\hat{C} \equiv C_1 \Sigma_1 - \sigma_{k+1} U B_1^T \tag{83}$$

$$\hat{D} \equiv D - \sigma_{k+1} U \tag{84}$$

where U is a unitary matrix which satisfies:

$$B_2 = -C_2^T U \tag{85}$$

and

$$\Gamma \equiv \Sigma_1^2 - \sigma_{k+1}^2 I \tag{86}$$

Then

$$G_r(s) = \left[\begin{array}{c|c} \hat{A} & \hat{B} \\ \hline \hat{C} & \hat{D} \end{array}\right]_s - F(s) \tag{87}$$

where $G_r(s)$ is the stable optimal Hankel norm approximation of order k, and $F(s)$ is an anti stable (all poles in the RHP) transfer function of order n-k-l. F(s) contains the unstable modes, hence, it should be removed then only the stable modes remain.

Chapter 3. Dynamical model of mobile rack vehicle.

In this chapter, the stability of longitudinal and lateral mobile rack vehicle is considered. The dynamical of longitudinal and lateral model is analyzed to establish the state space of system. Then base on that state space of model, the controller has built to keep the stability of platoon under affection of exogenous inputs or outputs such as disturbance or noise from sensors.

3.1 Dynamical model of longitudinal mobile rack vehicle

Consider the connected mobile-rack vehicles as shown in Fig. 26.

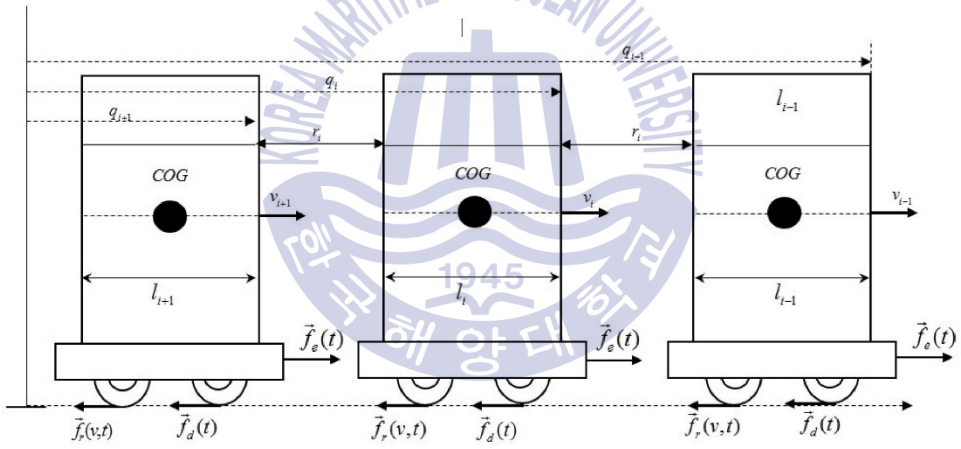

Fig. 26 Three adjacent vehicles in the string formation

Let $q_{i-1}(t)$, $v_{i-1}(t)$ and $a_{i-1}(t)$ denote respectively the position and velocity of the preceding $(i-1)^{th}$ vehicle (ego vehicle) in a platoon. Similarly, $q_i(t)$, $v_i(t)$ and $a_i(t)$ describe the position and velocity of the i^{th} vehicle. The vehicle $(i+1)^{th}$ in a platoon with position and velocity are also denoted by $q_{i+1}(t)$, $v_{i+1}(t)$, $a_{i+1}(t)$ respectively. The headway time $h_{di}(t)$ is the time necessary to the ego vehicle to travel the distance to the preceding vehicle, at its current speed (Yanakiev. D et al.,

2014). As shown in Fig. 26, three adjacent vehicles in a platoon, numbered $i+1$, i and $i-1$ following each other on the road. The safe distance r_i is defined as

$$r_i = q_{i-1} - q_i - l_{i-1} = q_i - q_{i+1} - l_i \tag{88}$$

where l_{i-1} and l_i are the length of the $(i-1)^{th}$ and i^{th} mobile-rack. To depict the vehicle motion to be controlled, the dynamical equation of the mobile-rack vehicle is described as follows:

$$m_i \dot{v}_i(t) = f_e(t) - f_r(v,t) - f_d(t) \tag{89}$$

where $f_e(t)$ represents the motor traction or braking force applied to the vehicle, m_i the mass of the i^{th} vehicle, $f_r(v,t)$ the force due to air resistance and friction typically described in nonlinear form, $v(t)$ the velocity of the mobile-rack vehicle, and $f_d(t) = m_i d(t)$ the gravity force due to the floor slope. Particularly, there may be limited traction available on the icy road surface. The longitudinal acceleration of the system is given as

$$a_i(t) = \dot{v}_i(t) = \frac{1}{m_i} f_e(t) - \frac{1}{m_i} f_r(v,t) - d(t) \tag{90}$$

Furthermore, the force that follows the position input is approximately described as a first-order lag with a time-delay

$$\tau_{pi} \dot{f}_e(t) + f_e(t) = g_{ui} u_i(t - \phi_i) \tag{91}$$

where τ_{pi} describes the i^{th} motor time constant, $u_i(t)$ the control input with ϕ_i time-delay, and g_{ui} the transmission gain of the input-force subsystem. The linear expression of the force due to air resistance and friction is given by

$$f_r(v,t) \approx \frac{m_i}{\tau_{mi}} v_i(t) = \lambda_i v_i(t) \tag{92}$$

where τ_{mi} the time constant. The motor force can be obtained as

$$f_e(s) = s(m_i s + \lambda_i) q_i(s) + m_i d(s) \tag{93}$$

From Eq. (93), the relationship between input and the motor force is given by

$$f_e(s) = \frac{g_{ui}}{(\tau_{pi} s + 1)} e^{-\phi_i s} u_i(s) \tag{94}$$

Therefore, the transfer function with the acceleration disturbance $a_{d_i}(s)$ is also given by

$$q_i(s) = \frac{\tilde{g}_{ui}}{s(\tau_{mi} s + 1)(\tau_{pi} s + 1)} e^{-\phi_i s} u_i(s) - \frac{\tau_{mi}}{s(\tau_{mi} s + 1)} a_{di}(s) \tag{95}$$

Hence, the transfer function $G_i(s)$ with state variables can be defined as

$$G_i(s) = [A_i, B_i, C_i, D_i] = C_i (sI - A_i)^{-1} B_i + D_i \tag{96}$$

In addition, the detailed system matrices with state space description are described by

$$\underbrace{\begin{bmatrix}\dot{q}_i(t)\\ \dot{v}_i(t)\\ \dot{f}_{ei}(t)\end{bmatrix}}_{\dot{x}_i}=\underbrace{\begin{bmatrix}0 & 1 & 0\\ 0 & -\frac{1}{\tau_{mi}} & \frac{1}{m_i}\\ 0 & 0 & -\frac{1}{\tau_{pi}}\end{bmatrix}}_{A_i}\underbrace{\begin{bmatrix}q_i(t)\\ v_i(t)\\ f_{ei}(t)\end{bmatrix}}_{x_i}+\underbrace{\begin{bmatrix}0\\ 0\\ \frac{g_{ui}}{\tau_{pi}}\end{bmatrix}}_{B_{ui}}u_i(t-\phi_i)+\underbrace{\begin{bmatrix}0\\ -1\\ 0\end{bmatrix}}_{B_{di}}a_{di}(t) \tag{97}$$

$$\underbrace{\begin{bmatrix}q_{pi}(t)\\ v_i(t)\end{bmatrix}}_{y_i}=\underbrace{\begin{bmatrix}1 & h_{di} & 0\\ 0 & 1 & 0\end{bmatrix}}_{C_i}\underbrace{\begin{bmatrix}q_i(t)\\ v_i(t)\\ f_{ei}(t)\end{bmatrix}}_{x_i} \tag{98}$$

where x_i denotes the state vector, y_i the output vector, and B_i the input matrix given by $B_i=[B_{ui}\ B_{di}]^T$. Note that the sudden change of acceleration $a_{d_i}(s)$ can be one of the exogenous disturbances to address the string stability in a platoon.

3.2 Dynamical model of lateral mobile rack vehicle

3.1.1 Kinematics and dynamics of mobile rack vehicles

The model used is a bicycle model (Wong. J.Y, 1993) with lateral and yaw planes. The MRV is moving with constant speed of magnitude V at the center of gravity (CG) along a desired path. It is assumed that the vehicle is equipped with appropriate sensors to detect some lateral motions from the center-line of the path and is also equipped with a set of actuators to generate the desired steering actions during a maneuvers. For simplification, the left and right wheels are steered by the same angles, and each pair of front and rear wheels are laterally lumped into one tire in the center-line. As shown in Fig. 27, the planar model is usually referred to as a bicycle model (You. S.S. et al., 1998) and its orientation with respect to some global coordinate (X,Y).

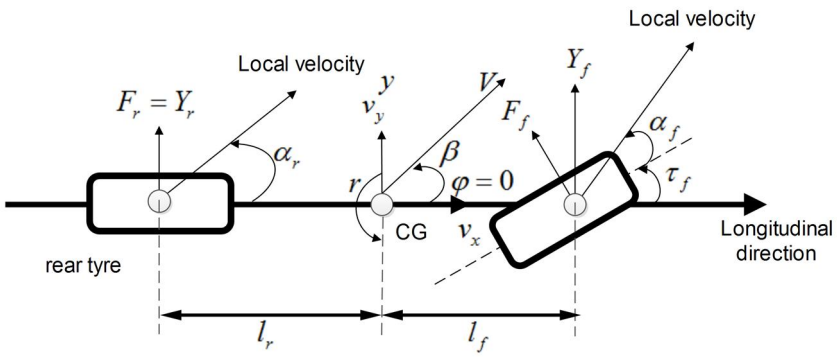

Fig. 27 Planar MRV model and coordinate systems

The coordinate system denoted by (x, y, z) with its origin at the CG, is introduced to describe vehicle motion. Next, the chassis sideslip β is the angle of linear velocity (V) of its CG with respect to the y axis, the chassis system, (x, y, z) is rotated by a yaw angle φ. If a set of angles (β, φ, τ_f) are small, then the following variables can be defined. First, the linear velocities are simplified to be:

$$\begin{aligned} v_x &= V\cos\beta \approx V; \\ v_y &= V\sin\beta \approx V\beta; \end{aligned} \tag{99}$$

Applying the Newton's second law of motion in the Y direction only.

$$ma_y = F_{yf} + F_{yr} \tag{100}$$

where the lateral forces F_{yf} and F_{yf} are those exerted from the front and rear wheels respectively, while a_y denotes the inertial acceleration at the center of gravity in the direction of the y axis. Decomposing this term further shows that it is the sum of two terms; the lateral acceleration $\dot{y}$ and the centripetal acceleration $V\dot{\varphi}$.

Substituting these term into the left-hand side of Eq. (99) yields the following relationship.

$$m(\ddot{y}+V\dot{\varphi}) = \sum lateralforce = F_{yf} + F_{yr} \tag{101}$$

Yaw motion or moments about the vertical z axis through the CG:

$$J_z\dot{r} = \sum \text{steering torque} = l_f F_{yf} - l_r F_{yr} \tag{102}$$

Here, the constants l_f and l_r denote the distance from the front wheel and rear wheel to the center of gravity, respectively, while J_z is the moment of inertia. In general, lateral tire force is a non-linear function of slip angle. In this thesis, the cornering stiffness for the front (rear) tire is denoted by $\left(C_f, C_r\right)$ respectively and its value depends on the tire road interaction. As long as the tire slip angle is small, a linear relationship between tire force and slip angle can be justified. Then, the lateral force generated by the front and rear tires vary linearly with their slip angles (Rajamani R., 2006).

$$F_{yf} = 2C_{\alpha f}(\tau_f - \theta_{vf}) \quad \text{and} \quad F_{yr} = 2C_{\alpha r}(-\theta_{vr}) \tag{103}$$

However, in many cases, the slip angles is not angle is not small and this necessitates the inclusion of uncertainty terms in the tire model. Thus, the cornering stiffness is an uncertain parameter that varies with the road –tire contact conditions. The vehicle performance should be achieved robustly for practical operating ranges from poor adhesion (low friction) on slippery roads to good adhesion on dry roads. Approximating for small angles and subtitling the notation $v_y = \dot{y}$, the tire velocity angles (Rajamani R., 2006) could be obtained as:

$$\theta_{vf} = \frac{\dot{y} + l_f \dot{\varphi}}{V}$$
$$\theta_{vr} = \frac{\dot{y} - l_r \dot{\varphi}}{V} \tag{104}$$

Combining Eq. (99) through Eq. (104) yields the lateral equations of motion:

$$m\dot{V}\dot{\beta} + \left[mV + \frac{2l_f C_{\alpha f} - 2l_r C_{\alpha r}}{V} \right] r + \left[2C_{\alpha f} + 2C_{\alpha r} \right] \beta = 2C_{\alpha f} \tau_f(t)$$
$$J_z \dot{r} + \left[\frac{2l_f^2 C_{\alpha f} - 2l_r^2 C_{\alpha r}}{V} \right] r + \left[2l_f C_{\alpha f} - 2l_r C_{\alpha r} \right] \beta = 2l_f C_{\alpha f} \tau_f(t) \tag{105}$$

A description of the coefficients in Eq. (105) appears in Table 1. Fig. 28 shows a two MRVs in a platoon with the same coordinate but different yaw angle and the deviation. The lateral deviation is the following's mobile rack vehicle's lateral offset from the target vehicle's position, can be modelled as relations of the two vehicle's states. In this section, the platoon of MRV is assumed that the velocity and distance are satisfied the longitudinal stability condition. In the other hand, each MRV has the same velocity and safety distance. The relation shows that the lateral deviation changes according to the rotation of the following vehicle as well as the difference in the direction of motion of the two vehicles.

Let $\Delta\gamma = \gamma_L - \gamma_{i-1}$ is the deviation, $\gamma_i, \varphi_i, \beta_i$ denote the lateral position, the yaw angle and the slip angle of i^{th} MRV, respectively. $\gamma_{i-1}, \varphi_{i-1}, \beta_{i-1}$ denote the lateral position, the yaw angle and the slip angle of $(i+1)^{th}$ MRV, respectively. The deviation from center of gravity (COG) of i^{th} MRV to COG of $(i-1)^{th}$ MRV can be described as:

$$\gamma_i(t) - \gamma_{i-1}(t) = V_i \int_{t_0}^{t} \left(\varphi_i(t) + \beta_i(t) \right) dt - V_{i-1} \int_{t_0}^{t} \left(\varphi_{i-1}(t) + \beta_{i-1}(t) \right) dt \tag{106}$$

No.	Description	Label	Unit
1	The mobile rack vehicle mass	m	kg
2	The yaw moment of inertia.	J_z	$kg.m^2$
3	The cornering stiffness rear	$C_{\alpha r}$	N/rad
4	The cornering stiffness front	$C_{\alpha f}$	N/rad
5	The distance from CG to rear axle	l_r	m
6	The distance from CG to front axle	l_f	m
7	The longitudinal velocity	v_x	m/s
8	The lateral velocity	v_y	m/s
9	The yaw rate about the c.g.	r	rad/s
10	The steering angle	τ_f	rad
11	The safety distance	ϑ	m

Table 1 The summary of coefficients of vehicle model

The projected point at a distance ϑ from the COG of i^{th} MRV to COG of $(i-1)^{th}$ MRV. By approximating for small angles:

$$\gamma_L(t) - \gamma_i(t) = \vartheta \sin\varphi(t) \approx \vartheta\varphi(t) \tag{107}$$

Substituting Eq. (107) to Eq. (106) and assuming that the longitudinal velocity of two MRVs are synchronized $V_i = V_{i-1} = v_x$. Then the following dynamic equation describing the rate of change of the later deviation is obtained as:

$$\Delta\dot{\gamma} = \vartheta r + v_x(\varphi_i - \varphi_{i-1}) + v_x(\beta_i - \beta_{i-1}) \tag{108}$$

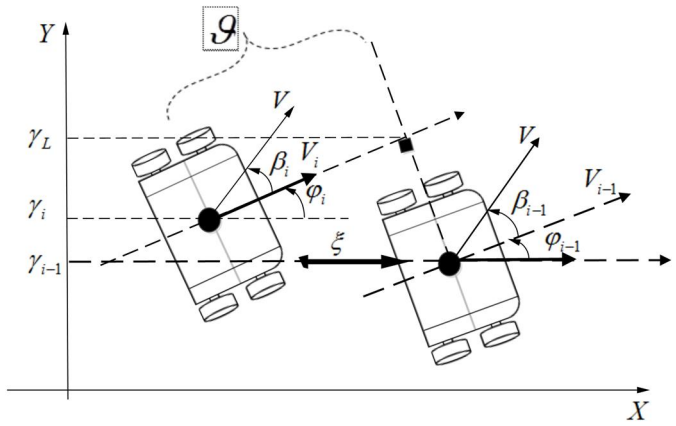

Fig. 28 Two adjacent MRVs in a platoon

Based on two equations Eq. (105) & Eq. (108), the transfer function describes the relation of the steering angle and yaw angle G_φ and the lateral position G_γ can be obtained:

$$G_\varphi = \frac{\varphi}{\tau_f} = \frac{a_0 s + a_1}{b_0 s^3 + b_1 s^2 + b_2 s}; G_\gamma = \frac{\gamma}{\tau_f} = \frac{c_0 s + c_1}{d_0 s^3 + d_1 s^2 + d_2 s} \tag{109}$$

where:

$$G_\varphi = \frac{\varphi}{\tau_f} = \frac{a_0 s + a_1}{b_0 s^3 + b_1 s^2 + b_2 s}; G_\gamma = \frac{\gamma}{\tau_f} = \frac{c_0 s + c_1}{d_0 s^3 + d_1 s^2 + d_2 s} \tag{110}$$

where:

$$a_0 = 2mC_{\alpha f}l_f v_x; a_1 = 4C_{\alpha f}C_{\alpha r}v_x^2(l_f + l_r); b_0 = mJ_z v_x;$$
$$b_1 = 2(mC_{\alpha f}J_z^2 l_f^2 + C_{\alpha f}J_z v_x^2 + mC_{\alpha f}J_z^2 l_r^2 + C_{\alpha r}J_z v_x^2);$$
$$b_2 = (C_{\alpha f}^2 l_f^2 + C_{\alpha r}^2 l_r^2)(4J_z^2 v_x - 4v_x^3) + 4C_{\alpha f}C_{\alpha r}J_z^2 v_x(l_f^2 + l_r^2)$$
$$-2mv_x(C_{\alpha f}l_f - C_{\alpha r}l_r) + 8C_{\alpha f}C_{\alpha r}l_f l_r v_x^3;$$
$$c_0 = C_{\alpha f}J_z; \mathrm{c}_1 = -C_{\alpha f}V_x L_f m + C_{\alpha f}V_x C_{\alpha r}L_r^2 + C_{\alpha f}V_x C_{\alpha r}L_f L_r;$$
$$d_0 = mJ_z; d_1 = C_{\alpha f}J_z V_x + mC_{\alpha f}l_f^2 V_x - C_{\alpha r}J_z V_x + mC_{\alpha r}l_r^2 V_x$$
$$d_2 = -C_{\alpha f}^2 J_z^2 l_f^2 + C_{\alpha f}^2 l_f^2 V_x^2 + 2C_{\alpha f}C_r J_z^2 l_f l_r + C_{\alpha f}C_{\alpha r}l_f^2 V_x^2$$
$$+C_{\alpha f}C_{\alpha r}l_r^2 V_x^2 - mC_{\alpha f}J_z^2 l_f - C_r^2 J_z^2 l_r^2 + C_r^2 l_r^2 V_x^2 + mC_{\alpha r}J_z^2 l_r;$$

3.1.2 Lateral vehicle model with nominal value

The nominal plant transfer function from the steering angle to the yaw angle and the lateral position, for the parameters in Table 2 can be obtained:

$$G_\varphi(s) = \frac{\varphi}{\tau_f} = \frac{1008s + 24500}{24s^3 + 21033600560s^2 + 490784000035s} \quad (111)$$

$$G_\gamma(s) = \frac{\gamma}{\tau_f} = \frac{700s + 158620}{30s^3 + 7273s^2 + 152495s} \quad (112)$$

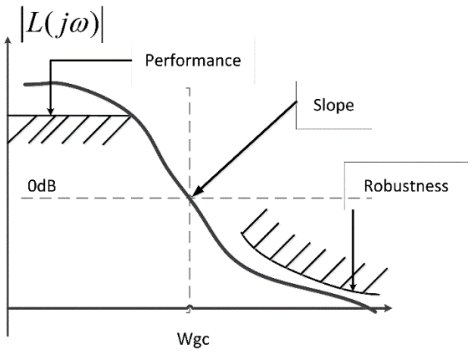

Fig. 29 The requirement shape responses for stable system description

The shape of transfer function must satisfy these condition as: in low frequency the gain margin of response must be high for disturbance attenuation and must be low in high frequency for noise rejection. The condition requirement is described in Fig. 29. However, the frequency response of open-loop plant $G_{\varphi}(s)$ and $G_{\gamma}(s)$ for min, max and nominal values are shown in Fig. 30.

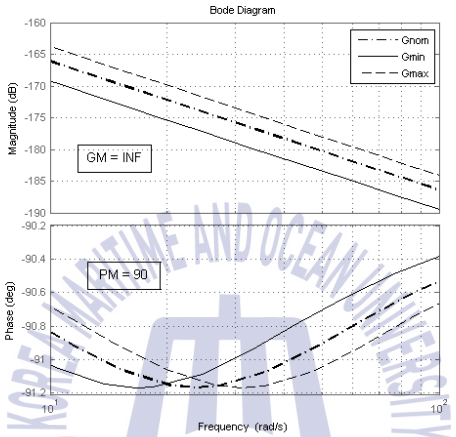

(a)

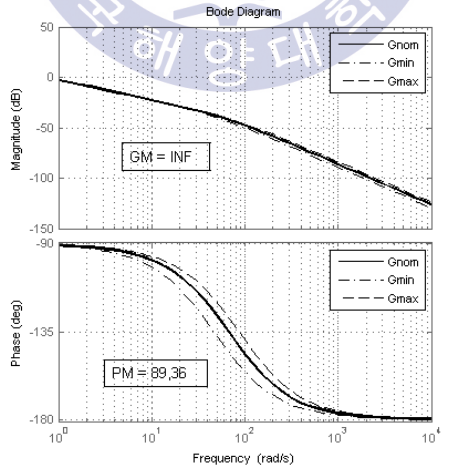

(b)

Fig. 30 The open-loop response of system for min max and nominal value: (a) Yaw angle frequency responses; (b) the lateral position frequency responses

It is noted that the system present different characteristics depending on the nominal min max value and the stability is critical issue which need to be considered. Hence, the objective of this paper shall present to build the controller which can keep the system is stable under affection of either noise and disturbance or uncertainty parameters.

Chapter 4. Controller design for mobile rack vehicle

4.1 Robust controller synthesis for longitudinal of mobile rack vehicles

For the dynamic model described in Eq. (97), the parametric uncertainty (Wang, 1998) is an inevitable in most practical applications. For example, the mass of mobile-rack vehicle significantly varies with its nominal value depending on dynamic loading conditions. Due to various uncertainties, the actual model parameters will vary over the given ranges around their nominal values. Assuming that the parametric uncertainties are real and structured (Young *et al*., 1991) the uncertainty plant $\tilde{G}_i(s)$ can be written as follows:

$$\tilde{G}_i(s) = G_i(s)(1 + \Delta_M(s) W_M(s)) \tag{113}$$

where the uncertainty block and weighting function are respectively described by

$$\Delta = \begin{bmatrix} \delta_1 & 0 \\ 0 & \delta_2 \end{bmatrix} \quad W_M = \begin{bmatrix} W_{M11} & 0 \\ 0 & W_{M22} \end{bmatrix} \tag{114}$$

Then the perturbed plant set with multiplicative uncertainty is defined as

$$\Pi = \left\{ \tilde{G}_i \mid \tilde{G}_i = G_i(1 + \Delta . W_M), \left| \Delta_M \right| < 1^{\forall} \omega \right\} \tag{115}$$

For obtaining the uncertainty weight W_M, the smallest radius $l_M(j\omega)$ at each frequency that includes the possible plant $\tilde{G}_i \in \Pi$ is defined as

$$l_M(j\omega) = \max_{\tilde{G}\in\Pi}\left[\frac{\tilde{G}_i(j\omega) - G_i(j\omega)}{G_i(j\omega)}\right] = \max\left|\Delta(j\omega).W_M(j\omega)\right| = \max L \tag{116}$$

The weighting function $W_M(s)$ to cover the set that satisfies the condition is chosen as follows:

$$\underline{\sigma}(W_M(j\omega)) \geq l_M(j\omega), \quad \forall\omega \tag{117}$$

The set of L and elements of W_M in Eq. (116) and Eq. (117) are illustrated in Fig. 31.

Recall that the weighting functions bound all the radius l_M (Skogestad and Postlethwaite, 2003) of partial set of the plant $\tilde{G}_i$. With above theory, the weighting function W_M is calculated as:

$$W_M = \begin{bmatrix} \dfrac{0.6617s^2 + 11.4s + 31.97}{s^2 + 20.56s + 49.63} & 0 \\ 0 & \dfrac{0.8244s^2 + 0.7216s + 0.6306}{s^2 + 0.9595s + 0.7965} \end{bmatrix} \tag{118}$$

Assuming there exists a controller block $K_i(s)$, the weighting function $W_p\{W_{p1}; W_{p2}\}$ is added to the output to manipulate the dynamic performances of position and velocity. The preceding mobile-rack vehicle input signal u_{i-1} represents the set points that the closed-loop system has to track. The input multiplicative uncertainty $\Delta_M(s)$ and the uncertain parameters $\Delta_{di}(s)$ are added to system to perform the system uncertainty which need to overcome successfully.

The weighting uncertainty $W_M(s)$ is also added to system for combining with the input multiplicative uncertain $\Delta_M(s)$ to make the perturbed plant.

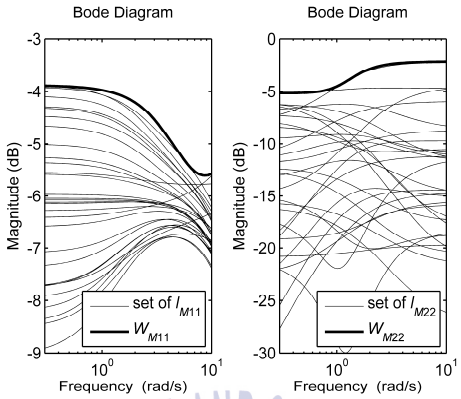

Fig. 31 Bode plots of weighting function and the bound sets

To realize the complete system, an acceleration disturbance a_{di} is also added to the control synthesis. Another factor that should be considered is the sensor noise W_n for the measurements of the distance and communications. The block diagram of MRVs connection in the platoon is described as Fig. 32 as bellow.

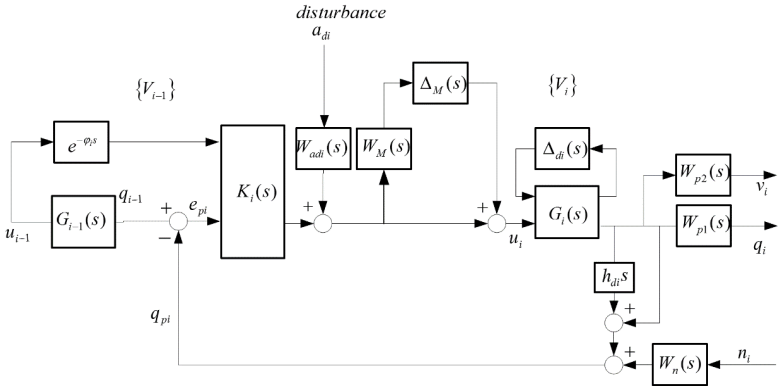

Fig. 32 The block diagram of MRVs connection in the platoon

In this figure, the connection between the leader and follower is descripted detail with the output signals of following MRVs need to control are position and velocity. These signals will feedback to the controller to evaluate and turning the error. The input signals are the position and velocity of leader MRV. From the control block diagram in Fig. 33, the generalized plant P is further described as

$$\begin{bmatrix} y_\Delta \\ z \\ \hline y \end{bmatrix} = \left[\begin{array}{cccc|c} 0 & 0 & 0 & 0 & W_M \\ W_p G_i & W_p W_{adi} & 0 & 0 & W_p G_i \\ \hline -G_i & -W_{adi} & -W_n & W_{re} & -G_i \end{array}\right] \begin{bmatrix} u_\Delta \\ a_{di} \\ n \\ q_{i-1} \\ \hline u_i \end{bmatrix} \tag{119}$$

The complete control structure block is redrawn from the MRVs connection block diagram to make it more overview and easier for designing the controller.

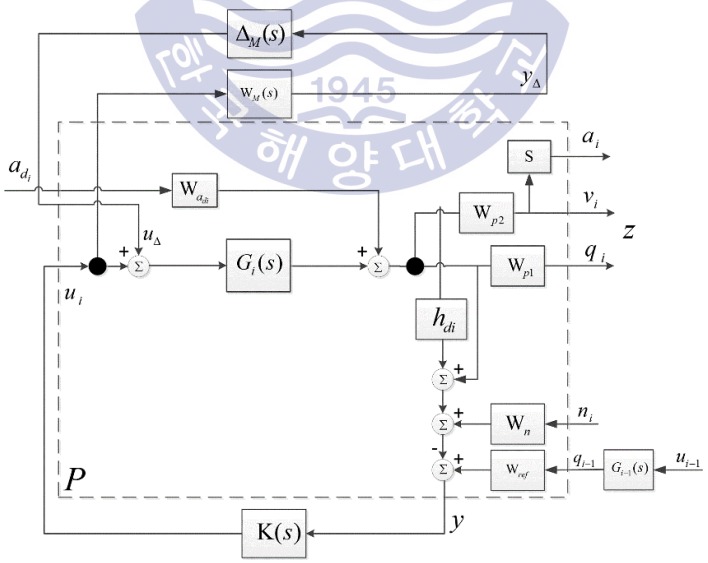

Fig. 33 Complete control structure with weighting functions

The closed-loop transfer matrix N that connects the generalized plant P with the controller K via lower linear fractional transformation (LFT), is depicted in Fig. 34. The interconnection matrix P is partitioned as $P = \left[\begin{array}{c|c} P_{11} & P_{12} \\ \hline P_{21} & P_{22} \end{array}\right]$. By the upper LFT manipulation, it can be derived that:

$$z = \left[P_{22} + P_{21}\Delta_M (I - P_{11}\Delta)^{-1} P_{12} \right] w \tag{120}$$

where $w = [\mathrm{a}_{di} \;\; n \;\; q_{i-1}]^T$; $z = [q_i \;\; v_i]^T$.

Such a lower LFT can be described by

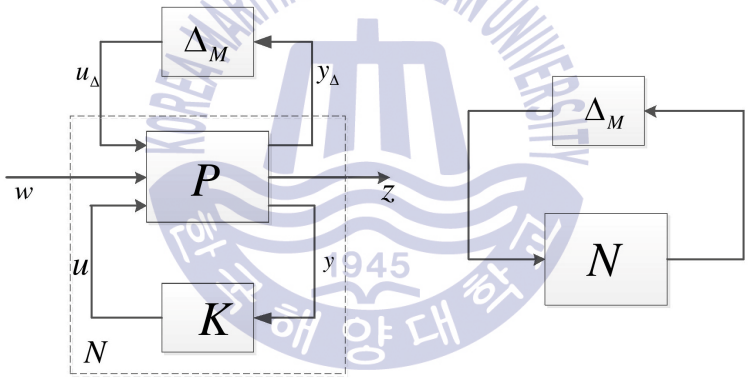

Fig. 34 The block diagram of closed-loop transfer N and $N-\Delta$ structure

$$N = F_l(P,K) = P_{11} + P_{12}K(I - P_{22}K)^{-1}P_{21}$$

$$= \left[\begin{array}{c|ccc} -W_M T_i & -W_M K S_0 a_{di} & -W_M K S_0 W_n & W_M K S_0 W_{ref} \\ \hline W_p S_0 G_{de} & W_p S_0 a_{di} & -W_p T_0 W_n & W_p T_0 W_{ref} \end{array}\right] \tag{121}$$

$$= \left[\begin{array}{c|ccc} N_{11} & N_{12} & N_{13} & N_{14} \\ \hline N_{21} & N_{22} & N_{23} & N_{24} \end{array}\right] = \left[\begin{array}{c|c} N_{y_\Delta u_\Delta} & N_{y_\Delta w} \\ \hline N_{zu_\Delta} & N_{zw} \end{array}\right]$$

where $S_0 = (I + G_i K)^{-1}$ describes the sensitivity function; $T_i = KG_i(I + KG_i)^{-1}$ and $T_0 = G_i K(I + G_i K)^{-1}$ are the input and output complementary sensitivity functions, respectively. For the $N - \Delta$ structure, the structured singular value μ_Δ is defined as follows:

$$\mu_\Delta(N) = \frac{1}{\min\{\bar{\sigma}(\Delta) \,|\, \Delta \in \Delta, \det(I - N\Delta) = 0\}} \tag{122}$$

For all perturbation Δ with the appropriate structure, it should satisfy the following criteria:

$$\max_\omega \bar{\sigma}[\Delta(j\omega)] < \frac{1}{\mu_\Delta(N)} \tag{123}$$

For example, $\mu_\Delta(N_{11}(j\omega))$ is the structured singular value of the closed-loop system $N_{11}(s)$ with respects to parametric uncertainty Δ_M. Based on D-K iteration, the stabilizing controller is obtained by such that

$$K = \arg\inf_K \left\| DF_l(P,K)D^{-1} \right\|_\infty \tag{124}$$

where D is a diagonal constant scaling matrix and can be determined by

$$D(j\omega) = \arg\inf_{D\in D} \bar{\sigma} \left\| DF_l(P,K)D^{-1}(j\omega) \right\|_\infty \tag{125}$$

The sensitivity function S_0 is a good indicator of addressing closed–loop system performance. To reduce the load disturbance effects on the controlled outputs in low frequencies, the sensitivity S_0 should be small and must satisfy the following condition:

$$\left\| W_p S_0 \right\|_\infty < 1 \quad {}^{\forall}\omega \Leftrightarrow \bar{\sigma}(S_0) < \frac{1}{\bar{\sigma}(W_p)} \tag{126}$$

If the control system is to be stable for all perturbed plants about nominal model up to the worst–case model uncertainty, the condition for robust stability is given as follows:

$$\left\| W_M T_i \right\|_\infty < 1 \quad {}^{\forall}\omega \Leftrightarrow \mu_\Delta(N_{11}(j\omega)) < 1 \tag{127}$$

Furthermore, the complementary sensitivity function T_0 should be small in high frequency range to reduce the effects of measurement noises on the controlled outputs as well as the control inputs. Fig. 35 represents the singular value plots of sensitivity S_0 and complementary sensitivity T_0, in which these results always satisfies the condition $S_0(s) + T_0(s) = I$ at all frequencies. Then the weighting performance W_p which chosen as above is reasonable and satisfies the condition given in Eq. (127). It is obvious that the robust controller can successfully attenuate the external disturbances and keep the complete system stable.

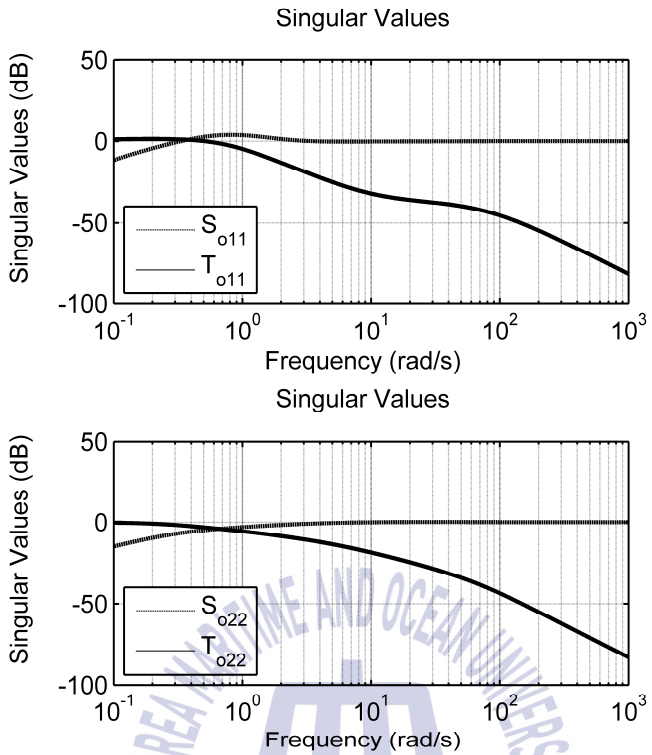

Fig. 35 Singular value plots of sensitivity and complementary sensitivity functions

Fig. 36 depicts nominal performance, robust stability and robust performance in which the structured singular values are all less than one and satisfy the conditions: $|W_p S| < 1$, $|W_M T| < 1$, and $|W_p S| + |W_M T| < 1$, respectively for all frequencies. Hence, the mobile rack system ensures the performance quality against disturbances and noises.

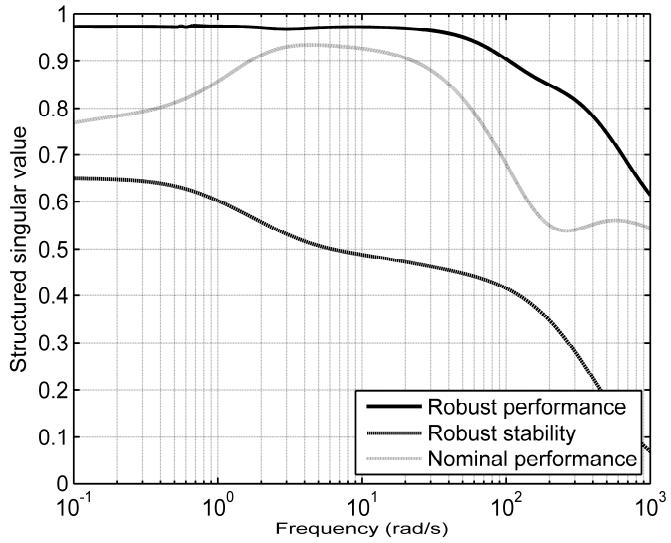

Fig. 36 Stability and performance tests of the control system

4.2 Robust controller synthesis for lateral of mobile rack vehicles

The lateral control problem is very important in the navigation procedure of mobile rack vehicle (MRV). To achieve precise navigation, lateral control should have good adaptability to the varieties of system parameters and different kinds of noises and disturbances. This is quite hard demand for design of the motion controller. The MRV considered in this work consist of a wheeled vehicle with autonomous movement, equipped with electric AC motors that are controlled by an on-board computer. In addition, for tracking the line and keeping the MRV in the lane, then the driver adjusts the yaw angle of the vehicle and the velocity of the wheel according to the command of the controller. It is assumed that the mobile rack vehicle is composed of a rigid body with wheels that do not get deformed and moves straight on a horizontal plane. Moreover, the vehicle lateral dynamics are affected by vehicle mass, longitudinal velocity, vehicle inertial, and the cornering stiffness of the tires. All of these parameters are subject to variation, even over the course of a single trip. Therefore a practical lateral control system must guarantee

stability, and ride comfort, over a wide range of parameters changes. This section aims to develop the controller which stabilizes the yaw angle of mobile rack vehicle in the extremely cold environment without rail track. It means that the system has ability to attenuate noise or disturbance and must be coped with the uncertainty parameters. The performance of the robust controller is then evaluated over the range of parameter variations through simulations.

4.2.1 Lateral vehicle model with uncertainty description

For the model at hand, parametric uncertainty is an inevitable issue, for example, the MRV mass varies about 30% around its nominal value. This change can be interpreted as a variation in the nominal model parameters in Eq. (111) and Eq. (112). This means that the MRV would be better and more precisely described if, instead of considering a single linear model, a family of linear model was stated. (Zhou. K et.al., 1996) shows that this family of models can be represented as follows:

$$G(s)=\left[\begin{array}{c|c} A+\sum_{i=1}^{k}\alpha_i A_i & B+\sum_{i=1}^{k}\alpha_i B_i \\ \hline C+\sum_{i=1}^{k}\alpha_i C_i & D+\sum_{i=1}^{k}\alpha_i D_i \end{array}\right] \tag{128}$$

where A,B,C,D represent the nominal model, and parameter uncertainty is shown by scalars $\alpha_i \in (-1,1)$. The coefficients in the state space realization matrices (A,B,C,D) are generally not fixed. Moreover, their exact values are uncertain at any fixed point in time, and should be accompanied by an uncertainty description that describes the set of all possible system variations. Let ρ is any uncertain parameters in $G(s)$; then each physical parameter ρ can be presented as the sum of a nominal and of an uncertain part. The summary of expected parameter changes is described in Table 3. Assuming that $\bar{\rho}$ is the nominal value of the parameter ρ and

that W_M is a constant scaling factor, it is possible to write ρ in terms of a norm-bounded perturbation as

$$\rho = \bar{\rho}(1 + W_M \Delta) \tag{129}$$

where $\Delta \in \Re$ represent the perturbation associated with ρ, with $\Delta \leq 1$ satisfied.

No.	Parameter	Nominal value	Range
1	m	3000	2100-3900
2	v_x	0.5	0.35-0.65
3	$C_{\alpha r}$	70000	49000-91000
4	$C_{\alpha f}$	70000	49000-91000
5	J_z	2000	constant
6	l_r	1.2	constant
7	l_f	1.3	constant
8	ϑ	1	constant

Table 2 The nominal parameter of longitudinal MRV system

It is worth noting that the perturbation is normalized to Δ by introducing W_M, which is the nominal dispersion of the working range of the model.

Then the block diagram for the uncertain parameter ρ in equation (141) is as shown in Fig. 37

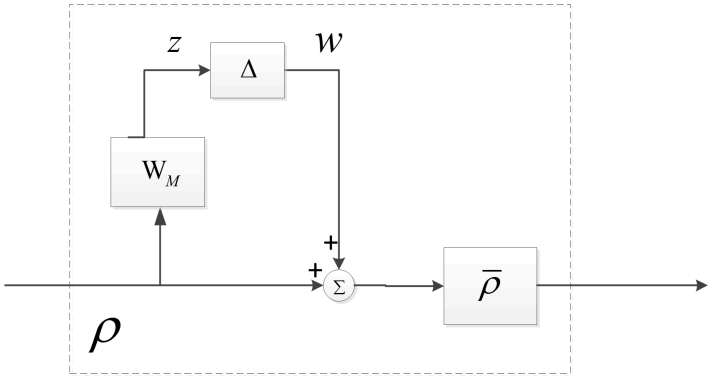

Fig. 37 The requirement shape responses for stable system description

In this thesis, the cornering stiffness depends on the tire-road contact conditions, and it is considered as an uncertain parameter. Consequently, the cornering stiffness in $G(s)$ can be replace by perturbed value in Table 3.

$$c_f = \bar{c}_f(1+W_{cf}\Delta_f) \text{ and } c_r = \bar{c}_r(1+W_{cr}\Delta_r) \tag{130}$$

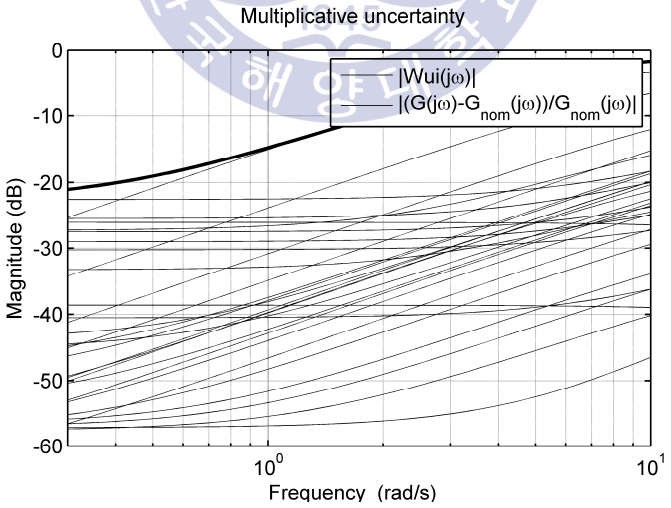

(a)

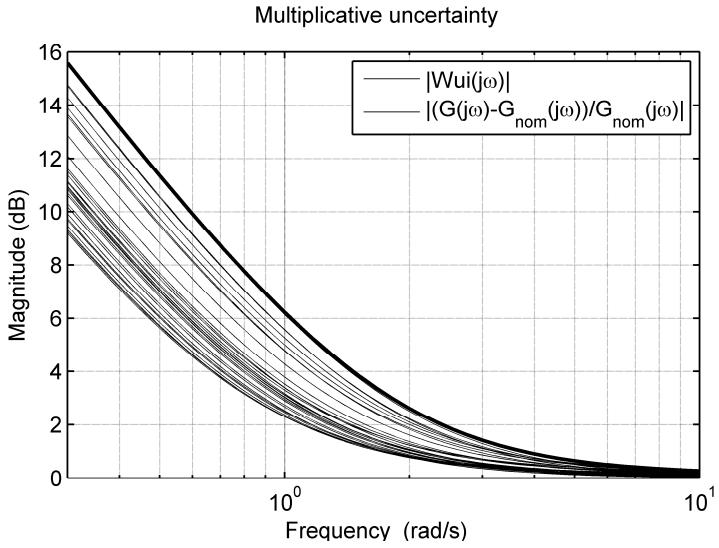

(b)

Fig. 38 The simulation of plan uncertainty: (a) yaw angle; (b) lateral position

where $\bar{c}_i$ is the nominal value and W_{ci} is a measure of the relative uncertainty size; each Δ_i may arbitrarily be changed between -1 and 1. Other parameters in $G(s)$ are assumed to be exactly known. The perturbed plant boundary $l_M(j\omega)$ at each frequency which includes the possible plant $\tilde{G}_{\Delta\gamma} \in \Pi$ is defined by Skogestad, et al. (2005) as follows:

$$l_M(j\omega) = \max \bar{\sigma}(\Delta(j\omega).W_M(j\omega)) \tag{131}$$

When max singular value $\bar{\sigma}(\Delta) = 1$, the weighting function W_M is chosen to cover the boundary $l_M(j\omega)$ that satisfies:

$$\underline{\sigma}(W_M(j\omega)) \geq l_M(j\omega), \quad {}^{\forall}\omega \tag{132}$$

The set of l_M and elements of weighting function W_M in (141) and (142) are plotted in Fig. 38. It can be seen that weighting function elements bound all the possible l_M .

4.2.2 Controller design

4.4.2.1 Interconnection structure and weighting function selection

This section discusses the performance specifications and weights from a practical point of view. Before, proceeding, it is necessary to formalize the uncertainties and system specifications in terms of a suitable general framework. The transfer function $Gnom(s)$ represent the nominal model of the lateral MRV dynamics.

$$G_{nom}(s) = \left[\begin{array}{c|cc} A & B_1 & B_2 \\ \hline C_1 & D_{11} & D_{12} \\ C_2 & D_{21} & D_{22} \end{array}\right] \tag{133}$$

To derive the linear fractional transformation (LFT) of an uncertainty model, the know part and the unknown elements are conveniently separated. All uncertainty elements are diagonally augmented in the perturbation matrix. Hence, the perturbed vehicle model with an LFT structure is shown in Fig. 39. The weighting matrix, which characterize the input/output signals of the control system, have to be formulated appropriately. For the robust controller to provide a desired degree of stability and performance robustness, it is necessary to translate the design specification into frequency-dependent weighting functions. The purposes of the different weighting functions are stated below. Consider a set of functions, $\{W_M(s), \Delta_M(s)\}$, where the weighting $W_M(s)$ is assumed to be known and reflects

the amount of unstructured uncertainty in the MRV model; $\Delta_M(s)$ is assumed to be stable and unknown, except for the norm condition, $\|\Delta_M(s)\|_\infty \le 1$.

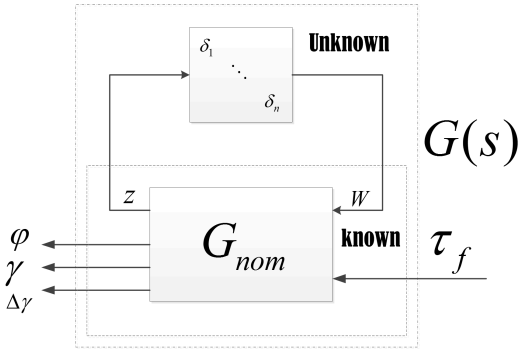

Fig. 39 The nominal MRV with parametric uncertainty

The high pass frequency weighting has been used to reflect this:

$$W_{M\varphi} = \frac{0.2764s + 4.26}{s + 51.78}; W_{M\gamma} = \frac{2.954s + 23.21}{s + 83.72} \tag{134}$$

At any frequency ω , the magnitude of $|W_M(j\omega)|$ can be interpreted as the percentage of the model uncertainty at that frequency. The performance weighting functions are used to define design specifications. The inverse of the performance weight indicates how much the external disturbance should be rejected at the output, or how much steady state tracking due to external input is allowed. The upper bound on $|1/W_\varphi(j\omega)|$ and $|1/W_\gamma(j\omega)|$ are the weight for the tolerable maximum angle φ , lateral position γ , respectively. In this case, the weight is assumed to be constant over all frequencies and is set as:

$$W_{\varphi} = \frac{4s+105}{10s+1}; W_{\gamma} = \frac{10s+155}{10s+5} \tag{135}$$

In order to reflect the magnitude and frequency content of signals, some weighting functions are chosen. Frist, to account for the fact that system outputs can never be sensed without noise, all measurement signals will always be corrupted by frequency – dependent noise. The noise varying frequency should be suppressed. In this paper, all noise occurs at high frequencies, and therefore each has to be weighted by high-pass characteristics. The weighting $W_n(s)$ on the sensors are set as:

$$W_{n\varphi} = W_{n\gamma} = \frac{0.02s}{0.5s+1} \tag{136}$$

where the upper bounds of $|1/W_n(j\omega)|$ represent the maximum expected noise gains. The interconnection structure for the mobile rack vehicle is described in Fig. 40.

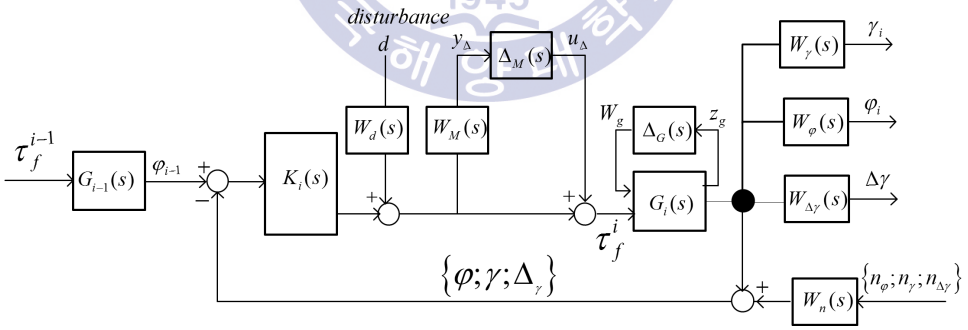

Fig. 40 The interconnection structure for MRVs control system in the platoon

4.4.2.2 General description for MRV control system

Assuming there exists a controller block $K(s)$, the weighting function $W_p\{W_\varphi; W_\gamma\}$ is added to the output to manipulate the dynamic performances of position and velocity. The preceding MRV yaw angle input φ_{i-1}, and the lateral position input γ_{i-1} . To realize the complete system, an external disturbance d is also added to the control synthesis. Another factor that should be considered is the sensor noise W_n for the measurements of the distance and communications. For general controlled system, there are three basic components: the generalized system P, the controller K and the multiple uncertainties $\Delta(\Delta_M(s); \Delta_G(s))$. Rearranging the feed-back system in Fig. 41 leads to the general structure shown in Fig. 42. The system P consists of recognizing three pairs of input/output variables. The first pair (u, y) consist of the control and the measurement signals.

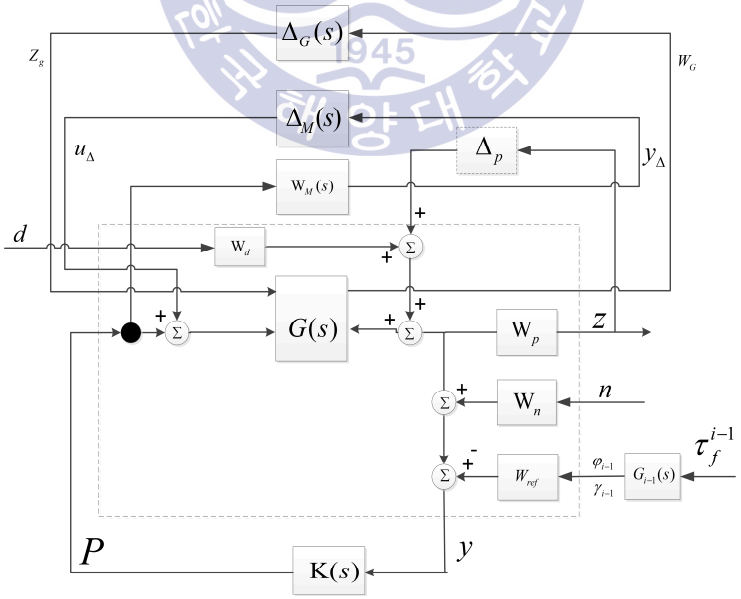

Fig. 41 The general description for closed-loop MRV system in the platoon

Next, the external and output signals (w,z) constitute the performance variables. Finally, the perturbation signals (y_Δ, u_Δ) connect the system through the perturbation Δ. Because of its general structure, this control description is suitable for synthesis as well as for the analysis problem. It is worth noting that P consists of a nominal MRV model and weighting functions.

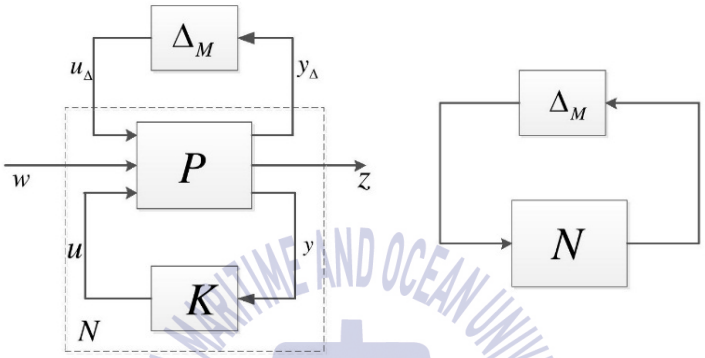

Fig. 42 Generalized control system P with the closed loop $N-\Delta$ structure

4.2.3 Robust performance problem

In this subsection, the stability and performance robustness for a vehicle control problem can be precisely defined by a scalar μ. A detail discussion of μ theory can be found in (Packard. A et.al., 1993). Therefore, only key theory are review for synthesis and analysis of controller. The controller K in Fig. 42 can be combine with

P via the lower LFT to yield the transfer function matrix N. For the $N-\Delta$ structure, the structured singular value μ_Δ is defined as follows:

$$\mu_{\Delta}(N)=\frac{1}{\min\{\bar{\sigma}(\Delta)\,|\,\Delta\in\Delta,\det(I-N\Delta)=0\}} \tag{137}$$

It is clear that the definition of $\mu_{\Delta}(N)$ depends strongly on the block structure Δ as well as the matrix N. The following lemma characterizes μ analysis and synthesis

Lemma *(*μ analysis)

1. Nominal performance: the system has performance if and only if

$$\|M_{22}\|_{\infty}=\sup_{\omega}\bar{\sigma}\{M_{22}(j\omega)\}\le 1,\forall\omega \tag{138}$$

2. Robust stability: $F_u(N,\Delta)$ shall be stable for all Δ if and only if

$$\|\mu_{\Delta}(M_{11})\|_{\infty}=\sup_{\omega}\mu_{\Delta}\{M_{11}(j\omega)\}\le 1 \tag{139}$$

3. Robust performance: $F_u(N,\Delta)$ shall be stable and $\|F_u(N,\Delta)\|_{\infty}\le 1$ if and only if

$$\left\|\mu_{\Delta_p}(M)\right\|_{\infty}=\sup_{\omega}\mu_{\Delta_p}\{M(j\omega)\}<1 \tag{140}$$

Following the definition as above, then for all perturbation Δ with the appropriate structure, it should satisfy the following criteria:

$$\max_{\omega}\bar{\sigma}[\Delta(j\omega)]<\frac{1}{\mu_{\Delta}(N)} \tag{141}$$

Based on D-K iteration, the stabilizing controller is obtained by such that

$$K = \arg\inf_{K} \left\| DF_l(P,K)D^{-1} \right\|_\infty \tag{142}$$

where D is a diagonal constant scaling matrix and can be determined by

$$D(j\omega) = \arg\inf_{D\in D} \bar{\sigma} \left\| DF_l(P,K)D^{-1}(j\omega) \right\|_\infty \tag{143}$$

The sensitivity function S_0 is a good indicator of addressing closed–loop system performance. To reduce the load disturbance effects on the controlled outputs in low frequencies, the sensitivity S_0 should be small and must satisfy the following condition:

$$\left\| W_p S_0 \right\|_\infty < 1 \quad {}^{\forall}\omega \Leftrightarrow \bar{\sigma}(S_0) < \frac{1}{\bar{\sigma}(W_p)} \tag{144}$$

If the control system is to be stable for all perturbed plants about nominal model up to the worst–case model uncertainty, the condition for robust stability is given as follows:

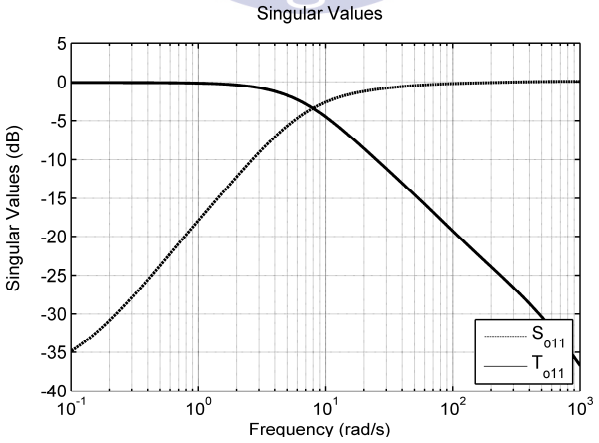

Fig. 43 The singular value plots of sensitivity and complementary sensitivity functions

$$\left\| W_M T_i \right\|_\infty < 1 \quad {}^\forall\omega \Leftrightarrow \mu_\Delta(N_{11}(j\omega)) < 1 \tag{145}$$

Furthermore, the complementary sensitivity function T_0 should be small in high-frequency range to reduce the effects of measurement noises on the controlled outputs as well as the control inputs. Fig. 43 represents the singular value plots of sensitivity S_0 and complementary sensitivity T_0 , in which these results always satisfies the condition $S_0(s) + T_0(s) = I$ at all frequencies. Then the weighting performance W_p which chosen as above is reasonable and satisfies the condition given in Eq. (144). It is obvious that the robust controller can successfully attenuate the external disturbances and keep the complete system stable.

4.3 String stability of connected mobile rack vehicle

Consider a group of the mobile-rack vehicles, in which the operation of each vehicle looks only one vehicle ahead. Each rack in this string can be modeled as follows:

$$q_i = \frac{1}{s} v_i \tag{146}$$

$$v_i = G_{vi}(s).v_{i-1} \tag{147}$$

where v_i is the velocity of i^{th} mobile-rack, and G_{vi} represents the mobile-rack-following algorithm of the i^{th} mobile-rack. For each mobile-rack, the following errors are defined as:

$$\begin{aligned} \varepsilon_i &= q_{i-1}(t) - q_i - r_i - h_{di} v_i(t) \\ \varepsilon_{i+1} &= q_i - q_{i+1} - r_i - h_{di+1} v_{i+1}(t) \\ \varepsilon_{vi} &= v_{i-1} - v_i \end{aligned} \tag{148}$$

In this paper, the constant time-headway policy has been adopted for control synthesis, and that is, the desired ranges are proportional to vehicle speeds. To investigate the string stability of such a system, a propagation transfer function $\bar{\Lambda}_{i,k}(s)$ is defined as the transfer function from range error of i^{th} vehicle to the range error of $(i+1)^{th}$ vehicle

$$\bar{\Lambda}_{i,k}(s) = \frac{\varepsilon_{i+1}}{\varepsilon_i} \tag{149}$$

Substituting Eq. (148) into Eq. (149) through Eq. (150) leads to

$$\bar{\Lambda}_{i,k}(s) = \Lambda_i.\Lambda_{i+1}....\Lambda_{i+k-1}.\frac{(1-\Lambda_{i+k} - s.h_{i+k}.\Lambda_{i+k})}{(1-\Lambda_i - s.h_i.\Lambda_i)} \tag{150}$$

It is clear that the output range errors must be smaller than or equal to the input range errors to avoid the errors propagate indefinitely along the connected vehicle string. Then the inequality $\left\|\bar{\Lambda}_{i,k}(s)\right\|_\infty \le 1$ needs to be satisfied to achieve string stability. The string stability based on the Eq. (150) can be described in Fig. 44.

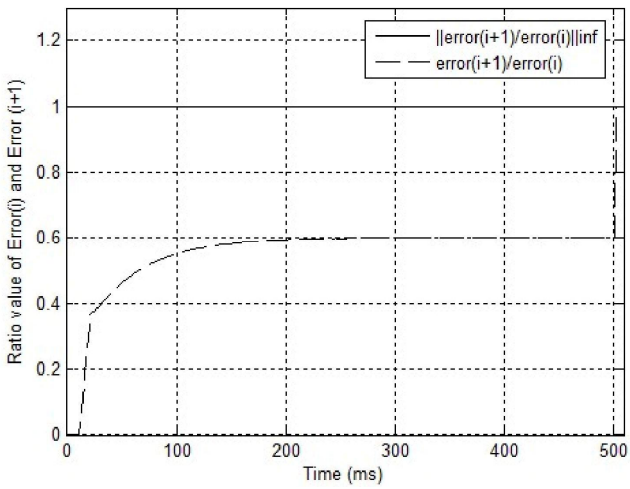

(a)

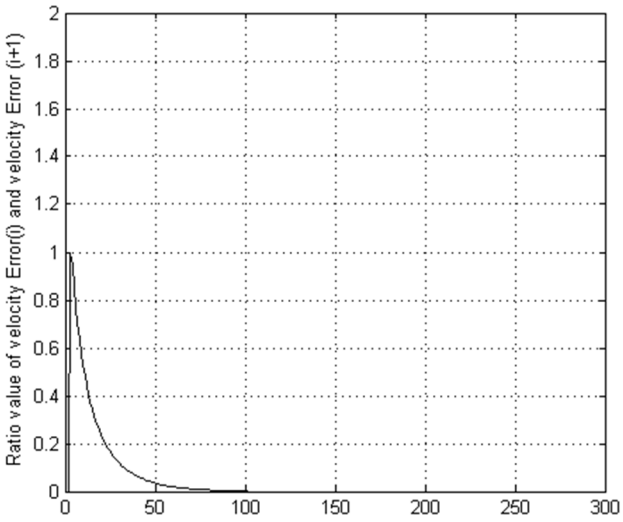

(b)

Fig. 44 String stability of the mobile rack vehicle system: (a) Position string stability, (b) Velocity string stability.

In this case, the ratio of $\bar{\Lambda}_{i,k}(s)$ (dashed) and the $\left\|\bar{\Lambda}_{i,k}(s)\right\|_{\infty}$ (solid) describes that the inequality $\left\|\bar{\Lambda}_{i,k}(s)\right\|_{\infty} \le 1$ is satisfied to ensure the safety spacing of mobile-rack vehicle system. Then the string stability will be guaranteed in a platoon. This means that the MRV's distance can be maintained in the operation term.

4.4 Lower order control synthesis

As it is well known the control system design using the H_{∞} method has high order in general. Evidently, the simple controller is normally preferred over complex ones for real implement. Note that there are fewer things to go wrong in the hardware or bugs to fix the software, and the computational requirements are less. There have been many efforts to invent new methods, which yield low-order

control system in comparison to the typical ones. In the following, some approaches for system reduction include such as truncation and residualization, balanced residualization and balanced truncation or optimal Hankel-norm approximation. It is useful to reduce as much as possible the closed-loop system order, which will simplify the implementation and increase the system reliability and maintainability. Based on the system balancing followed by optimal Hankel approximation, the Hankel-norm denotes the largest possible L_2 norm gain from past inputs to future outputs.

Let $G(s)$ represent the closed-loop system with state-space model, or $G(s)=[A,B,C,D]$. The Hankel singular values of $G(s)$ can be $\sigma_1 \geq \sigma_2 \geq ... \geq \sigma_k > \sigma_{k+1} = ... = \sigma_{k+l} > \sigma_{k+l+1} \geq ...\sigma_n > 0$. Then the reduced-order of the closed-loop system $G_h(s)$ is defined as

$$G_h(s) == [\hat{A},\hat{B},\hat{C},\hat{D}] = \hat{C}\left(sI-\hat{A}\right)^{-1}\hat{B}+\hat{D} \tag{151}$$

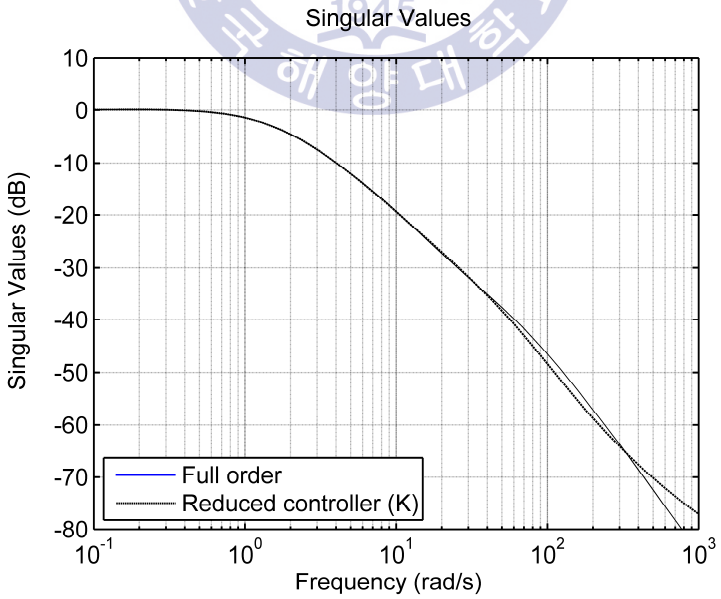

(a)

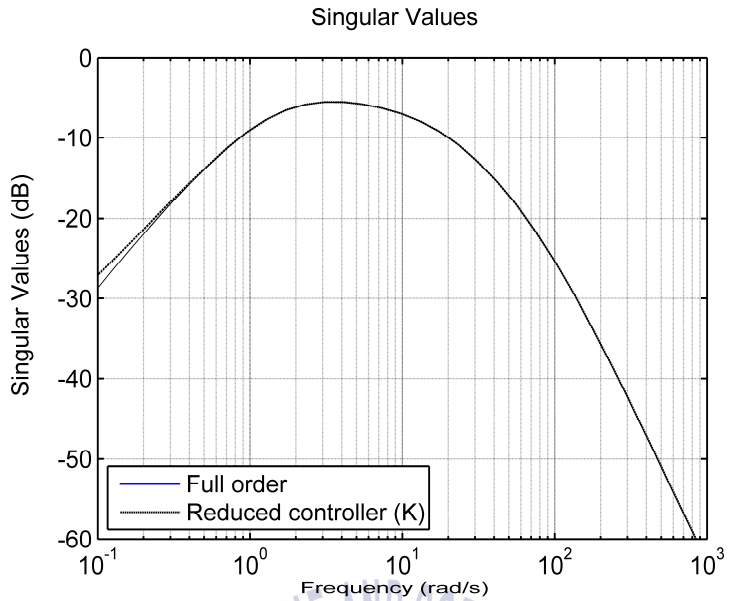

(b)

Fig. 45 Frequency responses of full-order (solid) and 3^{rd} order (dashed) closed-loop system: (a) the singular value of channel 1 and (b) the singular value of channel 2.

where $\hat{A} = \Gamma^{-1}(\sigma_{k+1}{}^2 A_{11}^T + \Sigma_1 A_{11} \Sigma_1 - \sigma_{k+1} C_1^T U B_1^T)$; $\hat{B} = \Gamma^{-1}(\Sigma_1 B_1 + \sigma_{k+1} C_1^T U)$; $\hat{C} = C_1 \Sigma_1 + \sigma_{k+1} U B_1^T$; $\hat{D} = D - \sigma_{k+1} U$; $\Gamma = \Sigma_1^2 - \sigma_{k+1}{}^2 I$, and U is unitary matrix satisfying the condition, $B_2 = -C_2^T U$. For the formula (102) to define an $(n-l)^{th}$ order of $\hat{G}(s)$, the $\hat{G}(s)$ is not stable but has exactly η stable poles. The η^{th}-order stable part $G_{h,\eta}(s)$ of $\hat{G}(s)$ is obtained by using modal decompositions and must satisfy the following condition:

$$\left\| G(s) - G_{h,\eta}(s) \right\|_H = \sigma_{k+1} \tag{152}$$

The closed-loop system is initially of 28^{th} order. Hence, the order of the closed-loop has been considerably reduced to third. The frequency responses of the full-

order and reduced-order system are depicted for comparisons in Fig. 45. The corresponding plots are practically almost identical, leading to similar performances for the closed-loop systems. In particular, the transient responses of the closed-loop system with full-order and those with the reduced-order system are practically same. However, as illustrated in Fig. 46, if the order of the system is further reduced to 2^{nd} order or more, the performances will be greatly degraded. The frequency responses with the reduced-order system are somewhat different, especially at high frequency ranges. Therefore, the final order of controller should be the third for simulation evaluation.

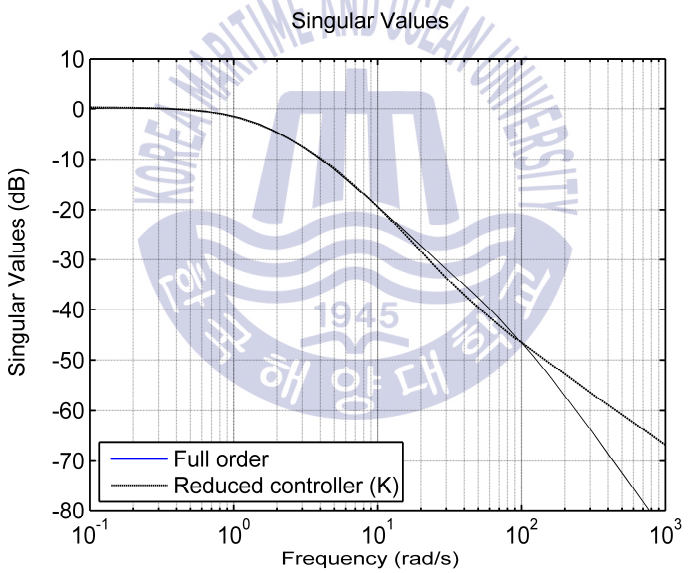

(a)

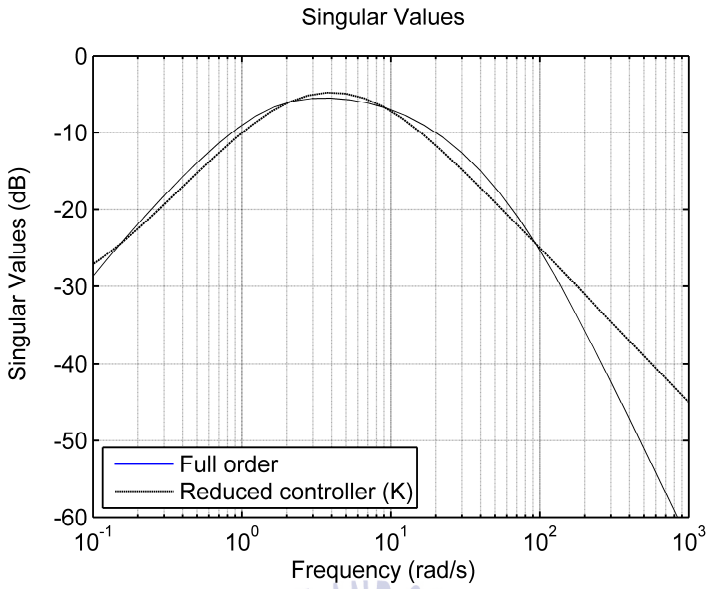

(b)

Fig. 46 Frequency responses of full-order (solid) and 2^{nd} order (dashed) closed-loop system: (a) the singular value of channel 1 and (b) the singular value of channel 2.

Chapter 5. Numerical simulation and discussion

5.1 Mobile rack longitudinal control simulation and discussion

In this section, a platoon of three vehicles is considered to evaluate the performances of the proposed control methods. The desired distance r_i for the mobile-rack vehicle is constant $1m$ and the length of each mobile-rack l_i is $2m$. The velocity range is given by $v_i(\mathrm{m/s}) \le 6$, consider the hardware limitation. The nominal parameters for the mobile-rack model are described in Table 3.

No.	Model parameters	Symbol	Value	Unit
1	Time constant	τ_{mi}	0.5 ± 0.15	s
2	Mass of mobile-rack vehicle	m_i	3000 ± 900	kg
3	i^{th} motor time constant	τ_{pi}	1 ± 0.3	s
4	System gain (input)	g_{ui}	0.7 ± 0.21	Unitless
5	Time headway	h_{di}	0.1 ± 0.03	s
6	Vehicle length	l_i	2	m

Table 3 The nominal parameter of longitudinal MRV system

For the anti-collision maneuvering, the safety distance between each mobile-rack must be taken into account. The lead mobile-rack shall track the reference input and the others will follow this vehicle via the distance sensor for maintaining safe distance. Moreover, to examine the system responses with the variations of parameters, three closed-loops of the controllers with the nominal, minimum and maximum systems are created, respectively. The nominal system uses the average parameters, the minimum and maximum system respectively use the minimum and maximum parameters. To understand the dynamic performances on those clearly,

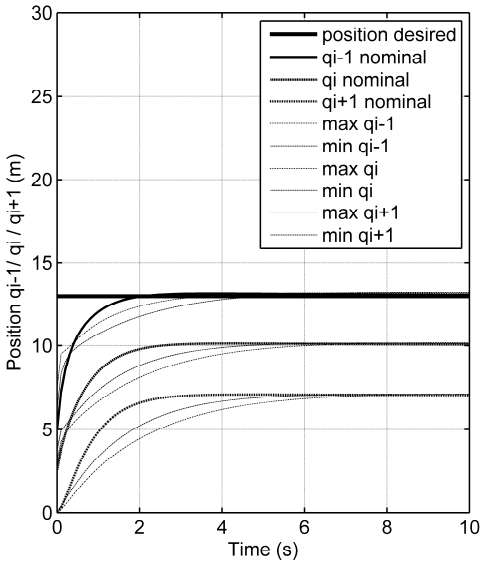

(a)

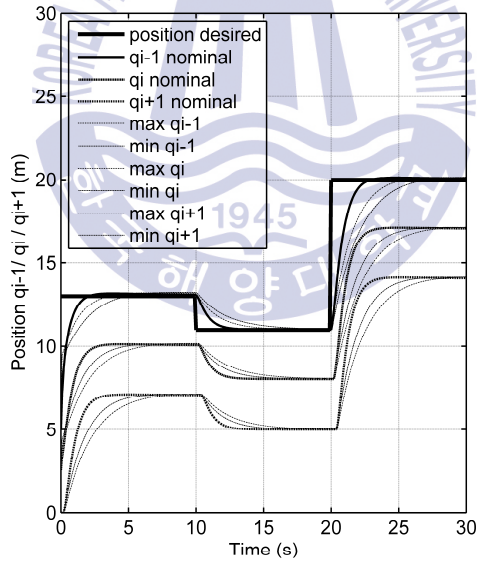

(b)

Fig. 47 Transient responses of MRV's position due to single target and multi targets: (a) single target, (b) multi target.

the simulations with three mobile-rack vehicles have been implemented, as shown in Fig. 47 (a) & Fig. 47 (b). It can be observed from those figure that the q_{i-1} output response reaches the reference targets at $13\,m$ in ten seconds without overshoot. The others q_i and q_{i+1} show similar responses within $3m$ spacing. This means that the controller can provide the safety spacing and the collision avoidance of three vehicles successfully. Furthermore, there are only slight differences among the transient responses of the nominal, minimum and maximum models. It proves that the proposed controller overcomes modeling mismatch effectively, and the set of perturbed systems under parametric variations satisfies the control requirements. The longitudinal acceleration responses of three-vehicle platoon are also represented in the simulation. The acceleration responses of this simple vehicle model were first of order delay with time constant is $0.1s$. Under the limiting conditions of string stability, the acceleration is diffused rather than amplified, but it is not attenuated. As described in Fig. 47, the transient responses of mobile-racks follow the lead vehicle without overshoot, the rising time less than three seconds.

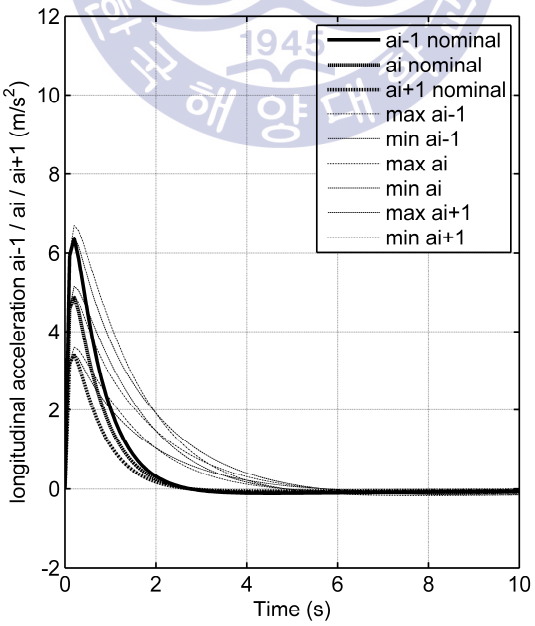

(a)

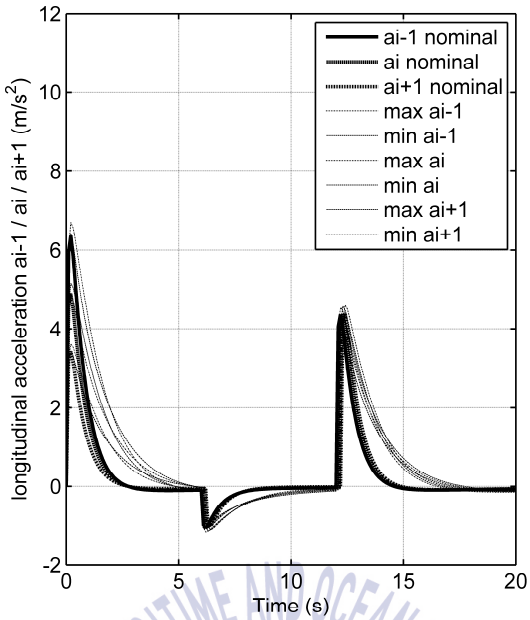

(b)

Fig. 48 Transient responses of MRV's acceleration due to single target and multi targets: (a) single target, (b) multi target.

For simulation maneuvering, the position response of lead vehicle has reached the desired position at $13\,m$. Suddenly, the lead vehicle is decreased to $2\,m$ to reach the new position desired which moving from $13\,m$ to $11\,m$. Finally, the lead vehicle is positioned more $9\,m$ to adapt the destination at $20\,m$. Similarly, in Fig. 48, the acceleration responses of three-vehicle platoon are also illustrated that track the acceleration desired, respectively. Then, Fig. 49 (a) represents the velocity performances which reach the maximum speed desired at $0.7\,m/s$. After the position of mobile rack vehicle- platoon reaches the position target, then the velocity responses converge to zero. For multi-destination case in Fig. 49 (b), the result illustrates that the best performance of velocity is always given. This means that the

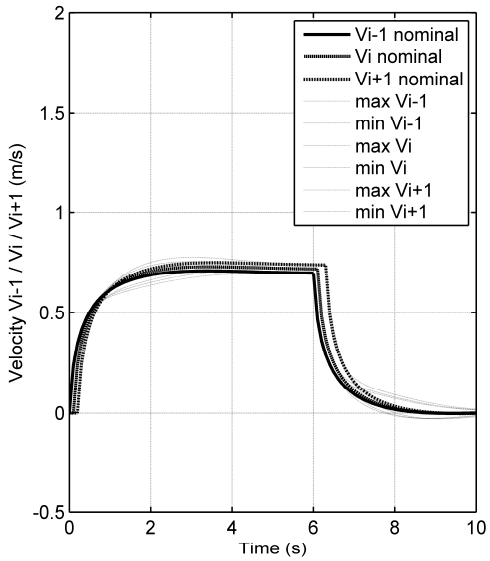

(a)

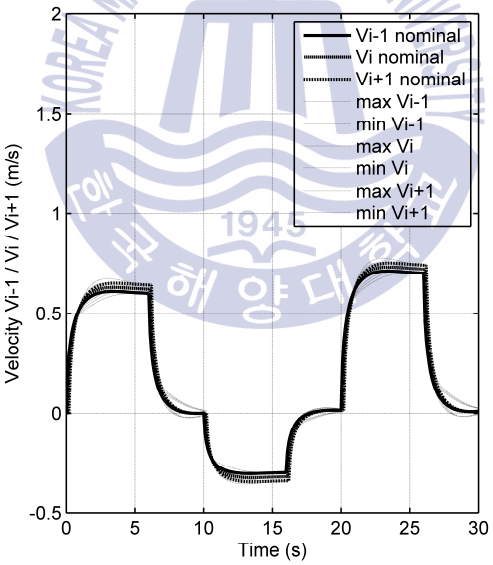

(b)

Fig. 49 Transient responses of MRV's velocity due to single target and multi targets: (a) single target, (b) multi target.

controller of vehicle platoon can adapt the stability requirement of the system under affection of uncertainty. However, the measured outputs are always distorted by

sensor noises in real plant operations, in which noises often occur in high-frequency ranges. It is obvious that the distortions caused by measurement noises can be attenuated with different levels depending on controllers. The ability to maintain the distance between vehicles regardless the measurement signals noises is important for the safety of the vehicle platoon. In this thesis, the robustness beside the measurement signals noises is considered. Fig. 50 shows the time history of system responses under measurement noises. The sensor noises can be eliminated up to 90% .

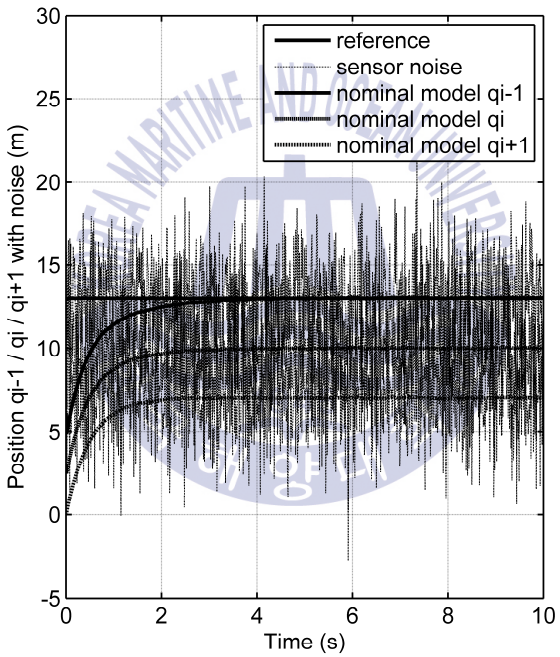

Fig. 50 Time history of vehicle control system due to sensor noises

The safety distance of vehicle system is maintained even under severe sensor noises. It means that the robust controller can provide safe operations for the mobile-rack vehicle system under large distortions caused by noises. In addition, the abilities of disturbances attenuation are likely to be important in verifying

control performance. The exogenous disturbances can be caused by the surface condition of the road, and the abrupt change of acceleration, etc. The identical disturbances have been imposed on representing an increase and decrease in position responses within ten seconds. Moreover, the random disturbances have been also added to test the motion stability of each vehicle. As illustrated in Fig. 51, the disturbance effects on the system performances have been reduced up to 90% in both cases. Whenever there are no changes in the external disturbances, the motion errors will go to zero. The system stability is not only depicted in the first case with the identical disturbance, which affected to the system at the same time, but also illustrated the ability to eliminate most of disturbances excited on each vehicle.

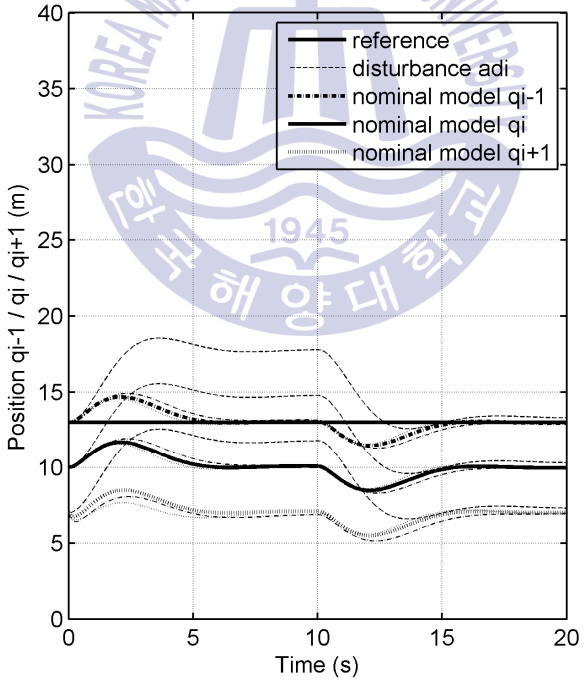

(a)

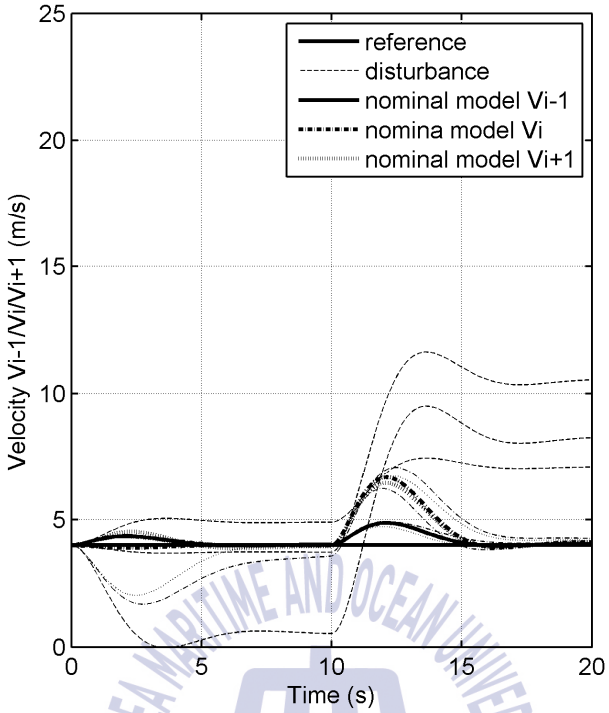

(b)

Fig. 51 Time history of vehicle control system due to external disturbances

Consequently, the closed-loop systems are stable even under large disturbances. While these disturbances occur faster than would usually occur in practice, the ability to eliminate them will insist on a controller that is also able to cope with slower disturbances.

5.2 Mobile rack lateral control simulation and discussion

Numerical simulations are conducted to verify the effectiveness of MRV model. The MRV specifications are list in Table 3. To avoid the obstacles in front of the MRV, a hook trajectory is used for testing the stable of model. For the lateral simulation, the velocity of both vehicles is $0.5m/s$ approximately constant over

time and their distance is 1m constant over time. The lead mobile-rack shall track the reference

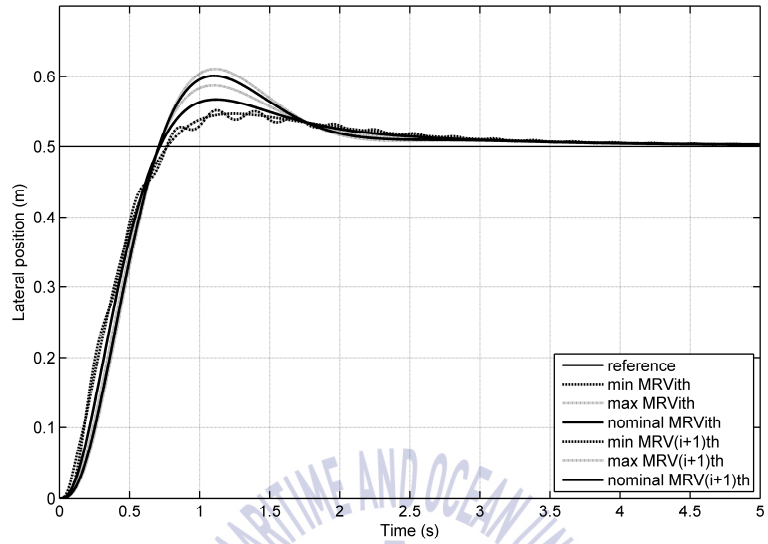

(a)

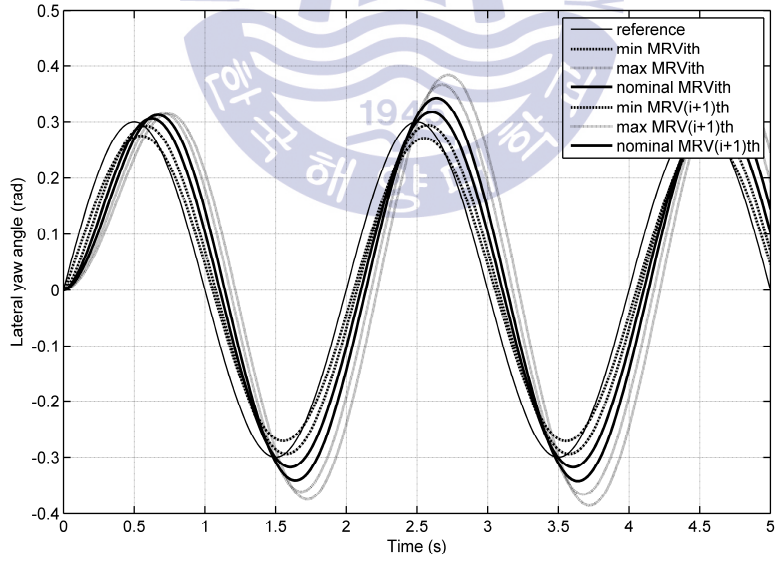

(b)

Fig. 52 The yaw angle response of the family of MRVs in the platoon: (a) yaw angle family step responses, (b) yaw angle family sine responses.

input and the following vehicle shall follow this vehicle via a sensor for maintaining the yaw angle and the lateral position. Moreover, to examine the system responses with the variations of parameters, three closed-loops of the controllers with the nominal, minimum and maximum systems are created, respectively. The nominal system uses the average parameters, the minimum and maximum system respectively use the minimum and maximum parameters. To understand the dynamic performances on those clearly, the simulations with three mobile-rack vehicles have been implemented, as shown in Fig. 52. It can be observed from Fig. 52(a) that the φ_{i-1} output response reaches the reference targets at $0.3(rad)$ in 2 seconds with small overshoot. The MRV following φ_i represents the similar response. Furthermore, there are only slight differences among the transient responses of the nominal, minimum and maximum models. It proves that the proposed controller overcomes modeling mismatch effectively, and the set of perturbed systems under parametric variations satisfies the control requirements. Moreover, to represents continues lane changes performed, a sinusoidal signal is used.

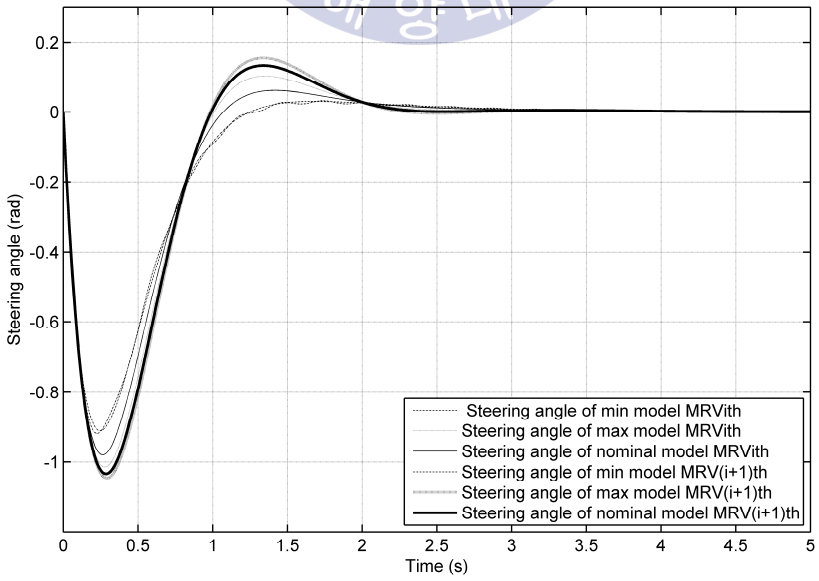

(a)

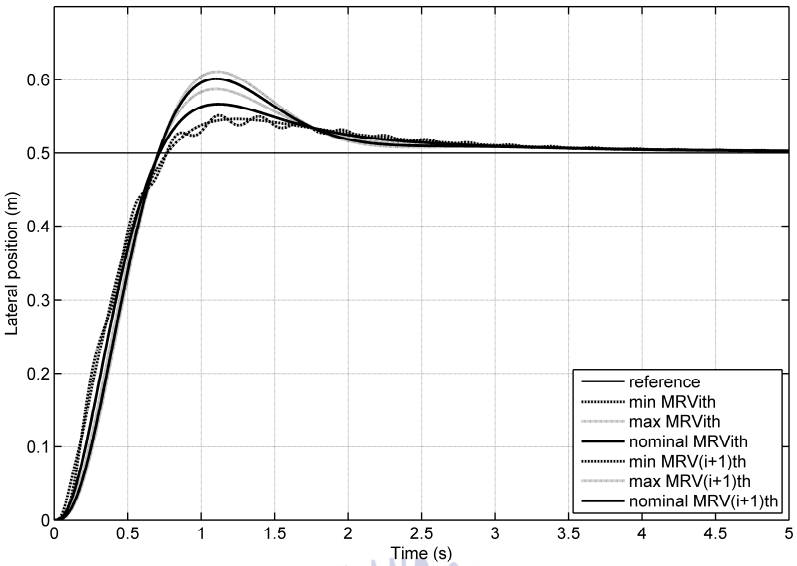

(b)

Fig. 53 The lateral position response of the family of MRVs in the platoon: (a) steering angle family with step input, (b) Lateral position family with step input

Furthermore, it provides the possibility to investigate the possible different dynamic behavior of the MRV to positive of negative side-slips angles. As a result in Fig. 52(b), with a sinusoidal input signal $\sin(\pi + 0.3)$, the output response of two MRVs are demonstrated that has the best tracking ability. This means that, the yaw angle of MRV leader can be reflected by the MRV follower exactly. These responses have a small overshoot in the range that can be accepted. The lateral position responses of two MRVs in the platoon are also represented in the simulation as Fig. 53. As this result, the family responses of the lateral position of two MRVs in the platoon are described. The result has performed the good tracking of follower MRV follows the lead vehicle with small overshoot, the rising time less than two seconds.

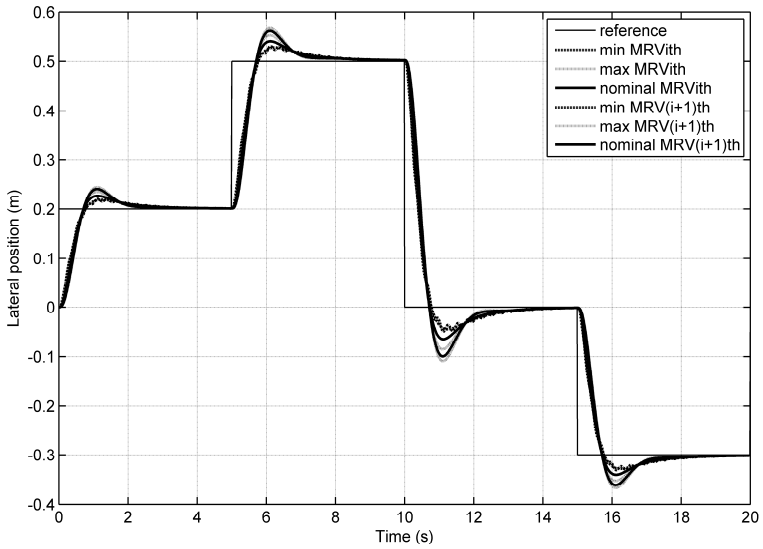

(a)

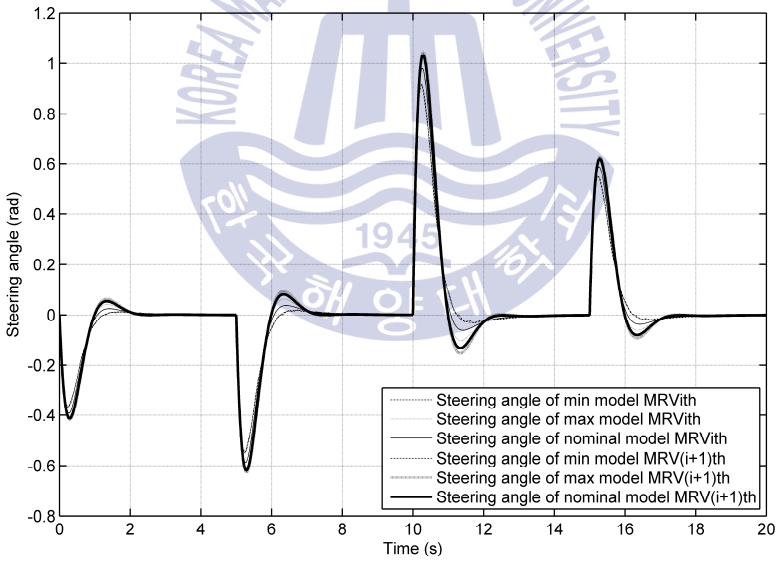

(b)

Fig. 54 The lateral responses with multi-destination of the family of MRVs in the platoon: (a) the lateral position responses (b) Lateral control input signal.

For maneuvering simulation as Fig. 54(a), the position response of lead vehicle has reached the lateral desired position at 0.1m.

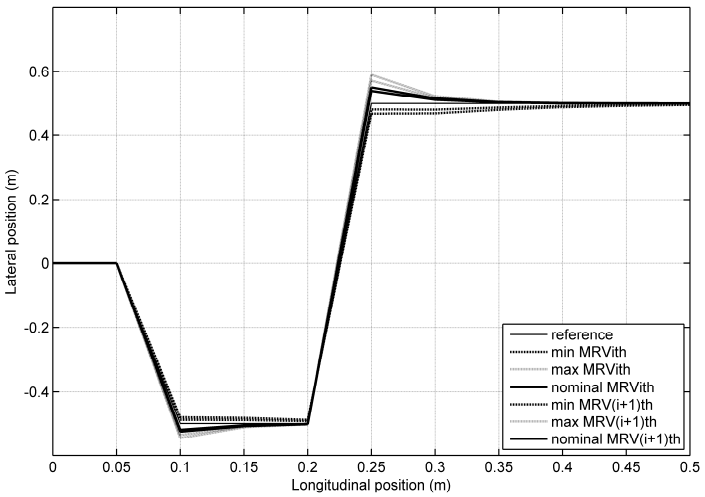

(a)

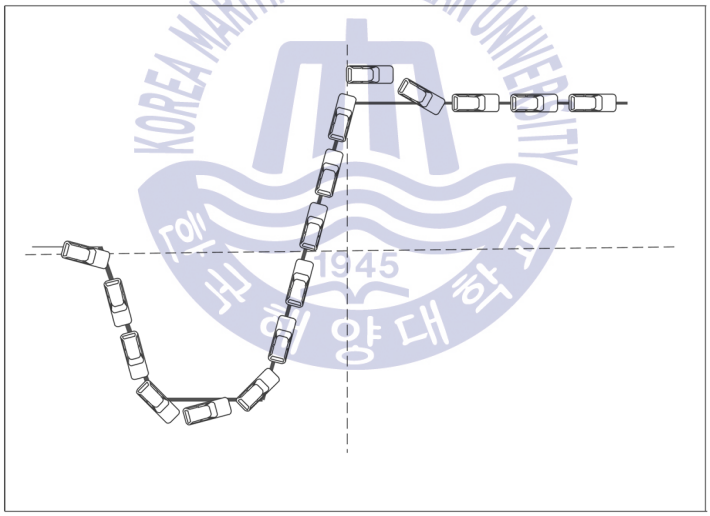

(b)

Fig. 55 The fishhook trajectory for MRV platoon: (a) the transient response of MRV in the platoon, (b) the description of platoon response with fishhook trajectory.

Suddenly, the lead vehicle changes the operation lane at 0.3m to reach the new position desired which moving from 0.1m. Then, the lead vehicle returns to the start position and turn right to -0.2m. Similarly, in Fig. 54(b), the lateral control

input responses of two MRVs in the platoon are also exhibited, respectively. The maximum value of steering angle is 1 rad and the minimum value is 0.4 rad. In order to illustrate the effectiveness of the developed approach, the vehicle equipped with the H_∞ controller is tested with fishhook maneuver in Fig. 55. As the result, although the fishhook maneuver is difficult to implement, so the transient responses of the platoon track the fishhook trajectory reference with small overshoot which can be accepted.

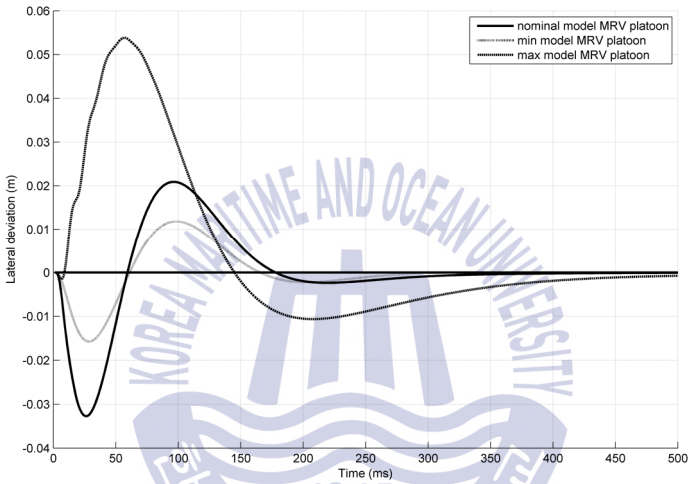

Fig. 56 The lateral deviation $\Delta\gamma$ of min, max and nominal model MRVs in the platoon.

In addition, the minimum and the maximum responses are also represented within small different from nominal response. Hence, the effectively of the MRV controller is proved that it has ability to track any reference desired input with the best result. Furthermore, as the description in Fig. 56, the MRV system which equipped with the robust controller has performed the best performance. The results have demonstrated by representing the lateral deviation responses with the maximum rate of deviation is 5.5cm and minimum rate is 1.1cm which are correlated to the maximum model and minimum model. The deviation at this case

is optimized as well as possible. However, in a real case, low-cost sensors are generally used, so that measurements are usually highly noise-corrupted. In the following simulation, in order to take into account robustness against the noise in the measurement signals, the measurement noise of the proposed algorithm, the noise signal at 102 rad/s are added to the measurement signals of the relative distance. The performances of the MRV platoon control system under noise in the measurement signals are shown in Fig. 57. As a simulation result in Fig. 57(a) the lateral position responses of the platoon without robust controller are deformed and cannot track the lateral position desired. In the opposite way, the MRV which equipped the H_∞ controller can maintain the stability of lateral position.

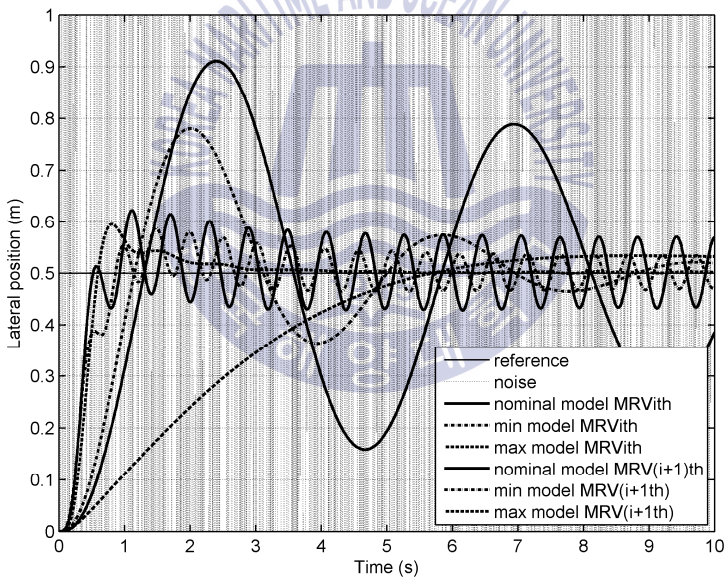

(a)

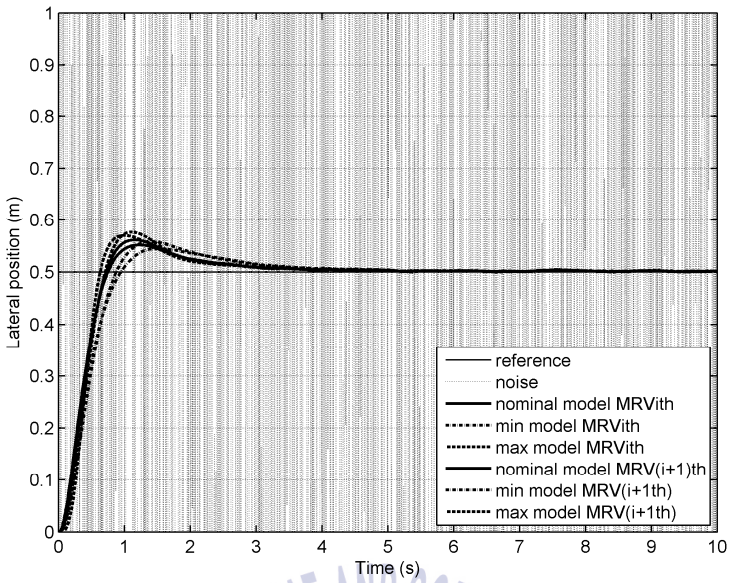

(b)

Fig. 57 The lateral position response due to noise: (a) without H_∞ controller, (b) with H_∞ controller.

The result in Fig. 57(b) illustrates the controller ability that can cope with noise or external disturbance to ensure the stable operation of MRV platoon. In addition the lateral stability of MRV platoon is affected by external disturbance such as the road surface is covered by ice in the cold warehouse. So, to test the abilities of disturbances attenuation, two simulations with and without robust controller are implemented and compared which is shown in Fig. 58. The external disturbance affected to the MRV system without H_∞ controller is shown as Fig. 58(a). The result shows the lateral position responses are deformed and undefined. This means that this system cannot maintain the stability if the robust controller is not equipped in. Inversely, the external disturbances have been attenuated completely in the Fig. 58(b).

Whenever there are no changes in the external disturbances, the errors will go to zero. Hence, the closed system is stable even under large disturbances.

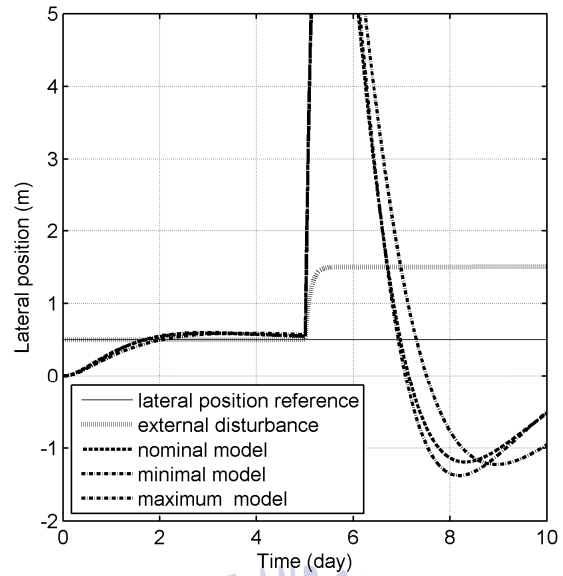

(a)

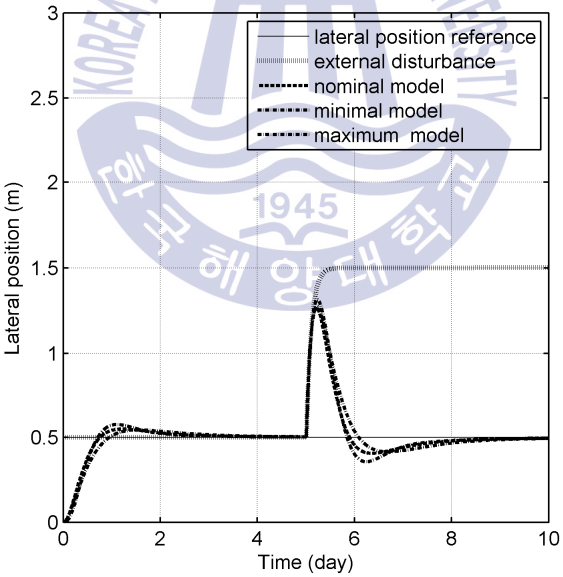

(b)

Fig. 58 The lateral position response due to disturbance: (a) without H_∞ controller, (b) with H_∞ controller.

While these disturbances occur faster than would usually occur in practice, the ability to eliminate them will insist on a controller that is also able to cope with slower disturbances.

Chapter 6. Conclusion

An autonomous mobile rack vehicles (MRVs) are used in the smart warehouses in order to storage the large product in the small area by moving the rack automatically. Working with automated guided vehicles (AGV) for automating the internal material flow. The MRVs is useful in the smart warehouse cause the flexible movement and convenient. The MRV can overcome the disadvantage of traditional rack. The main problem of MRVs are position tracking, string stability and lateral synchronization.

The focus of this thesis is on the design of longitudinal and lateral controllers for the autonomous mobile rack vehicles. At first, MRV longitudinal control was concerned, a string stability of MRV platoon was demonstrated and the robust controller was designed. Theoretical analysis showed that the controller could ensure the string stability and provide the stable operation of platoon. The results show that the system can cope with the uncertainty of system and has ability to attenuate the noise from sensors and external disturbances. Next, the lateral control was studied, considering the mass, the cornering stiffness, the velocity of MRV have great influence on lateral dynamics, a robust controller which ensures the stability of MRVs to overcome those critical issue as above either or noise and disturbance.

The simulation results showed that the proposed controller was able to perform accurate longitudinal control and lateral control as well as provide good ride quality. To demonstrate the stability of longitudinal control, so the position and velocity, acceleration simulations are implemented. The controller give the best position tracking result in Fig. 47. The position responses of three mobile racks are 13m, 10m and 7m, respectively. The transient responses track the reference input without overshoot and 8 seconds for settling time. Corresponding to the position responses, the velocity responses of three MRV are also represented the best results which can achieve the max speed of MRV at 0.7m/s. Along with these position and velocity responses, the transient responses of acceleration are also illustrated in Fig.

48 with the maximum value at $1.2 m/s^2$ and the minimum value at $-0.55 m/s^2$. In the other hand, the lateral control has performed stability of the yaw motion such as the yaw angle family response and lateral position responses with step input and rectangular input. The results shows the yaw angle family responses reach the reference targets at $0.3rad$ in 2 seconds with small overshoot. To demonstrate the stable of yaw angle, the sinusoidal input signal $\sin(\pi + 0.3)$ is used. The results shows the best tracking between yaw angle responses and the input signal in Fig. 52(b). The lateral position responses of the family of MRVs have illustrated that the following MRVs can be after the leading MRV with small overshoot. Moreover, to demonstrate the following vehicle can follow the leading vehicle with small errors, the lateral deviation results of nominal, minimum and maximum system have performed in Fig. 56 with the maximum rate is 5.5cm and the minimum rate 1.1 cm. In addition, to ensure the MRV system can operate in any environment, then the noises and disturbance case are added to the simulation. The results is compared to the PID controller and shows that in the noise or disturbance case, the PID controller cannot overcome that affection with the bad result in Fig. 57(a) and Fig. 58(a). However, the system is equipped with robust controller can cope with noise and disturbance in Fig. 57(b) and Fig. 58(b). In that Figure, the noise is attenuated 90% and the disturbance is ne

Finally, further validation and reliability, the controller of MRV shall be implemented with DSP board TMS320F28335 or ARM STM32F407-VET6 to evaluate the reliability and stability of platoon.

Reference

Becker, G., Packard, A., Philbrick, D., & BALAS, G., 1993. Control of Parametrically-Dependent Linear Systems: A Single Quadratic Lyapunov Approach. *Proceedings of the American Control Conference*, San Francisco, pp. 2795–2799.

Becker, G., & Packard, A., 1994. Robust Performance of Linear Parametrically Varying Systems Using Parametrically-dependent Linear Feedback. *Systems & Control Letters*, 23, pp. 205–215.

Caudill, RJ. & Garrard, WL., 1977. Vehicle follower longitudinal control for automated transit vehicles. *Journal of Dynamic Systems, Measurement and Control*, 99(4), pp. 241–248.

Doyle, J., 1978. Guaranteed margins for LQG regulators. *IEEE transactions on Automatic Control* 23, pp. 756–757.

Doyle, J., 1982. Analysis of feedback systems with structured uncertainty. *IEE Proceeding of Control Theory Application,* 129**,** pp. 242–250.

Fujioka, T. & Suzuki, K., 1994. Control of longitudinal and lateral platoon using sliding control, *Vehicle System Dynamics*, 23(8), pp. 647–664.

Juergen, G., Hanshue, T. & Satyajit, P., 1996. Analysis of Automatic Steering Control for Highway Vehicles with Look-Down Lateral Reference System, *Vehicle System dynamics*, 26(4), pp. 243–269.

Gao, F., Dang, D. F., Huang, S.S. & Li, S. E., 2017. Decoupled robust control of vehicular platoon with identical controller and rigid information flow. *International Journal of Automotive Technology,* 18(1), pp. 157–164.

Gao, F., Li, S. E., Zheng, Y. & Kum, D., 2016. Robust control of heterogeneous vehicular platoon with uncertainty dynamics and communication delay. *IET Intelligent Transport Systems*, 10(7), pp. 503-513.

Georgieva, P. G. & Feyo De Azevedo, S., 1999. Robust control design of an activated sludge process. *International Journal of Robust Nonlinear Control,* 9, pp. 949–967.

Godbole, D. N. & Lygeros, J., 1994. Longitudinal control of the Lead Car of a Platoon. *IEEE Transaction on Vehicular Technology,* 43(4), pp. 1125–1135.

Guo, G. & Yue, W., 2012. Autonomous platoon control allowing range limited sensors. *IEEE Transaction on Vehicular Technology,* 61(7), pp. 2901–2912.

Herman, I., Martinec, D., Hurak, z. & Sebek, M., 2015. Nonzero bound on fiedler eigenvalue causes exponential growth of H-infinity norm of vehicular platoon. *IEEE Transaction on Automatic Control,* 60(8), pp. 2248–2253.

Hsu, C. F., Wang, W. J., Lee, T. T. & Lin, C. M., 2004. Longitudinal control of vehicle platoon via wavelet neural network. *IEEE International Conference on Systems,* Man and Cybernetics, pp. 3811–3816.

Lanzon, A., Engelken, S., Patra, S. & Papageorgiou, G., 2012. Robust stability and performance analysis for uncertain linear systems-the distance measure approach. *International Journal of Robust and Nonlinear Control,* 22(11), pp. 1270–1292.

Liang, C.Y. & Peng, H., 2000. String stability analysis of adaptive cruise controlled vehicles. *JSME International Journal Series C-Mechanical Systems, Machine Elements and Manufacturing*, 43, pp. 671–677.

McFarlane, D. C. & Glover, K., 1992. A loop shaping design procedure using synthesis. *IEEE Transactions on Automatic Control,* pp. 759–769.

Petersen, U. N., Ruekgauger, A. & Schiehlen, W. O., 1996. Lateral control of a convoy vehicle system. *In Proceedings of 14th IAVSD- Symposium*, pp. 519–532.

Pascal, D. & Michel, P., 1996. Longitudinal and lateral servoing of vehicle in a platoon. *In Proceeding of the IEEE Intelligent Vehicle Symposium,* pp. 41–46.

Peng, H. & Tomizuka, M., 1993. Preview control for vehicle lateral guidance in highway automation. *Trans. ASMR, J. Dynamic Systems, Measurement Control*, 115(4), pp. 678–686.

Pham, H., Hedrick, K. & Tomizuka, M., 1994. Combined lateral and longitudinal control of vehicle for IVHS. *In Proceedings of American Control Conference*, 2, pp. 1205–1206.

Rajamani, R., Choi, S. B., Law, B. K., Hedrick, J. K., Prohaska, R. and Kretz, P., 2000. Design and experimental implementation of longitudinal control for a platoon of automated vehicles. *Journal of Dynamic Systems Measurement and Control* 122, pp. 470–476.

Rajamani, R. & Shladover, S. E., 2001. An experiment comparative study of autonomous and co-operative vehicle- follower control systems. *Transportation research part c: emerging technologies,* 9(1), pp. 15–31.

Sam-sang, Y., & Seok-kwon, J., 2002. Controller design and analysis for automatic steering of passenger cars. *Mechatronics*, 12, pp. 427–446.

Samar, R., Postlethwaite, I. & Gu, D.W., 1994. Applications of the Singular Perturbation Approximation of Balanced Systems. *IEEE Proceedings of Control Applications Conference* 28, pp. 24–26.

Skogestad, S., and Postlethwaite, I., 2005. *Multivariable feedback control: analysis and design,* 2nd edn, Josn Wiley & Sons, Ltd., Chichester, West Sussex PO19 8SQ, England.

Sivaji, V. V. & Sailaja, M., 2013. Adaptive cruise control systems for vehicle modeling using stop and go manoeuvres. *International Journal of Engineering Research and Applications (IJERA)*, 3(4), pp. 2453–2456.

Stankovic, S., Stanojevic, M. J. & Siljak, D. D., 2000. Decentralized over-lapping control of a platoon of vehicles. *IEEE Trans. Control System Technology,* 8(5), pp. 816–831.

Steven, E. S., Nowakowski, C., Lu, X.Y. & Ferlis, R., 2015. Cooperative adaptive cruise control (cacc) definitions and operating concepts. *In Proceedings of the 94th Annual TRB Meeting . Transportation research board.*

Swaroop, D. & Hedrick, JK., 1996. String stability of interconnected systems. *IEEE transactions on automatic control*, 41(3), pp. 349–357.

Tai, M. & Tomizuka, M., 2000. Robust longitudinal velocity tracking of vehicle using traction and brake control. Proceedings of international workshop on advanced motion control, pp. 305–310.

Vincente, M., Steven, E. S., John, S., Christopher, N., Hiroshi, K. & Masahide, N., 2014. Cooperative adaptive cruise control in real traffic situations. *IEEE Transactions on Intelligent Transportation Systems*, 15(1), pp. 296–305.

Walker, D. J., 1996. On the structure of a two-degree-of-freedom Hinf loop shaping controller. *International Journal of Control*, 63(6), pp.1105–1127.

Yanakiev, D. & Kanellakopoulos, I., 2008. Variable time headway for string stability of automated heavy-duty vehicles. *IEEE Proceedings of Conference on Decision and Control* 34, pp. 4077–4081.

Young, P. M., Newlin, M. P. & Doyle, J. C., 1991. μ Analysis with Real Parametric Uncertainty. *IEEE Proc. Decision and Control Conf.* 30, pp. 1251–1256.

Young, J. S., 2010. The best optimal Hankel-Norm approximation of railway active wheelset models. *IEEE Proc. American Control Conf*erence, pp. 2724–2729.

Zoran, G. & Muhidin, L., 2000. Singular perturbation analysis of system order reduction via system balancing. *Proceeding American control conference*, pp. 2420–2424.

Zames, G., 1981. Feedback and optimal sensitivity: Model reference transformations, multiplicative seminorms and approximate inverses. *IEEE Transactions on Automatic Control*, 26, pp. 301–320.

Zhang, P., Yuan, M., & Wang, H., 2008. Improvement of nitrogen removal and reduction of operating costs in an activated sludge process with feedforward-cascade control strategy. *Biochemical Engineering Journal*, 41(1), pp.53–58.

Zhou, K., Khargonekar, P. P., Stoustrup, J., & Niemann, H. H., 1992. Robust stability and performance of uncertain systems in state space. In *Proceedings of the 31st IEEE Conference: on Decision and Control,* Tucson, AZ, pp.662–667.